Anina Barth

Dynamics of Solubilisation Processes in Amphiphilic Systems Studied by Highly Time-Resolved Stopped-Flow Experiments

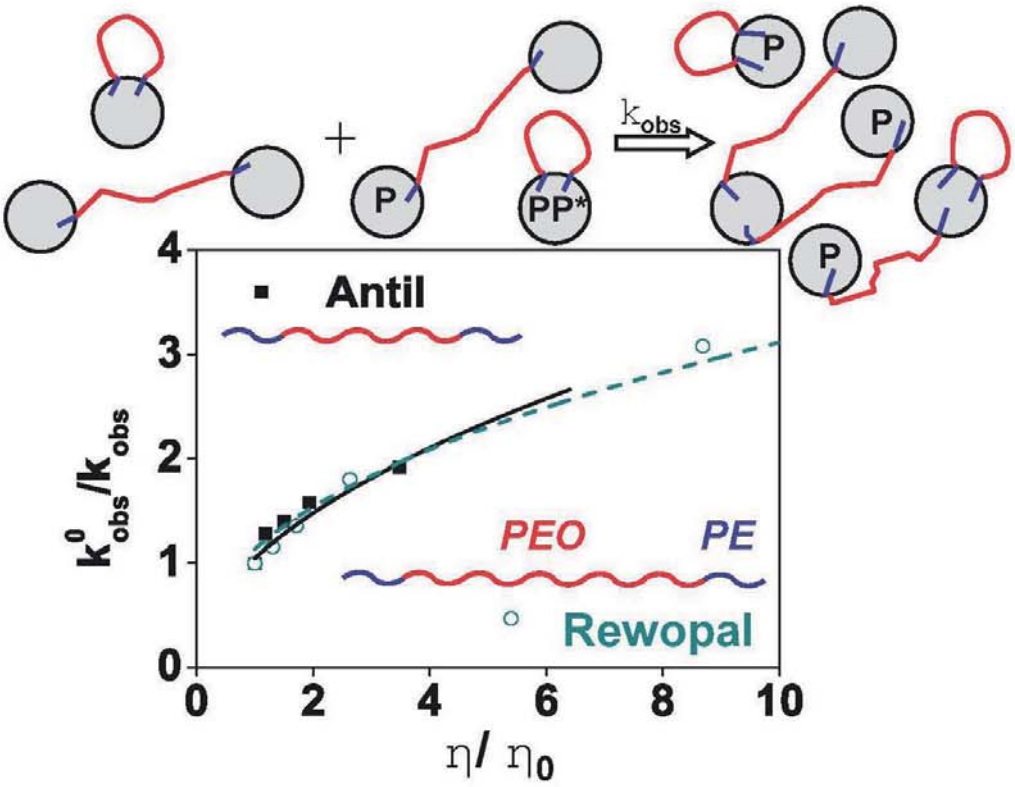

Cuvillier Verlag Göttingen
Internationaler wissenschaftlicher Fachverlag

Dynamics of Solubilisation Processes in Amphiphilic Systems Studied by Highly Time-Resolved Stopped-Flow Experiments

vorgelegt von
Diplom-Chemikerin
Anina Barth
Potsdam

Von der Fakultät II - Mathematik und Naturwissenschaften
an der Technischen Universität Berlin
zur Erlangung des akademischen Grades

Doktor der Naturwissenschaften
(Dr. rer. nat.)

genehmigte Dissertation

Promotionsausschuss:

Vorsitzender:	Prof. Dr. Reinhard Schomäcker
1. Berichter:	Prof. Dr. Michael Gradzielski
2. Berichter:	Prof. Dr. Joachim Koetz

Tag der wissenschaftlichen Aussprache: 23.08.2011

Berlin 2011
D 83

Bibliografische Information der Deutschen Nationalbibliothek
Die Deutsche Nationalbibliothek verzeichnet diese Publikation in der Deutschen Nationalbibliografie; detaillierte bibliografische Daten sind im Internet über http://dnb.d-nb.de abrufbar.
1. Aufl. - Göttingen : Cuvillier, 2011
Zugl.: Berlin, Univ., Diss., 2011

978-3-86955-974-5

Nonnenstieg 8, 37075 Göttingen
Telefon: 0551-54724-0
Telefax: 0551-54724-21
www.cuvillier.de

1. Auflage, 2011
Gedruckt auf säurefreiem Papier

978-3-86955-874-5

Abstract

In this work a comprehensive study of the solubilization dynamics in ternary and quaternary surfactant systems is presented. Microemulsion either with the zwitterionic tetradecyldimethylamine oxide or the nonionic pentaethyleneglycol monododecyl ether were employed to study intensively the dynamics of the exchange of oil between microemulsion droplets. The stopped-flow method - in which two volumes of solutions are rapidly mixed and the properties of the mixed solution followed as a function of time and - was employed intensively throughout this work. Complementary stopped-flow measurements (turbidity, fluorescence and Small Angle X-ray Scattering) served as a suitable tool to monitor the kinetics of solubilisate exchange between and the equilibration of microemulsions and in addition the process of formation of vesicles. For that purpose pyrene butyric acid stearyl ester was specially designed and used as fluorescent probe and by a systematic variation of the molecular composition of the microemulsion a comprehensive understanding of the solubilization dynamics has been achieved.

Fluorescence measurements proved that not the bending elasticity but the curvature of the surfactant monolayer is the decisive factor during the exchange of oil in a ternary, nonionic microemulsion system. Consequently, at identical values of the bending elasticity, coalescence is slower the smaller the aggregates. Furthermore, through addition of small amounts of charge (introduced by admixing an ionic surfactant) and amphiphilic polymers, the coalescence of microemulsions necessary during the process of oil exchange and equilibration, could be decelerated significantly due to the electrostatic and steric repulsion induced in the system. At the same time the activation energy for these two processes was found to increase as a consequence of the hindrance to coalescence.

In a second approach the structural transition from micelle/microemulsion to vesicles was investigated. The spontaneous formation of the vesicles depends strongly on the preparation of the sample and are therefore controlled by the kinetics of their formation process and was found to be slower the higher the distance between the starting composition and the final composition.

Zusammenfassung

Die vorliegende Arbeit beschäftigt sich mit der Solubilisationsdynamik in ternären und quaternären Tensidsystemen. Es wurden Mikroemulsionen, bestehend aus dem zwitterionischen Tetradecyldimethylaminoxid oder dem nichtionischen Penta-ethylenglycolmonododecylether, verwendet, um die Ölaustauschkinetik zwischen diesen Mikroemulsionstropfen zu untersuchen. Die Stopped-flow-Methode – bei der identische Volumina zweier Lösungen sehr schnell gemischt werden und die Eigenschaften der Mischung als Funktion der Zeit untersucht werden können – wurde für diese Untersuchungen eingesetzt. Komplementäre Detektionsmethoden (Trübung, Fluoreszenz und Kleinwinkelröntgenstreuung) dienten dazu, die Kinetik des Ölaustausches und der Bildung von amphiphilen Strukturen zu untersuchen. Zu diesem Zweck wurde ein Pyrenstearylester synthetisiert und als Fluoreszenzfarbstoff verwendet, der es ermöglichte, einen umfassenden Überblick über die Solubilisationskinetik zu erlangen, während die molekulare Zusammensetzung der Mikroemulsionen systematisch verändert wurde.

Fluoreszenzmessungen zeigten, dass nicht die Biegesteifigkeit, sondern die Krümmung der Tensidschicht der entscheidende Faktor des Ölaustauschs in einem ternären, nichtionischen Mikroemulsionssystem ist. Bei gleicher Biegesteifigkeit, verläuft der Ölaustausch umso langsamer, desto kleiner die Aggregate. Durch Zugabe kleiner Mengen von Ladung und amphiphilen Polymers und der daraus resultierenden zunehmenden elektrostatischen und sterischen Abstoßung, wurde die Geschwindigkeit des Koaleszenzprozesses gezielt verlangsamt. Gleichzeitig stieg die Aktivierungsenergie für diesen Schritt aufgrund der zusätzlichen Behinderung an.

Ein weiteres Ziel war die Untersuchung des Strukturübergangs Mizelle/Mikroemulsion zu Vesikeln. Die spontane Bildung der Vesikel wird durch die Zusammensetzung der Probe beeinflusst und hängt daher entscheidend von deren Bildungsprozess ab. Die Bildungsgeschwindigkeit ist dabei umso langsamer, je größer der Unterschied in der Zusammensetzung des Anfangs- und Endzustandes.

Table of Contents

1 Introduction

In aqueous solution many surfactants exhibit a rich phase behavior due to their ability to self-assemble into a large variety of morphologically different structures. The simplest ones are micellar structures of e.g. spherical or cylindrical shape to more complex ones like lamellar, vesicle or sponge phases.

Originally proposed by Tanford [1] but later refined,, Israelachvili et al. [2] introduced the concept of the so-called packing parameter in 1976, a theoretical framework that relates molecular parameters (head group area, chain length, hydrophobic tail volume) and intensive variables (temperature, ionic strength etc.) to surfactant microstructures and which provides the opportunity to ´tailor´ the amphiphilic morphology as desired.

The (critical) packing parameter P is given by

equation 1.1

$$P = \frac{\upsilon}{a \cdot l_c}$$

where υ, a, and l_c are volume, head group area and length of the amphiphile, respectively.

For surfactants with a broad head group and a short tail, $P < 1/3$ and spherical micelles are formed, where the water forms the solvent phase. Shifting the packing parameters to higher values (by decreasing a_h and/or increasing l) the surfactant microstructure changes from cylindrical aggregates [3, 4] ($1/3 < P < 1/2$) to bilayers (lamellar phase [5, 6] and vesicles [5, 7-10] ($P = 1$) and finally to the corresponding inverse structures as displayed in chart 1.1.

In the past the static behavior of these morphological structures has been studied intensively due to their central importance for technical and biological applications, which will be discussed in detail later. However, the dynamic properties of amphiphilic systems are only poorly understood and this applies also to the criteria determining the kinetics of structural reorganization processes of such systems.

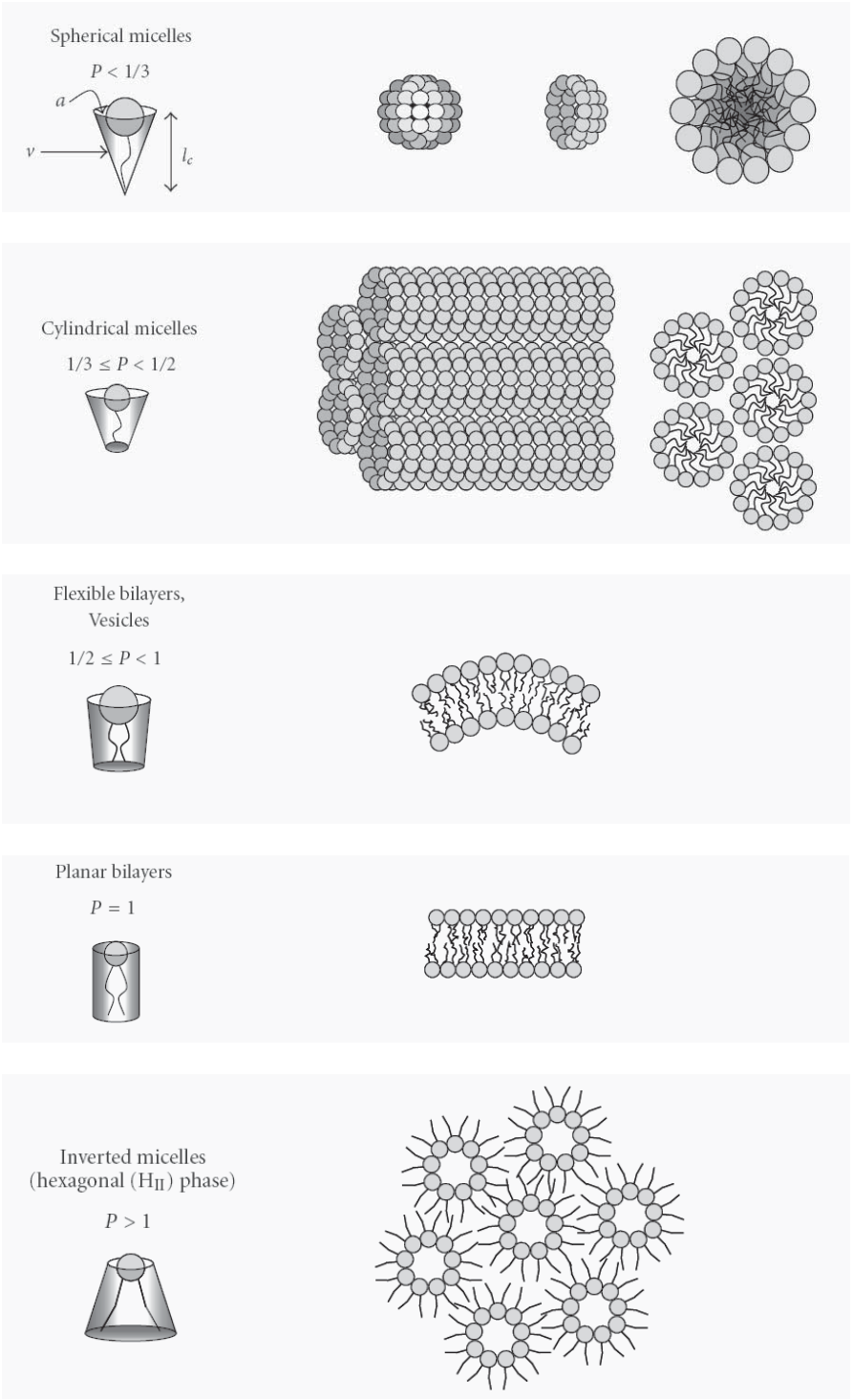

chart 1.1 Morphological structures predicted by the packing parameter [11].

Hence, the present work dealt with kinetical aspects in surfactant systems and the influence of parameters, such as charge, steric interactions, and temperature thereof. Three kinetic approaches of fundamental importance for technical applications will be investigated:

The kinetics of the **formation** of amphiphilic structures.
The kinetics of the **exchange** of solubilisate between surfactant aggregates.

On the one hand the morphological transition from micelles/microemulsions to metastable multilamellar vesicles and the formation of thermodynamically stable microemulsions was studied (where the latter is not a process of formation in the common sense because the amphiphilic structure of the starting and the final solution are MEs in both cases; it is therefore more appropriate to speak of equilibration of ME aggregates). The former one is of special technological interest since it has been known for some time now that metastable amphiphilic structures are controlled by the dynamics of their formation [12]. Studying the dynamics of morphological transitions in surfactant systems has become an increasingly active field of colloid research due to the improved experimental time resolution which offers the possibility to gain a more detailed picture of the structural changes involved [13]. Therefore the dynamics of these two formation processes were investigated i.e. by means of time-resolved SAXS measurements. Subsequently specific control of the metastable intermediate structures can be of key importance e.g. in template synthesis and formulations etc.

On the other hand the kinetic of the exchange of oil between ME aggregates was studied in detail. As amphiphiles two technical-grade surfactants were employed. Their structure and properties will be introduces in the following paragraph, where a brief introduction to microemulsions (definition, relevance and application) will be given. The last paragraph of the introduction will deal with the principles of vesicle formation and their importance for technical and biological tasks.

Microemulsions

Microemulsions are thermodynamically stable dispersions of either water-in-oil (W/O) or oil-in-water (O/W), the stability being the result of the presence of a suitable surfactant [14, 15]. They have been studied intensively due to their enormous potential in many technical applications, e.g. in detergency, ternary oil recovery, formulation of cosmetic, agricultural or pharmaceutical products, and lately the preparation of nanoparticles [16-21]. ME aggregates saturated with hydrophilic (water) or hydrophobic (alkanes) solubilisate, consist of small, spherical droplets, exhibiting radii in the range 3 - 30 nm [22]. MEs are thermodynamically stable (they form spontaneously and droplet size is independent of variations in preparation method [23]) which renders them most suitable as reaction medium for enzyme-catalyzed reactions [24, 25], the controlled and selective synthesis [26] and lately the preparation of nanosized particles [19-21].

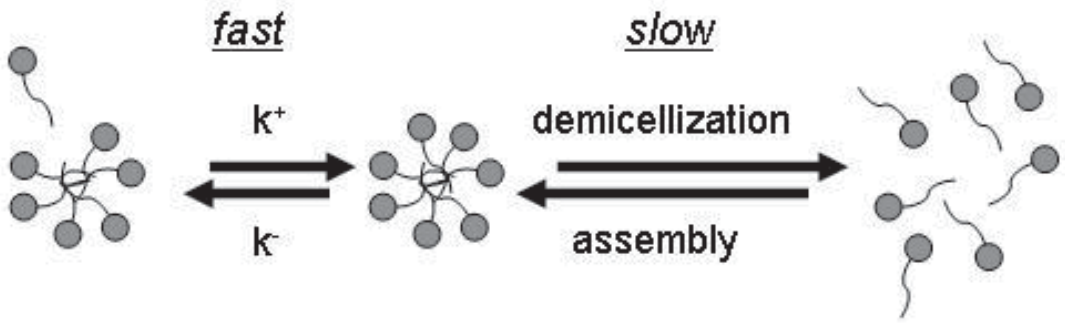

chart 1.2 Surfactant exchange mechanism and micelle formation and break-down according to Aniansson and Wall [27] where k^+ and k^- are the exit and entry rates of surfactant molecules (displayed as hydrophilic head group in blue and hydrophobic tail)

Quite a number of publications about micelle dynamics come from chemical relaxation experiments [28-31] that are a powerful means of determining the rates of various relaxation processes. Two well-separated relaxation times have been identified: a rapid relaxation τ_1, which requires microseconds and a slower process τ_2 that occurs on a timescale of seconds or longer. A cartoon describing these two processes is presented chart 1.2. The fast process has been assigned to an association-dissociation process (exchange of individual surfactant molecules between micellar aggregates and the

continuous phase) [27, 32] and values for k^+ and k^- have been determined, e.g. by performing T-jump experiments for a number of surfactants [33]. The slow process was attributed to the reestablishment of equilibrium through cooperative condensation or dissolution of surfactant monomers (creation and breakdown of entire micelles). However it is difficult, with data from relaxation experiments alone, to establish the mechanism associated with each rate particularly the one of the slow process [34].

When hydrophobic compounds are solubilised into the micellar core, another type of dynamics becomes important: the exchange of solute molecules between micelles/MEs [35]. In contrary to micelles, MEs contain a dispersed state consisting of domain of nanometer dimension. In addition the interfacial tension in a solution of MEs is very small [35]. Both structures represent a thermodynamically stable state of the respective system. Regarding solute exchange between the aggregates three different mechanisms have been proposed:

- The first one involves the exit of individual solute or surfactant molecules into the aqueous phase and the entry into another droplet. This exit-reentry mechanism (represented by the relaxation rate k^-) becomes dominant when the water solubility of the species is sufficiently high.
- During the second mechanism the exchange of solute proceeds via collision of two micelles, followed by their separation. This collision-exchange-separation process, often called fusion-fission mechanism (and represented by the relaxation rate k_2), has been suggested as the dominant exchange mechanism in nonionic MEs and nonionic surfactant micelles at high concentration or at elevated temperature [35].
- The third possibility for solute exchange involves the fragmentation of a micelle/ME into two sub-aggregates and the subsequent growth into normal micelles/MEs. This fragmentation-growth (represented by the relaxation rate k_{fr}) has been suggested as a mechanism to explain rapid exchange between ionic micelles and MEs at high ionic strength [1].

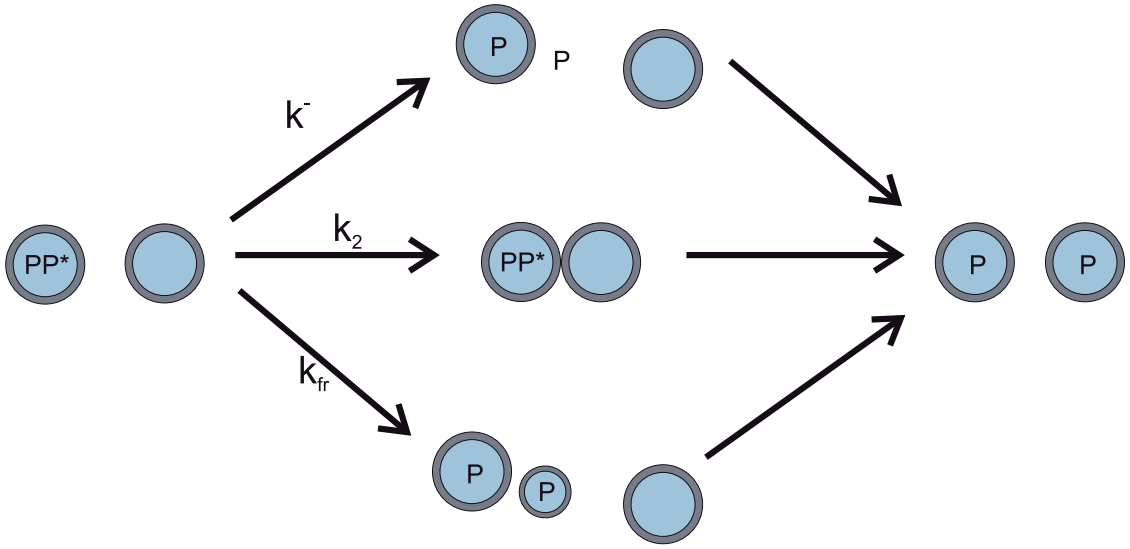

chart 1.3 Three different mechanisms for solute exchange between microemulsions (black circles refer to the surfactant monolayer; the hydrophobic solute is illustrated as gray-colored interior) where P is the fluorescent probe, k^- the exit rate for the probe molecule, k_2 the exchange rate for the fusion-fission mechanism and k_{fr} the exchange rate for the fragmentation-growth mechanism [35]

These three different solute exchange mechanisms are displayed in chart 1.3. The circles refer to the ME (surfactant monolayer: black, solute: gray) and the letter P´s refer to both a generic solute and a pyrene derivative that will give excimer fluorescence (see chapter 2.1.2) from aggregates containing two P molecules. The reaction rates k^-, k_2 and k_{fr} correspond to the exchange processes of the exit-reentry, the fusion-fission and the fragmentation-growth mechanism, respectively. In reaction kinetics, in general, the overall rate of a reaction is controlled by the rate of the slowest step. Depending on the number of participating molecules/aggregates etc. the order of reaction can be determined and from that an eligible fit function is selected. For the exit-reentry and the fragmentation-growth mechanism, only one aggregate is involved in the rate determining step. Therefore first-order kinetics is observed as shown in

equation 1.2

$$y = y_0 + A \cdot exp(-k_{obs} \cdot t)$$

where y is the measured variable as function of the time t, for instance the decreasing excimer intensity, y_0 the offset, A the amplitude of the signal and k_{obs}, the observed

relaxation rate. In many cases a mono-exponential fit function can be employed. The middle path of chart 1.3 will exhibit kinetics second order in ME concentration and can universally be expressed as

equation 1.3

$$y = y_0 + \frac{A}{1 + k_{obs} \cdot t}.$$

In the last 30 years only a limited number of authors presented results to understand the mechanism of the slow relaxation process described in chart 1.2. Hence there is a need to attempt to establish parameters of this process in more quantitative terms. As part of such an attempt, we investigate here O/W-microemulsions applying the stopped-flow technique [36, 37] which is a versatile method to study fast kinetics after a rapid mixing process with a time resolution of down to 1 ms, and has been employed in various studies before [38-44]. Details about the mode of operation are given in the experimental section 2.1.1.

Properties of microemulsion systems are to a large degree determined by the elastic properties of the amphiphilic monolayer [45, 46]. Description of MEs in that context is very simple, "*since, because of their low interfacial tensions, the leading term in the free energy should be given by the bending energy, which can be described in terms of two elastic constants, the mean bending modulus* κ*, and the Gaussian modulus* $\bar{\kappa}$" [47]. Here the influence of the composition, especially the cosurfactant concentration, was found to be of particular interest. In the course of this discussion the interrelation between the observed rate constants of the stopped-flow experiments and the macroscopic interfacial tension will be elucidated.

Multilamellar vesicles

Vesicles are closed amphiphilic bilayers where parts of the solvent is entrapped inside the aggregate and which are often formed in the low-concentration range. In general, vesicles can structurally be subdivided into two main classes. As a first case, they may just be comprised of one single bilayer, as displayed in the chart below and are than referred to as unilamellar vesicles/ ULVs with sizes between $4 - 20$ nm for small unilamellar vesicles /SUV and 50 nm - 10 μm for large unilamellar vesicles/ LUVs (denotation used in this work see chart 1.4). In addition to the first case there exists also the possibility of multilamellar vesicles/ MLVs (see chart below) where one has various concentric shells of vesicles, thus, these phases are also sometimes called 'onion phases' [48]. Vesicles especially from phospholipids (ULVs in this case are often called liposomes) have been investigated widely [10, 49]. They serve as model(s) for membranes and allow therefore studying the basic mechanisms of membrane function. Due to their closed interface they are convenient architectures for encapsulation necessary for pharmaceutical, cosmetic and chemical application.

The kinetic of morphological transitions in amphiphilic systems is important for the understanding of many applications but so far no comprehensive study has been done. The formation of vesicles is not a thermodynamically controlled process. In many cases the final vesicle phase is not in thermodynamic equilibrium but instead long-lived metastable structures are observed. Accordingly the properties of such systems depend strongly in the preparation of the sample and are therefore controlled by the kinetics of their formation process. The knowledge of the dynamics during the formation of the vesicles is crucial to influence the properties of the final state which is especially important in industrial applications.

As already mentioned above, the elastic properties of amphiphilic monolayers and bilayers, as they are typically formed in self-assembling structures, are an important factor in understanding their properties [47] and can be described by a spontaneous curvature c_0 and two elastic constants κ and $\bar{\kappa}$ associated with the mean curvature and the Gaussian curvature, respectively. These parameters are very important in the determination of the structure and phase sequences in surfactant systems, i.e. droplets or sponge-like structures and are interrelated in the harmonic approximation of the

continuum bending free energy, F_b, of a monolayer or bilayer established by Helfrich in 1973 [50]:

equation 1.4

$$F_b = \int dA\left[\left(\frac{\kappa}{2}\right)\cdot\left(c_1 + c_2 - 2c_0\right)^2 + \bar{\kappa}\cdot c_1 \cdot c_2\right]$$

where c_1 and c_2 are the principal curvatures of the amphiphilic film, κ and $\bar{\kappa}$ are the mean and Gaussian bending moduli and A is the surface area. With this approximation one can calculate the energy of the different topologies of a surfactant film and thus determine the most stable structures. The expression for F_b in equation 1.4 is essentially an expansion of the free energy for small curvatures and is correct in the limit of radii of curvatures that are large compared with the thickness of the film [51].

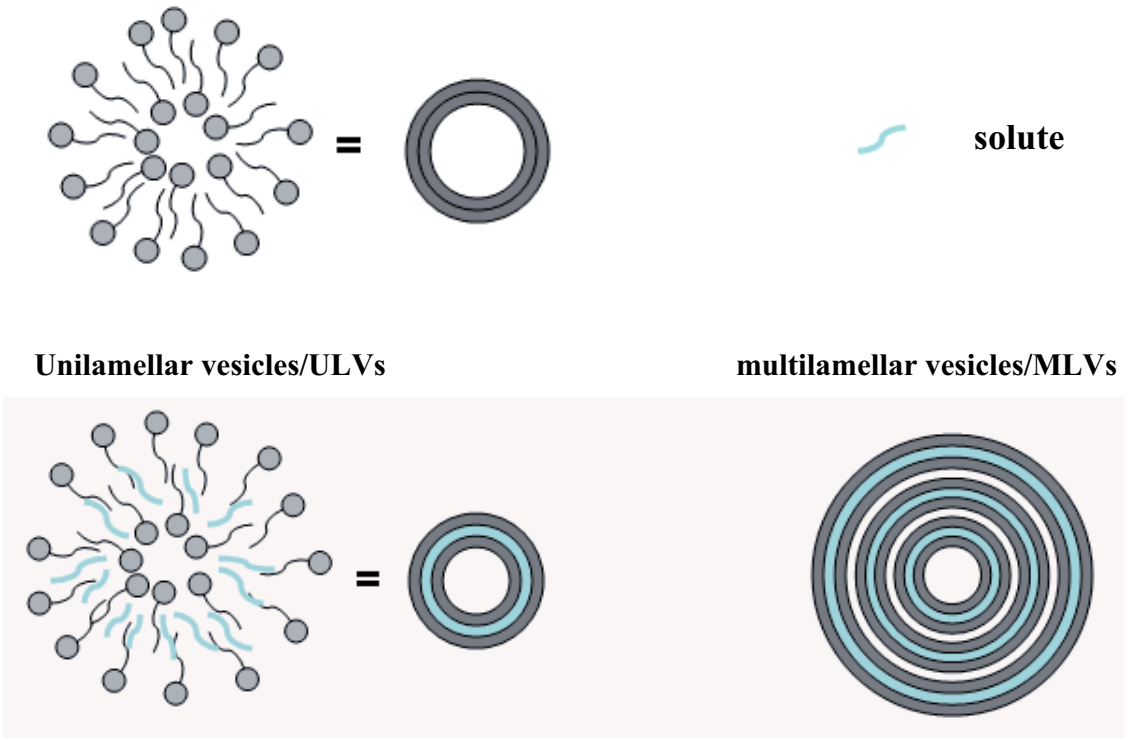

chart 1.4 Illustration of unilamellar and multilamellar vesicles

Depending on the spontaneous curvature of the surfactant monolayer, O/W-MEs are stable for positive c_0 and W/O-MEs for negative values. For the balanced state (phase inversion temperature) of the monolayer, breaking on the emulsion is to be expected [52]. In many droplet microemulsions, the magnitude of c_0 also determines the maximum droplet size (maximum solubilization power [53]. Values for κ are always positive. The second term of equation 1.4 takes into account the fact that the system can change its topology: $\bar{\kappa}$ is negative for lamellar or spherical, whereas positive favours saddle-splay structures as in bicontinuous cubic or sponge phases. Usually F_b is negligible compared to the interfacial tension contribution. However, in ME systems, the interfacial tension is small or even zero and the bending energy becomes a very important term [53].

By means of e.g. neutron spin echo experiments, it is possible to determine values of κ exclusively. However, a combination of data sets of complementary methods is necessary to calculate $\bar{\kappa}$. Therefore, it has been found that the sum of the mean and Gaussian bending modulus for liquid films, $2\kappa + \bar{\kappa}$ can be used to describe the elasticity of an amphiphilic film. Values for $2\kappa + \bar{\kappa}$ can be derived relatively easily e.g. from interfacial tension or SANS measurements. In 1999, Safran has given a nice overview of the field of curvature elasticity that discusses fundamentals, the effects of fluctuations and inhomogenieties and gives a brief review of experimental characterizations on surfactant system [51]. A special task of this work was the comparison of the experimentally obtained values of the sum $2\kappa + \bar{\kappa}$ of the bending constants with the generated phase diagrams in a ternary surfactant system which will be discussed in detail in chapter 6.

Investigated surfactant systems

As amphiphiles, the zwitterionic semipolar surfactant tetradecyldimethylamine oxide (TDMAO) (see chart 1.5) was employed throughout this work to study both kinetic approaches, (a) and (b). The class of alkylamine oxides, with their mesoionic character, shows a behavior between those of typical nonionic and cationic surfactants of identical chain length [54-56]. At ambient temperature TDMAO can serve as a model system for nonionic surfactants with a reasonable solubilisation capacity as it has been reported for the ternary system TDMAO/decane/water [57].

For the formation of microemulsions very often the presence of a cosurfactant is required that lowers the interfacial tension between the oil phase and the water phase which for a pure surfactant often is too high [58, 59]. Cosurfactants like the medium-chain hexanol are amphiphilic compounds of low molecular weight. They are not able to build micellar structures by themselves but, due to their molecular structure, they increase the packing parameter of the surfactant interface, thereby increasing the solubility for hydrophobic compounds significantly.

TDMAO

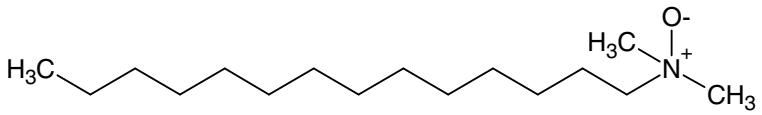

$C_{12}E_5$

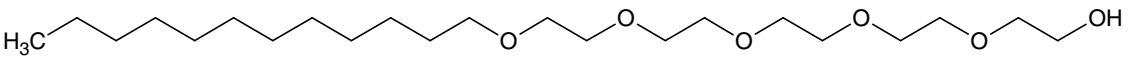

chart 1.5 Structures of both surfactants employed in this work (tetradecyldimethylamine oxide/TDAMO] and penta(ethylene oxide) monododecyl ether/$C_{12}E_5$)

In the quaternary system 100 mM TDMAO/hexanol/decane/water described previously [60] the addition of 1.3 molecules of hexanol per surfactant molecule leads to a reduction of the interfacial tension by a factor of ~ 100, and causes an increase of the solubilisation capacity from 0.35 to 12 molecules of decane per surfactant molecule compared to the ternary system without cosurfactant. In the phase diagram of the quaternary system at constant surfactant concentration is displayed in figure 1.1, where one observes a very extend range of an oil-in-water (O/W) microemulsion (the so-called L_1-phase; blue area) with very different droplet sizes and droplet concentrations, at a given surfactant concentration. In the phase diagram in figure 1.1, beyond the range of the L_1-phase, without the addition of decane and separated by a two-phase region, the isotropic L_α-phase is found (green area). At low hexanol concentration, vesicles ($L_{\alpha l}$-phase)

exhibiting flow-birefringence are present (Pictures of the ternary and quaternary system taken under normal conditions (||) and crossed polarizers (⊥) are presented in figure 1.1). When the hexanol concentration is increased further, this phase will become increasingly birefringent and is now composed of a mixture of vesicles with lamellar chunks ($L_{\alpha h}$-phase). Finally at still higher hexanol concentrations a L_3-phase (sponge phase) is observed. Addition of decane leads to the formation of a liquid crystalline lamellar phase that swells by taking up the oil into the lamellar sheets [61].

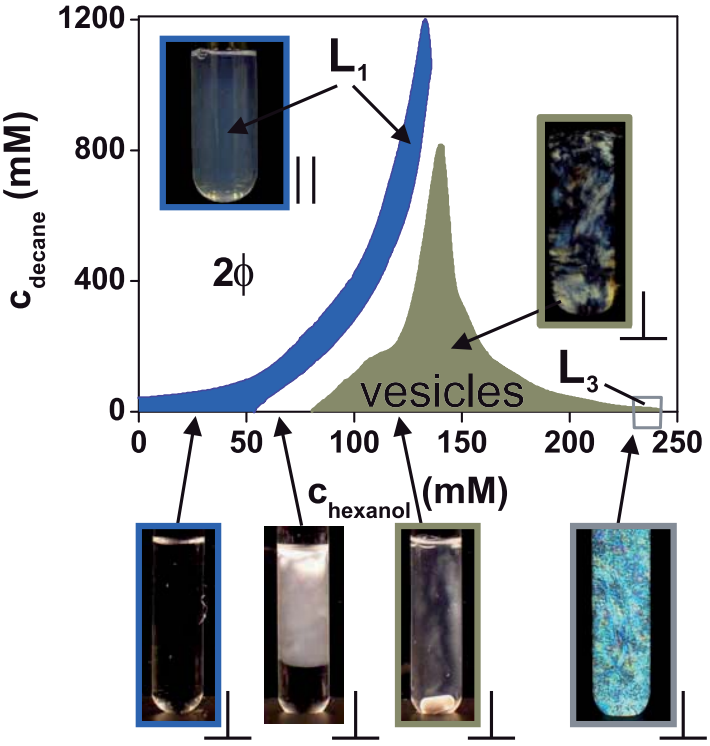

figure 1.1 Phase diagram of the system 100 mM TDMAO/1-hexanol/decane/water [61] at 25 °C. L_1, isotropic O/W microemulsion (blue); vesicles, partially birefringent phase (green); L_3, sponge phase; 2Φ, two-phase region. Picture of the ternary and quaternary system taken under normal conditions (||) and crossed polarizers (⊥). Vesicles in the ternary system (without decane) show flow birefringence

The above mentioned L_1-phase contains ME droplets of spherical shape with a maximum size and perfect sphericity at the upper solubilisation limit (emulsification boundary). This renders this system interesting as it allows following equilibration of microemulsions after mixing two differently sized microemulsions. Therefore

stopped-flow measurements with complementary detection methods (turbidity, fluorescence and SAXS) were performed to monitor the equilibration process in detail. Alternatively one can also follow the exchange of solubilisate in identically composed and sized microemulsions by appropriate methods. For that task stopped-flow fluorescence measurements were conducted. The first approach is in general experimentally more easily done but rather difficult to analyze while the second is experimentally more demanding but simpler to analyze.

However, in order to study the influences of different participations to the experimentally achieved exchange rates, as a pre-condition, the surfactant system at hand should be dilutable at least by a factor of 10. This is not possible in the quaternary system with the amine oxide, whereas it is easily achieved for nonionic surfactants of the poly(ethylene oxide) monoalkyl ether type. Here, ternary MEs with penta(ethylene oxide) monododecyl ether, $C_{12}E_5$ (were i and j denote the length of the alkyl chain and the ethoxy unit respectively) (see chart 1.5) as surfactant proved to be easier for the investigation of solute exchange. The micellar solution was loaded with octane, decane and dodecane and oil-swollen spherical ME at the solubilisation limit were achieved which is a prerequisite to gain reliable information during kinetic measurements.

In both the quaternary and the ternary system, the influences of temperature and the addition of additives, like ionic surfactants and polymers, were tested. This then allows learning how electrostatic interactions and thickness of the amphiphilic film affect these processes. An interesting class of adsorbing polymers consists of the so-called hydrophobically modified (HM) water-soluble polymers, with a water-soluble polymer backbone and covalently bounded hydrophobic side chains [62]. They were found to have considerable impact on the exchange kinetics and a quantitative analysis will be given here.

Concerning the spontaneous formation of multilamellar vesicles, in this work the phase diagrams of four ternary systems with TDMAO as dispersant are presented. As solute, esters of different alkyl chain length were incorporated and the impact of the decreasing polarity on the phase behavior was studied. Due to the symmetric vesicle phase, the ternary system TDMAO/enanthic methyl ester (EME)/water [63] at a constant surfactant concentration of 200 mM, i.e. ~ 5 wt% was employed, and the structural transition from a

mixture of the micellar and microemulsion phase to form a vesicle phase was studied. Furthermore the question of having charged amphiphilic mono- and bilayers present during the process of vesicle formation (as introduced by admixing an ionic surfactant) was addressed. The quantitative results were studied i.e. by stopped-flow measurements with simultaneous detection in turbidity and conductivity mode are presented.

This thesis is structured as follows:

In chapter 3 a comprehensive study will be presented on the exchange dynamics between MEs of a ternary system with $C_{12}E_5$ as surfactant. In addition quantitative information about solubilisate exchange and the equilibration of MEs in the quaternary system TDMAO/1-hexanol/decane/water were obtained and presented in chapter 4.

In the second part of this work the influence of cosurfactants of medium polarity (esters) on the phase behavior of TDMAO in water were investigated. These systems proved most suitable to study the kinetics of morphological transitions, i.e. in this case the formation of multilamellar vesicles, in mesoscopically structured amphiphilic systems. This process has been investigated for various starting conditions and as a function of the charging of the amphiphilic system with advanced time-resolved methods, e.g. stopped-flow DLS and SAXS.

2 Experimental Section

Abstract

The experimental section of this work deals with the techniques that have been used to gain information about the static and dynamic behavior of the surfactant systems investigated. The major part of the results discussed is based on kinetic measurements performed by using the stopped-flow method. The principle of this technique and the different modes used will be discussed in more details. Supplementary information which is important to define kinetic parameters was obtained by means of UV/Vis- and fluorescence spectroscopy and dynamic light scattering (DLS) measurements. For the investigation of the static properties, e.g. phase diagrams, conductivity, rheology, small angle neutron scattering, surface tension and interfacial tension measurements were performed.

2.1 Methods

2.1.1 Stopped-flow method

Experimental setup

Stopped-flow studies were carried out using a Bio-Logic SFM400/S stopped-flow instrument as displayed in chart 2.1. During measurements small volumes of solution are driven from high performance syringes through a high efficiency mixer and the resulting mixture passes through a measurement flow cell (figure 2.1). The flow is abruptly stopped by a shutter triggered electronically, which allows the observation of the mixed system about 1 ms (depending on the flow-rate) after the mixing time. Structural changes in the observed system can be detected by transmission, fluorescence, and conductivity measurements. Additionally we are even able to detect transmission and conductivity

signals simultaneously which allows more reliable information about decisive steps during the kinetic process. In order to obtain more detailed structural information this technique can also be coupled to small-angle x-ray or neutron scattering and even nuclear magnetic resonance spectroscopy (SAXS, SANS, NMR). In order to receive a proper mixing result, the standard berger ball (BB) mixer right before the flow cell can be replaced by a high density (HDS) mixer, which includes an internal siphon-like frame and allows blockage of convection created by density or temperature differences.

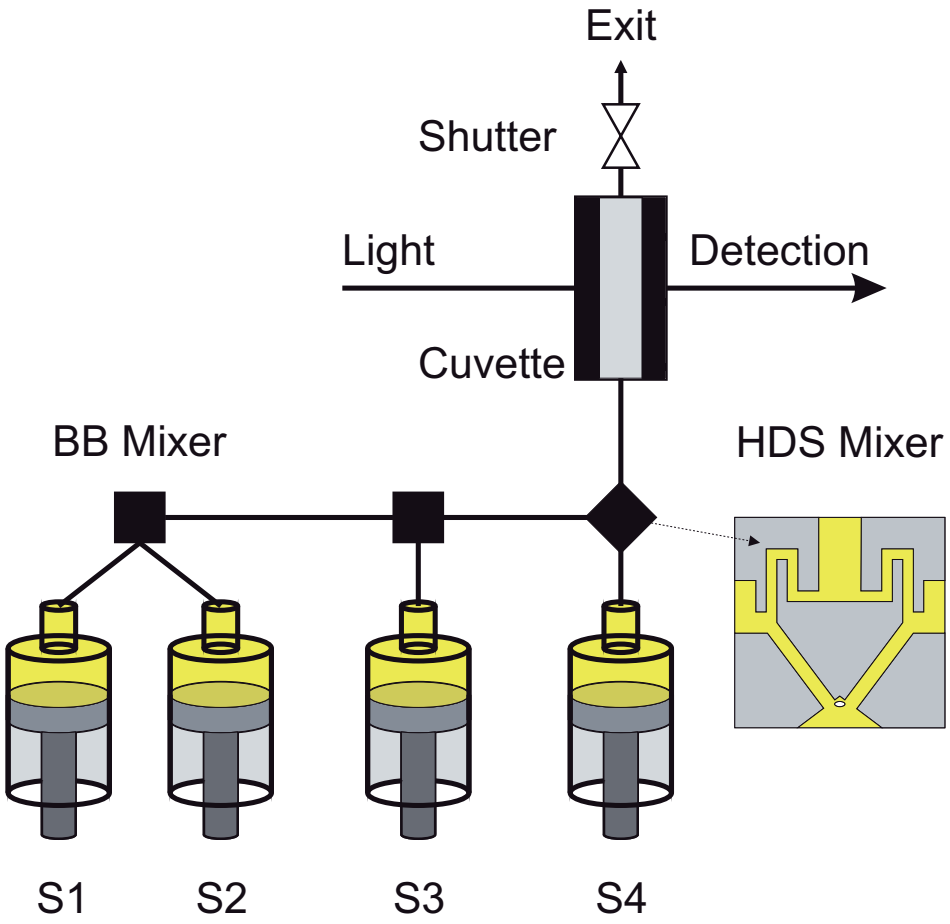

chart 2.1 Schematic diagram of the set-up for stopped-flow experiments (for Bio-logic SFM400/S) with four syringes (S1-S4), Berger ball mixer (BB) and high density mixer (HDS)

Turbidity and fluorescence mode

Most kinetic measurements were performed in turbidity and fluorescence (principle see 2.1.2) mode with the Modular Optical System/MOS-200. As light source served a 150 W Xe(Hg) lamp with shielded lamp house. Light passed through a monochromator for improved signal to noise ratio and stray light rejection and afterwards through the measurement cell (figure 2.1). The size of the exit slit is fixed at 1 mm which corresponds to a 4 nm band pass. The wavelength can be set manually. For transmission measurements the incident wavelength was adjusted to 405 nm; the transmitted light was monitored in 180 ° angle between 180 – 999 nm. In fluorescence mode curves were monitored in 90 ° angle in the range of the emission wavelength λ_{em} = 435 – 999 nm with an excitation wavelength λ_{ex} = 350 nm using a GG435 cut-off filter (ITOS) to eliminate the monomer emission bands. The incident light and the photomultiplier tube is converted into an electrical signal and then digitized by the A/D board in the host microcomputer [64]. Under normal conditions, i.e. a flow rate of 7 ml/s and a total volume of 150 µl, we achieve a dead time of 5.2 ms (which was calculated by division of the dead volume of the mixing path, 36.6 µl by the flow rate).

figure 2.1 Observation head of a SFM400/S stopped-flow device. Inside the head the standard measurement flow cell (fluorescence cuvette: FC-15) with an edge length of 1.5 mm and four transparent sides for measurements in transmission or fluorescence mode is visible. The mixture passes the head from the bottom to the top

Conductivity mode

In our experimental setup we are able to perform turbidity and conductivity measurements simultaneously. In figure 2.2 the setup of the Modular Conductivity System, MCS-200, with additional turbidity components is displayed. At the observation head (cubicle in the middle of the picture) the light source is connected via a standard optical fiber (silvery cable) with the detector (PMT) in 180 ° angle. Perpendicular to that, two cables (red and black) connect the electrodes at the flow cell with the detection unit MSC-200.

figure 2.2 Setup for simultaneous measurements in turbidity and conductivity mode. Observation head with optical fiber (silvery cable) and detector (photo cathode with secondary electron multiplier tube/PMT) in 180 ° angle. Perpendicular cable (red and black) to connect the electrodes at the flow cell with the detection unit

The standard stopped-flow cuvette has been modified with two special electrodes (on opposite sides of the cell) consisting of glassy carbon (a material which is more inert than Platinum and which avoids adhesion of air bubbles on the surface). In this geometrical setup the electrical cell constant k = 8 cm^{-1} (that represents the cell geometry and allows to calculate the universal comparable, specific conductivity with the measured value). The MCS-200 allows to measure steady-state spectra of the impedance of a solution and to follow rapid changes during kinetic measurements. The impedance spectrum yields the real and imaginary part (the former representing the electrical resistance) of the solution as a function of the excitation frequency (see figure 2.3).

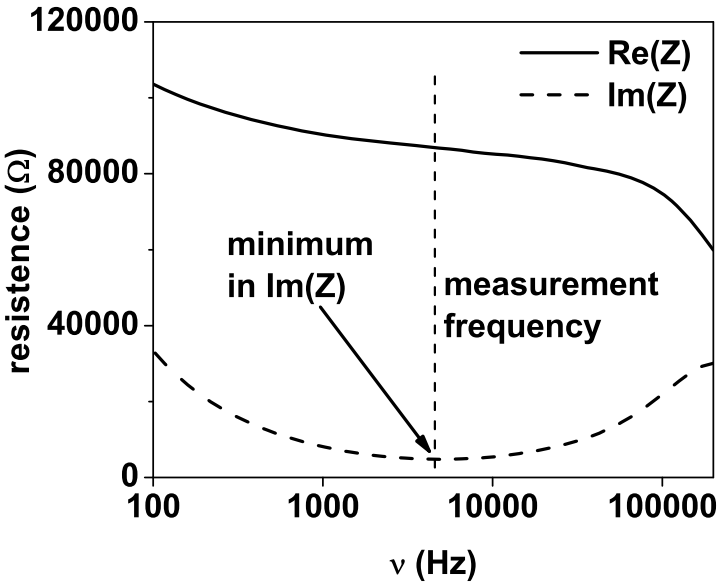

figure 2.3 Typical impedance (Z) spectrum for the final solution of the mixing 199 mM TDMAO/1 mM TTAB 1:1 199 mM TDMAO/1 mM TTAB/ 450 mM EME (at 22 °C; a flow rate of 14 ml/ s and a total volume of 150 µl) in a classic representation (x-axis: frequency in logarithmic scaling; y-axis: real (black) and imaginary part (red) of Z in Ohm (Re(Z), Im(Z)). The dashed line indicates the point where the imaginary part is minimal, which would be optimal for rapid kinetics recordings (optimal frequency here: υ = 4833 kHz)

The spectral mode of the conductometer allows to determine the optimal frequency at which the imaginary part is minimal and the real part does not show a considerable dependency on the frequency. In kinetic mode a high-frequency electrical voltage is

applied to the solution between the electrodes in the cuvette and the resulting current is monitored over time. By means of a Fast-Fourier-Transform technique, real and imaginary part of the complex impedance can be computed at sampling rated up to 200 μs per data point [64].

SAXS mode

Stopped-flow SAXS studies were done using an identical stopped-flow device as for transmission and conductivity measurements which has been specifically adapted for SAXS experiments (principle see [65]). The home-made observation cell of the stopped-flow apparatus was made of a thin-walled quartz capillary with diameter of 1.6 mm and a wall thickness of 10 μm. Mixing was performed at a total flow rate of 6.67 ml/s and a total volume of 600 μl After the mixing sequence, the flow was disrupted with millisecond accuracy using a solenoid driven stopper; and the SAXS-scattering observed for an acquisition time of 12 000 ms. The minimum dead time is defined by the sum of the mixing time (< 0.1 ms) and the time needed for the mixed solution to flow from the mixer to the observation point (< 3 ms). Under normal conditions we achieve a dead time of 2.3 ms. Typically, the data acquisition is triggered at the beginning of the mixing phase, and the total number of frames was determined by the growth kinetics and the SAXS detector used.

Time-resolved SAXS experiments were carried out at the beam line ID02 of the European Synchrotron Radiation Facility (ESRF) in Grenoble, France. Monophasic stock solutions were stored in a thermostatic bath at 25.0 ± 0.1˚C before placing them into the stopped-flow device and mixing them at the same temperature. SAXS-data were recorded using a fiber optically coupled FReLON (Fast-Readout, Low-Noise) Kodak CCD detector, with an input field of 100 mm x 100 mm, a nominal dynamic range of 16 bit, a 4 x 4 binning (resolution 512 x 512) and a read out rate of 5 frames/sec, reducing the dead time of 80 ms between each frame while using the fast shutter. The wavelength was kept at 1 Å (FWHM 0.015%) and a sample-to-detector distance of 10 m to cover the range of scattering vector $q = 0.0085 – 0.5$ nm^{-1}, where θ is the scattering angle. Additional static (for the initial and final states) measurements were acquired at exposure

times of 5 and 2 ms, respectively. The measured SAXS-intensities were normalized to an absolute scale using standard procedure described elsewhere [66]. The normalized two-dimensional SAXS patterns were azimuthally averaged to obtain the scattering intensity as a function of q. The corresponding background intensity of the stopped-flow cell filled with water was subsequently subtracted. The resulted background subtracted scattered intensity is denoted by I(q).

DLS mode

We were also able to combine the stopped-flow with a dynamic light scattering DLS setup. Here, the change of particle radii and of sample dynamics can be followed in time. The laboratory-built DLS setup adapted to the stopped-flow system is shown in figure 2.4.

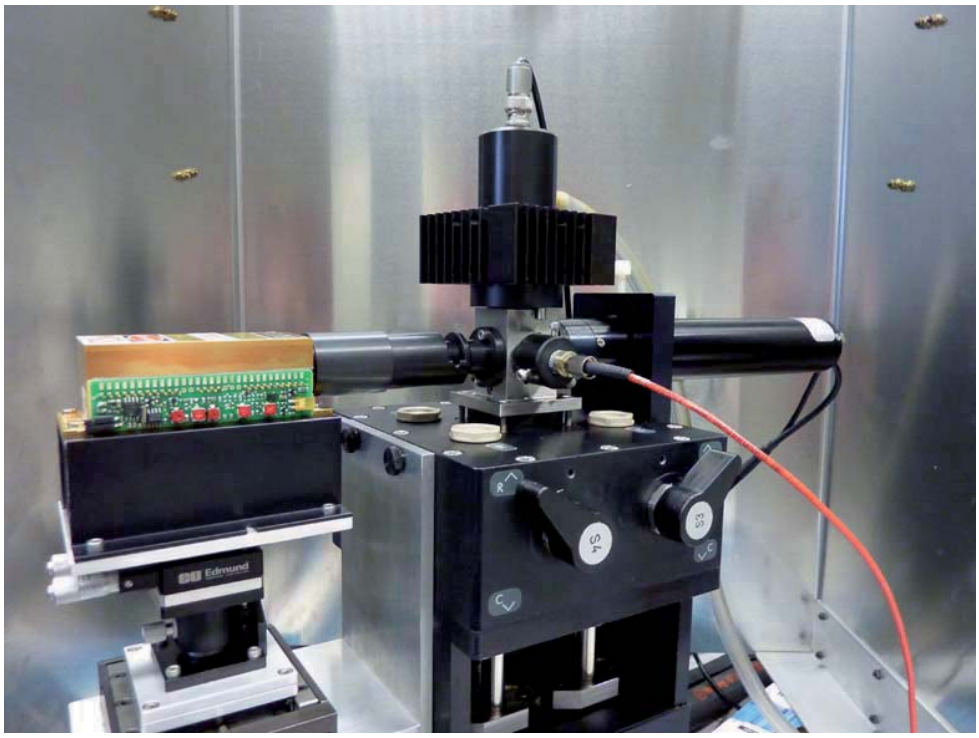

figure 2.4 Setup for simultaneous measurements in turbidity and DLS mode. Left side: 20 mW Laser (Compass 215M-20) with detector in 90 ° angle (red cable). Right side: PMT in 180 ° angle to light source for detection of the transmission

It consists mainly of a diode-pumped Nd:YAG laser (Compass™ 215M CWGreen Lasers, Coherent) operating at λ = 532 nm and at 20 mW output power and a single high resolution real time MT-64 multiple tau digital correlator (Flex02-01D/C, Correlator) that calculates the homodyne autocorrelation function g2(τ). The Laser beam was aligned perpendicular to the cell wall (in this case we have chosen the standard stopped-flow cell FC-15). Scattering vector was 90 °. An avalanche photo diode with fiber connection (60 FC-0-M8-33, Schäfter + Kirchhoff) detects the photons that are correlated in the hardware correlator. Because of statistical and software reasons the shortest measurement time was 1s.

2.1.2 Fluorescence spectroscopy

In fluorescence spectroscopy a species is first excited by photons from a beam of light, usually ultraviolet light, from its ground electronic state to one of the various vibrational states in the excited electronic state. Due to collisions with other molecules, the excited species loses vibrational energy until it reaches the lowest vibrational state of the present excited electronic state. The electron then relaxes back to the ground state thereby emitting light of longer wavelength than that of the initial light. A special kind of fluorescence is the formation of excimers (excited dimmers). They are formed between two (identical) atoms or molecules that would not bond if they were in the ground state. The lifetime of excimers is only in the order of nanoseconds. A prominent molecule is pyrene whose molecular structure is symmetric so that conclusions about the micro-polarity of the surrounding medium from the ratio of the monomer intensities can be drawn.

Steady-state fluorescence measurements were carried out with a Hitachi fluorescence spectrophotometer (F-4500). The intensity was kept below 10^6 counts/s to maintain the linearity of the detector response. For emission spectra, λ_{ex} = 350 nm, whereas excitation spectra were obtained for both λ_{em} = 378 nm (monomer) and λ_{em} = 470 nm (excimer).

2.1.3 Scattering methods

Scattering methods are essential tools in the characterization of polymers, colloids and interfaces. When radiation interacts with a sample either scattering or absorption occurs. The first case can be divided in elastic (static) and inelastic scattering methods; in the former case there is no energy exchange. Static light and small angle neutron scattering (SLS and SANS) are elastic methods and they monitor the time averaged scattering intensity. Dynamic light scattering and neutron spin-echo spectroscopy are inelastic scattering methods and analyze the energy transfer between sample and the incoming radiation. The most important quantity evaluating scattering experiments is the magnitude of the so-called scattering vector, q, given by:

equation 2.1

$$q = \frac{4\pi}{\lambda} \cdot sin\frac{\theta}{2}$$

where λ is the wavelength of the incident radiation (e.g. neutrons or light) in the scattering medium and θ the scattering angle. The scattering vector is the reciprocal length of the radiation applied to the sample. By adjusting q, the spatial resolution can be chosen depending on range that has to be investigated; using Bragg's law we can associate to each q value a characteristic length scale $s = 2\cdot\pi/q$. Therefore, at low q information about the overall size and shape of molecules or aggregates can be gained. At high q the internal structure and the interface of the scatterer can be studied. SLS and DLS are well suited to study the overall particle size and shape of large objects. Because of the shorter wavelength, SANS and neutron spin echo/NSE can be utilized to study the internal structure of e.g. polymers or colloids in detail. In the following sections a brief introduction to the principles used in this work is given.

2.1.3.1 Dynamic light scattering

In DLS experiments monochromatic, coherent light sources (laser) with a wavelength bigger than the diameter of the particles investigated are used. In that case

time-dependent fluctuations of the light are observed that are due to the small particles in solution undergoing Brownian motion. From the intensity fluctuations the second order autocorrelation curve at a certain delay time τ can be derived:

equation 2.2

$$g_T^2(q;\tau) = \frac{\langle I(t)I(t+\tau)\rangle + \langle I(t)\rangle^2}{\langle I(t)\rangle^2}$$

Values of I(t) and I(t + τ) are correlated for smaller τ but this correlation is lost as τ becomes large with the period of fluctuations [67]. In the first case $g_T^2(q;\tau) = \langle I(t)^2\rangle / \langle I(t)\rangle^2 + 1$ and $g_T^2(q;0) > 1$, in the second case $g_T^2(q;\infty) = 1$. Therefore a continuous decay of $g_T^2(q;\tau)$ to 1 can be observed.

For an ergodic medium the time-averaged autocorrelation function is equivalent to the ensemble average in the course of an experiment of the duration T and becomes valid.

equation 2.3

$$g_T^2(q;\tau) = g_E^2(q;\tau)$$

The time-averaged autocorrelation function is than related to the normalized ensemble-averaged autocorrelation function by the Siegert relationship [68]:

equation 2.4

$$g_E^2(q;\tau) = 1 + c\left[g^1(q;\tau)\right]^2$$

where c is a baseline parameter that is proportional to the ratio of coherent area to detector area. In many applications the autocorrelation function decays like a single exponential a is represented by

equation 2.5

$$g^1(q;\tau) = exp(-\Gamma\tau)$$

with the decay rate $\Gamma = Dq^2$, D being the translational diffusion coefficient and hence the one meaningful parameter characterizing the sample. Usually, samples are polydisperse and the evolution of $g^1(q;\tau)$ must be described by a weighted sum of

exponentials. From the mean value $\overline{\Gamma}$ and under certain experimental conditions, e.g. sphericity of the particles, low-concentration rage, non-interacting particles etc., the hydrodynamic radius, R_H, of the aggregates in solution can be derived from Stoke´s equation

equation 2.6

$$D = \frac{kT}{6\pi\eta R_H}$$

where k is the Boltzmann constant, T the temperature, η the viscosity of the solvent.

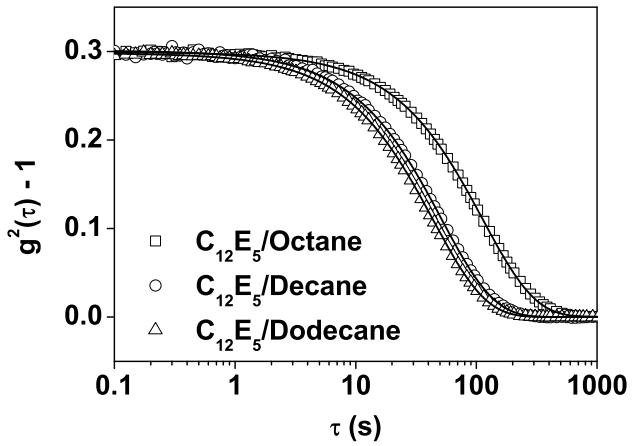

figure 2.5 (Normalized intensity autocorrelation functions – 1) of three ternary MEs (squares: 56.98 mM $C_{12}E_5$/275.5 mM Octane; circles: 60.13 mM $C_{12}E_5$/161.02 mM decane; triangles: 78.02 mM $C_{12}E_5$/134.68 mM decane). From the corresponding mono-exponential fit hydrodynamic radii of 12.3, 8.80 and 7.49 nm where calculated. It is clearly visible, that $[g^{(2)}(\tau) - 1]$ decreases faster, the smaller the ME droplets

For the dynamic light scattering experiments (DLS) we used a ALV/ CGS-3 Compact Goniometer System with a He-Ne–laser (λ_{ex} = 632.8 nm). Measurements were done at a scattering angle of 90 ° and a temperature of 25 °C controlled by a thermostated toluene bath. The data were analyzed with the program ALV-7004 version 3.0, which does an inverse Laplace transformation using a constrained regularization method, and thereby yielding a relaxation spectrum of the autocorrelation function. Details of this method are described in [69].

2.1.3.2 Small angle scattering

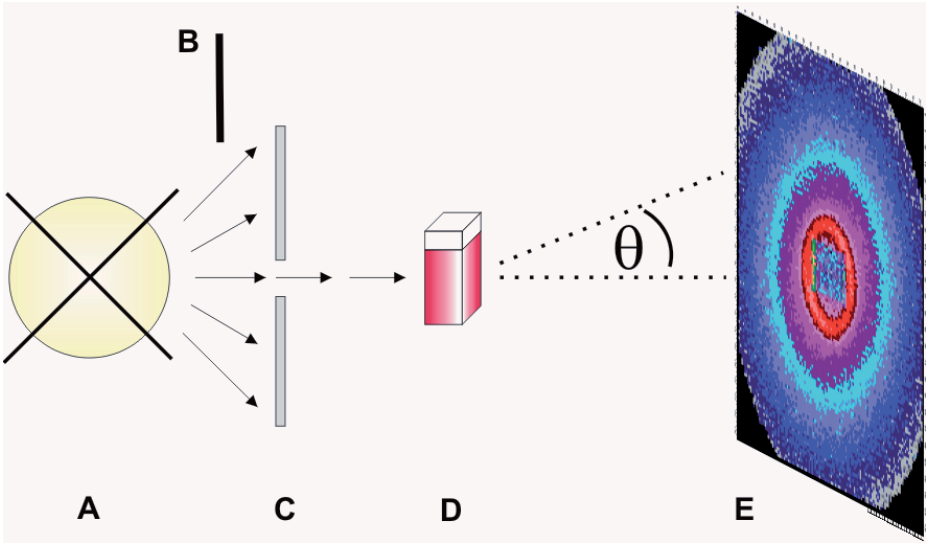

chart 2.2 General setup for small-angle scattering technique with A = radiation source, B = monochromator, C = aperture, D = sample, E = detector and θ = scattering angle

Small angle scattering (SAS) is a collective name including small angle neutron (SANS), X-ray (SAXS) and light (SALS) scattering. We will discuss the first two techniques, as they where utilized in this work, in more detail below.

In chart 2.2 the general set-up for scattering experiments with neutrons or X-rays is displayed. Independent of the radiation used, a monochromatic, collimated beam is directed at a sample. Radiation is then elastically scattered by a sample and recorded at very low angles (typically 0.01 - 30 °). Hence, according to the reciprocity law these methods are most suited to study particles with colloidal dimensions (1 - 100 nm). The fundamental difference of both techniques is the mechanism by which the incident radiation interacts with the sample. X-rays have a charge which will interact with the orbital electrons of the sample.

As a consequence, in the case of X-rays the scattering cross-section increases proportionally to the number of electrons, i.e. to the atomic number. Neutrons are neutral particles and are therefore unaffected by the charge of the orbital electrons but interact with the nucleus of the atom. Accordingly a neutron with the wavelength of 0.15 nm has

an energy of 34.6 meV, whereas the energy of a X-ray photon of the same wavelength is 200 000 times greater (calculated from equation 2.7 and equation 2.8 respectively).

equation 2.7

$$E_n = \frac{p^2}{2m_n} = \frac{(\hbar \cdot k`)^2}{2m_n}$$

(E_n: energy of a neutron, p: momentum, $\hbar$: reduced Planck constant, k`: wave vector, m_n: mass of the neutron)

equation 2.8

$$E_X = h \cdot \nu = h \cdot \frac{c}{\lambda}$$

(E_X: energy of a X-ray photon, h: Planck constant, c: speed of light, λ: wavelength of the photons)

Hence, X-ray radiation can result in radiative heating of the sample and can easily bring about serious molecular degradation [70] which has to be considered especially for biological applications. The strength of the neutron interactions varies in an apparently unpredictable way with the atomic number and is not even identical for isotopes of the same elements. The most significant isotopic variation appears for hydrogen and deuterium. So, unlike X-rays, neutrons can differentiate between them. As many applications occur in water, the isotopic substitution in the solvent is the essential property in planning structure analysis (contrast matching conditions, etc.).

For both methods the resulting scattering pattern is analyzed to provide information about the size, shape and orientation of some components of the sample containing inhomogeneities in the nm-range. SAS techniques are widely used to study polymers, biological molecules, nanoparticles, micelles and microemulsions, etc. The decisive factors about what sample can be investigated and which information can be gained, are strongly depending on the type of radiation used in the SAS experiment. For many applications these techniques are complementary.

In the following the principles of SANS and SAXS will be discussed in further detail and with respect to the parameter and information that we wanted to extract from our data.

Small angle neutron scattering

Neutrons interact with the nucleus of the atom via the strong nuclear force. Since its interaction probability is small, it offers the advantage of deep penetration making it a unique tool for investigating bulk condensed matter. There are two ways of producing neutrons in sufficient quantity. The majority of scientific facilities for SANS use nuclear reactors, the others spallation neutron sources. For detection, in many cases gas proportional and scintillation neutron detectors are used. The resulting SANS pattern are treated following a regular procedure to account for the electronic noise, the detector efficiency and the scattering from the empty cell. In this work the corrected curves were initially analyzed using a model-free analysis as described in detail in chapter 6 to evaluate the validity of the data (by comparing the theoretical and experimental invariant) and to gain information about the particle size (intensity at low q) and shape (surface-to-volume ratio) and potential interactions (Guinier-radii at low- and mid-q-range).

Chapter 3 and 4 in this work deal with the kinetic of solubilisate exchange between MEs. Therefore most SANS measurements were performed verifying spherical shape of the ME samples which is a prerequisite to gain reliable information during kinetic measurements as already mentioned above. In figure 2.6, SANS curves of three MEs with TDMAO as dispersant are displayed. Due to the packing parameter of TDMAO, in the binary system of 100 mM surfactant (in D_2O) cylindrical micelles are present (black curve). Addition of 35 mM decane, gives oil-swollen, dilute MEs of spherical shape (magenta curve). By adding hexanol as cosurfactant, the packing parameter will be changes and up to 1200 mM decane can be incorporated into the ME. The scattering curve of such a concentrated, spherical ME is presented as olive curve in figure 2.6. In the mid-q range a pronounced minimum, indicating low polydispersity, is visible and the particle size can be estimated by calculating π/q. At low scattering vector, a distinct decrease in the intensity is observed which can be attributed to the presence of repulsive interactions (due to the increased size) between ME aggregates. Combining information about the sizes/shape of and the interactions between the particles from the model-free analysis are crucial to select the appropriate model which will then be employed to fit the experimental data.

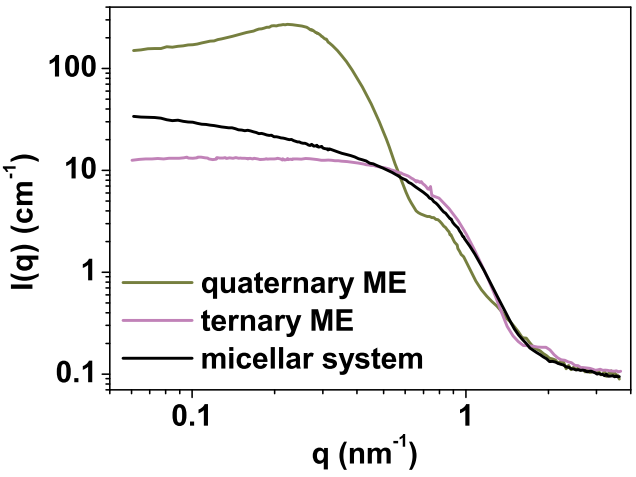

figure 2.6 Static SANS spectra of MEs with different shape; black: cylindrical, dilute ME (100 mM TDMAO/D_2O); pink: dilute, spherical ME (100 mM TDMAO/n-decane/D_2O); olive: concentrated, spherical ME (100 mM TDMAO/1-hexanol/n-decane/D_2O) with low polydispersity and repulsive interactions

The small-angle neutron scattering (SANS) experiments in chapter 4 were performed at the instrument NG7, NIST, Gaithersburg (USA), in chapter 6 at V4 (BERII reactor) at the Helmholtz-Zentrum Berlin für Materialien und Energie, Lise-Meitner Campus, Berlin, and KWS2 of the Forschungs-Neutronenquelle Heinz Meier-Leibnitz (FRMII, Munich, Germany). The detailed description of the experimental parameter and the data treatment can be found in the experimental section of the corresponding chapters.

Small angle X-ray scattering

Small angle X-ray scattering (SAXS) techniques use short wavelength radiation to gain information about the averaged particle sizes or shapes of a sample which can contain solid, liquid or gaseous domains. In this method, an X-ray photon, as an electromagnetic wave, interacts (weakly) with the charge of the orbital electrons in the sample. Thus X-rays can penetrate matter (e.g. a few millimeter of aluminium) as well as neutron but not as deep as the latter.

In order to receive reliable information from SAXS spectra several pre-conditions must be fulfilled: (1) X-rays must `see` a contrast, i.e. particles investigated must have an electron density different from that of the matrix (e.g. the solvent); (2) the energy loss of the initial radiation must be kept as low as possible. Apart from the scattered light, a certain fraction of X-rays will be absorbed by the sample and transformed into other forms of energy (heat, fluorescence radiation etc.). In order to increase the quality of the SAXS data the absorption must kept small by choosing the optimal sample thickness d, which is the reciprocal value of the absorption coefficient μ. Another fraction of the incident X-ray radiation will be lost by Compton scattering (incoherent scattering) when the photon of the beam hits an electron inside the sample and is bounced away thereby loosing fraction of its energy, which is take over by the electron. The emitted radiation has a different wavelength and contains no structural information of the sample. The SAXS data can be improved by correct subtraction of the featureless background radiation. (3) The particle sizes should be as monodisperse as possible as the signal strength is related to the squares volume of the particle [71].

2.1.4 Zero-shear viscosity measurements

The viscosity in the Newtonian regime is called the zero shear viscosity η where the shear rate is proportional to the stress rate. The zero shear viscosity gives valuable information on the molar mass, e.g. for polymer solutions, or shape, e.g. micelles and microemulsions.

For the determination of the zero shear viscosity an Ubbelohde viscometer and micro Ubbelohde viscometer were used. The flow time was automatically determined with a mgw-Lauda viscoboy 2 and the average out of three measurements was corrected according to Hagenbach depending on the type of the capillary.

2.1.5 Interfacial tension measurements

Interfacial tensions were determined from spinning drop measurements using a spinning drop tensiometer SITE (Krüss, Germany). The spinning drop tensiometer is based on the theory derived by Vonnegut [72]. A glass capillary is filled with a dense fluid, the pure surfactant solution, placed horizontally and equilibrated at 25 °C for 10 min under rotation at ~ 1000 rpm. One drop (V ≈ 6 µl) of the less dense fluid, the ester, is placed in the middle of the capillary via glass syringe. The rotational speed was increased to 2000 - 4000 rpm until macroscopic droplets of cylindrical shape were observed in the middle of the capillary. After an initial waiting time of 10 min, when the shape of the droplet is determined by the balance between interfacial (~γ/d; where d is the thickness of the droplet) and centrifugal ($\sim \Delta\rho \cdot \omega^2 \cdot d^2$) forces, the thickness of the droplet was measured every 10 min for five times to ensure stable values over one hour. The interfacial tension was calculated according to the following approximation:

equation 2.9

$$\gamma = a` \cdot d^3 \cdot \omega^2 \cdot \Delta\rho$$

from the average value of the diameter d at a rotational speed ω and a given density difference Δρ. The constant a` ($1.237 \cdot 10^{-8}$) corresponds to the correction term for the conversion of the units and the optical amplification [73].

2.1.6 Surface tension measurements

The energy required to expand the interface (under constant temperature and pressure) is called surface tension, γ. Water hat a value of γ ~ 72 mN/m. Compounds that are able to lower the interfacial tension to at least 30 mN/m are called surface active agents, surfactants. In figure 2.7 (filled squares) the typical development of γ with successive addition of TDMAO is displayed. At very low surfactant concentration TDMAO molecules accumulates and γ decreases slowly until the water-air-interface is saturated

(~ 10^{-4} mol/l in the figure 2.7 below). The surface tension keeps constant and micelles, as a new phase, are formed. The intersection point of the linear fits of the data before and after that concentration is the critical micellar concentration, cmc, which is a characteristic value of each surfactant. Impurities in the solution will lead to divergence of the ideal slope (figure 2.7; crossed circles). In that case the purification procedure of the surfactant has to be repeated.

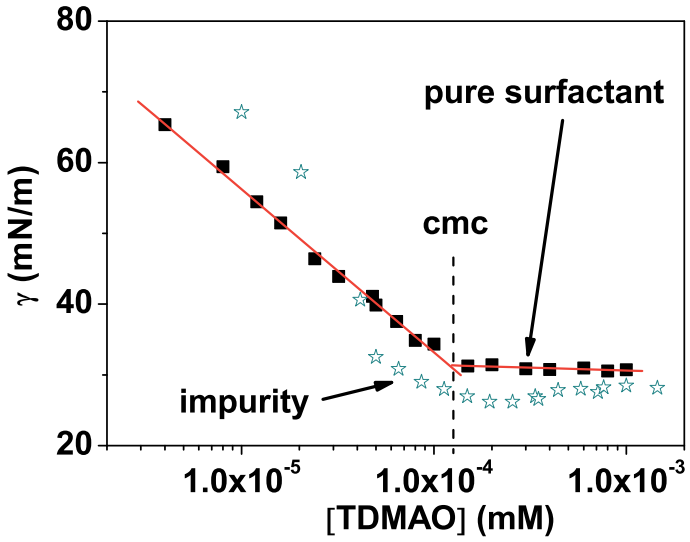

figure 2.7 Surface tension of synthesized TDMAO in water as a function of concentration of the surfactant measured at 25 °C; squares: pure surfactant, crossed circles: sample with impurities; red lines denote the linear fits, the concentration at the point of intersection is the critical micellar concentration (cmc)

For surface tension measurements a Krüss Digital Tensiometer (K10ST) with a thermostated vessel was employed. Values of were derived by applying the deNoüy Ring method where the maximum pull on a platinum ring by the surface is measured.

2.1.7 Conductivity measurements

Electric conductivity was measured with a 712 Conductometer from Metrohm operating at a constant frequency of 300 Hz ($\kappa < 200$ µS/cm) or 2.4 kHz ($\kappa > 200$ µS/cm) which was chosen automatically. As sensor a separate double Pt-sheet electrode (Metrohm, 0.15 × 8 × 8 mm) was employed. The electrical conductivity κ depends greatly on the temperature. Therefore all conductivity values measured where corrected by a temperature coefficient and recalculated according to equation 2.10.

equation 2.10

$$\kappa = \frac{\kappa_{exp}}{1 + \frac{\alpha}{100}\left(T_{exp} - T_{Ref}\right)}$$

2.1.8 Rheology

Rheological measurements were performed with a Gemini 200 HR rheometer from Malvern Instruments GmbH. The measurements were carried out with plate-plate geometry (∅ = 40 mm) and a gap size of 0.15 mm was used. To determine the linear viscoelastic area an amplitude sweep was performed and from that a deformation of 0.04 for the sample with EME and 0.01 for the one with PME was taken to perform the frequency sweep in controlled strain mode.

2.1.9 NMR-spectroscopy

Nuclear magnetic resonance (NMR) spectroscopy is the most important spectroscopic method for structure determination of organic and metal-organic compounds. In addition it is a powerful tool to determine physical and chemical properties of atoms and molecules, therefore providing detailed information about dynamics, reaction state and chemical environment. NMR relies on adsorption of electromagnetic radiation (radio waves) at the resonance (Larmor precession rate) frequency of the NMR active nuclei with a spin $I_S \neq 0$ (e.g. ^{2}H, ^{13}C, ^{14}N, ^{19}F). Its Larmor frequency can be determined either at constant magnetic field or through variation of the frequency of the alternating electrical field.

Modern NMR spectrometers consists of an extremely stable and homogeneous magnetic field (B_0) of $1 - 20$ T (tesla) and coils introducing the electrical field perpendicular to B_0. During measurement, the sample placed in a thin-walled glass tube is kept rotating around its vertical axis to diminish inhomogenities of the field to improve the quality of the spectra. Depending on the local chemical environment, different NMR active nuclei (e.g. protons in ^{1}H-NMR or carbon atoms in ^{13}C-NMR spectroscopy) resonate at slightly different frequencies. Both frequency shift and resonance frequency are proportional to the strength of the magnetic field. Therefore the shift is converted into a field-independent dimensionless value called the chemical shift. Finally, in the simplest case of an ^{1}H-NMR or ^{13}C-NMR spectrum, chemical shifts of the isotopes are compared to tabulated values and together with the ratio of signal intensities, the structure of an unknown compound can be gained.

^{1}H-NMR spectra were taken with a Bruker AC 200 MHz spectrometer. $CDCl_3$ was used as solvent.

2.2 Materials and preparation methods

The nonionic surfactant $C_{12}E_5$ was a chromatographically pure sample supplied by Nikkol and used as received. Tetradecyltrimethylammonium bromide (DTAB, $C_{12}H_{29}N(CH_3)_3Br$) (99%) was obtained from Sigma Aldrich and used as supplied. Tetradecyldimethylamine oxide (TDMAO, $C_{14}H_{29}N(CH_3)_2O$) was obtained from Julius Hoesch (Düren, Aromox14D-W970, 24 - 26%) as a gift. The solutions were freeze-dried until the amount of water reached a value of 2.5 wt% which was determined via Karl-Fischer-Titration. It was checked by surface tensions measurements that the cmc agreed with the literature value of 0.12 - 0.14 mM [74]. Tetradecyltrimethylammonium bromide (TTAB, $C_{14}H_{29}N(CH_3)_3Br$) (99%) was obtained from Sigma Aldrich. All esters, valerian methyl ester (VME), capronic methyl ester (CME), enanthic methyl ester (EME), and pelargonic methyl ester (PME) were purchased from Fluka in p. A. quality and used without further purification. Some relevant properties of the esters are summarized in table 2.1.

As amphiphilic polymers dioleyl- and distearyl-polyethyleneoxide compounds (R-EO_x-R) Antil and Rewopal with a length of the polyethylene oxide (EO) part of x = 55 (Antil) or 150 (Rewopal) were employed. Antil® 141 Liquid (Antil) and REWOPAL® PEG 6000 DS (Rewopal) were received as a gift from Evonik with a distribution of the length of the polyethylene unit with x being the average degree of polymerization and used as received.

The fluorescent probe pyrene butyric acid stearyl ester (see chart 2.3) was synthesized using a standard procedure by reacting 0.50 g (1.73 mM) pyrene butyric acid with 0.46 g (1.73 mM) stearyl alcohol in presence of 0.72 g (3.47 mM) dicyclohexyl-carbodiimide in 20 ml dichloromethane. The mixture was stirred for 3 days at 38 °C. Column chromatography on silica gel and recrystallization in ethanol (2 times) gave the pure product with 26% yield. ^{1}H-NMR ($CDCl_3$): 0.875 (t, 3H, -CH_3), 1.235 (m, 30 H, Alkyl-CH_2), 1.628 (m, 2H, O-CH_2-CH_2-), 2.194 (m, 2H, Ar-CH_2-CH_2-), 2.459 (t, 2H, -CH_2-CO-), 3.395 (t, 2H, Ar-CH_2-), 4.079 (-O-CH_2-), 7.842-8.333 (m, 9H, Ar).

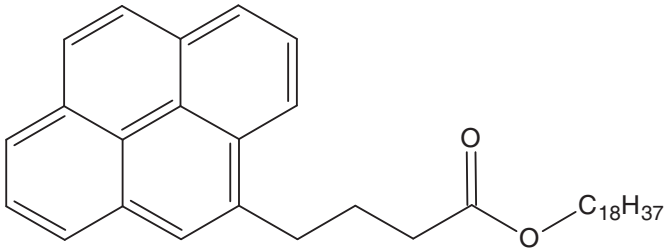

chart 2.3 Structure of the fluorescent dye pyrene butyric acid stearyl ester

For SANS measurements D_2O of 99.9% isotopic purity was obtained from Euriso-top. Scattering length densities of $6.36 \cdot 10^{-4}$ nm^{-2} for D_2O, $-0.195 \cdot 10^{-4}$ nm^{-2} for TDMAO, $-0.488 \cdot 10^{-4}$ nm^{-2} for decane und $-0.327 \cdot 10^{-4}$ nm^{-2} for hexanol were employed, respectively. For all samples not prepared with heavy water millipore water was used.

table 2.1 Solubility in water, density and scattering density of employed esters at 25 °C

	molar mass ($g \cdot mol^{-1}$)	**solubility in water[75] ($mg \cdot l^{-1}$)**	**density ($g \cdot cm^{-3}$)**	**SLD [10^{-4} nm^{-2}]**
VME	116.16	5060	0.88507	0.303
CME	130.18	1330	0.87970	0.235
EME	144.21	309	0.87569	0.181
PME	172.26	23	0.87017	0.107

All microemulsions of the ternary system $C_{12}E_5$/oil/water contained 57 - 78 mM surfactant and were diluted down to 1:10 with water were necessary. The samples were prepared by taking the required amount of surfactant and oil. Water was added to achieve the final concentration. The samples were heated to the lamellar phase under vigorous stirring. After cooling down to the two-phase region (ME with oil-excess phase) the samples were kept for equilibration in a thermostated oven at 25 °C until used for measurements. The polymer/ ionic surfactant containing microemulsions were prepared by mixing weighed amounts of microemulsions with varying amounts of polymers/ ionic surfactant and stirring the mixtures at 25 °C for several hours to ensure complete dissolution of the additive.

All microemulsion samples in the quaternary system with TDMAO/1-hexanol/ n-decane/water contained 100 mM (~ 2.6 wt%) surfactant. The samples were prepared by taking the required amount of a stock solution of 120 mM of surfactant. The appropriate amount of cosurfactant, oil, ionic surfactant and water was added to achieve the final concentration. After homogenizing with a vortex mixer the samples were kept for equilibration in a thermostated oven at 25 °C until used for measurements. The polymer containing microemulsions were prepared by mixing weighed amounts of microemulsions with varying amounts of polymers and stirring the mixtures at 25 °C for several hours to ensure complete dissolution of the additive.

All microemulsion samples contained 200 mM surfactant. The samples were prepared by adding a stock solution of 210 mM of surfactant to the required amount of ester, ionic surfactant and water was added to achieve the final concentration. After homogenizing with a vortex mixer the samples were kept for equilibration in a water bath at 25 °C.

3 The kinetics of solubilisate exchange in a nonionic surfactant system - correlation of measured rates with interfacial rigidity, charge and addition of polymer

Graphical Abstract

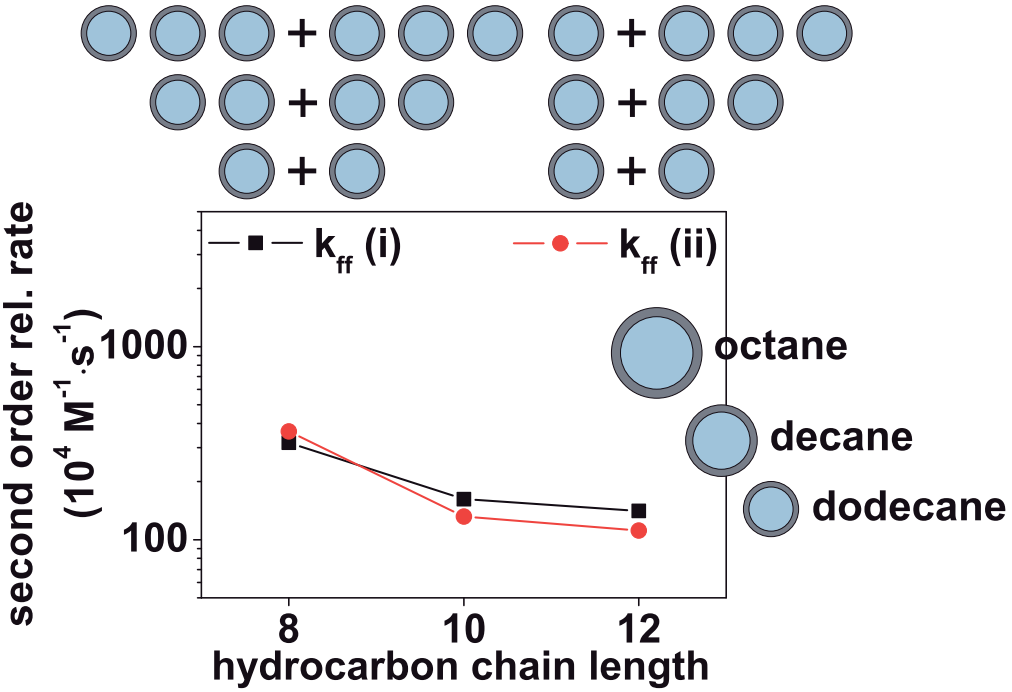

Abstract

In this chapter it is shown that the increase of the oil exchange rate constant, determined from a stopped flow kinetic study, and of the surfactant concentration of the ternary system $C_{12}E_5$/oil/water are directly related. The decrease of the excimer intensity during the mixing of microemulsions with octane, decane and dodecane was monitored. The observed coalescence rate at the solubilisation boundary depends linearly on the concentration of surfactant and of the microemulsion aggregates for the 1:1 mixing of microemulsions of the same concentration of droplets. Coalescence rates were obtained for a second mixing process, where the concentration of one solution was increased steadily. The exchange of oil is much faster for the bigger aggregates with octane than for the smaller ones with decane and dodecane. As the sum of the bending constant is identical for all three microemulsions, the difference can be explained by the higher curvature of the smaller aggregates with dodecane. Coalescence rates calculated from both mixing steps were identical under appropriate data treatment.

In addition we investigated the influence of additives, hydrophobically-modified polymers and cationic surfactant, on the kinetic. The polymer with the longer hydrophilic mid-block (150 ethoxy units) shows a much bigger effect of slowing down oil exchange than the shorter one (55 ethoxy units), apparently due to the enhanced steric hindrance. Much more pronounced is still the effect of introducing charge into the surfactant monolayer of the microemulsion and already 2-3 mol& ionic surfactant effectively slows down the coalescence rate by a factor of 10^3. The exchange of oil between the smaller aggregates with decane is slowed down by a factor of 20 more than the one with dodecane, at the same amount of surface charge which can be explained by the smaller interparticle distance in the case of decane.

3.1 Introduction

In this chapter the dynamics of the exchange of oil between MEs in the ternary system $C_{12}E_5$ has been studied intensively. Starting with the work of McBain and Woo [76] more than 70 years ago, the process of solubilisation of solutes into micellar media has been investigated with continued interest ever since. Two models have been introduced describing the take-up of solute directly from the solute surface, referred to as direct solubilisation and alternatively from the continuous phase, referred to as indirect solubilisation [77]. However, despite the fact that the thermodynamic aspects of microemulsions have been rather well understood [45, 78, 79] the time-dependent aspects have been studied to a much lesser extent.

Based on the work of Ward and Tordai, [80] who developed a model for adsorption at a planar interface from an infinite medium, Kabalnov et al. published a detailed theoretical study concerning the problem of adsorption from micellar solutions and the problem of solubilization kinetics [81]. At the same time, the group of Winnik examined the rates of solute exchange between nonionic and charged micelles in water and demonstrated the influence of the nature of surfactant and salinity on the exchange mechanism [34, 35, 82]. Some years before, Fletcher and Robinson [23] already published a comprehensive study investigating the influence of exchange rates between W/O-microemulsions and studied the effect of droplet size, temperature, chain length of oil and effects of additives thereof intensively. For AOT as dispersant, exchange rates of aqueous solubilisates between water droplets were found to be independent of the ion transferred (used as indicators for exchange), but dependent on droplet size and temperature. Exchange occurred with a second-order rate constant of 10^6 - 10^8 $M^{-1} \cdot s^{-1}$.

Fletcher and Holzwarth [83] performed iodine laser temperature-jump experiments in the system $C_{12}E_5$/tetradecane/water. Their second-order rate constants for droplet coalescence between W/O microemulsions show a linear dependence on the droplet concentration and exhibit values of 0.6, 1.9 and $10.0 \cdot 10^7$ M^{-1} s^{-1} for ω` (weight fraction of water) = 1, 2 and 4, respectively. However, as the temperature had to be changed to give the resultant values for ω`, and the particle size respectively, coalescence rates at

different ω` could not be compared due to the high temperature sensitivity of the nonionic surfactant. Therefore our aim in this kinetic study was to fix as many parameters as possible to be able to compare ternary MEs of different size, charge, composition with each other and get quantitative information about the system.

With $C_{12}E_5$ as dispersant and alkanes of increasing chain length as solute, the MEs (with low concentration of aggregates) were kept as close as possible to the solubilisation limit, where exchange kinetics are the slowest [84] and the droplets are close to spherical. The temperature of the solubilisation boundary was fixed at 25 °C, so the composition of the ternary ME had to be adjusted depending on the molar ratio of alkane (octane, decane, dodecane) to $C_{12}E_5$ ([O]/[S]) (corrected by the cmc of the surfactant in water of $5 \cdot 10^{-5}$ M [84]). In this series one observes that with decreasing chain length of the oil, larger amounts of it can be solubilised.

In figure 3.1 a partial phase diagram of the isotropic ME phase at the solubilisation boundary at 25 °C is displayed where the concentration of oil versus the concentration of surfactant is given. In the upper part of the graph the two-phase region with a ME phase and an excess oil phase is displayed. In the lower part the L_1-phase with spherical MEs with a constant molar ratio of oil-to-surfactant close to the solubilisation limit can be found. At constant ratio [O]/[S] one essentially fixes the spherical droplet radius. Under this conditions the variation of the number density of ME droplets at constant composition, temperature and radius is accomplished. This is a pre-requisite to determine the mechanism of solute exchange and participations of the rate constants when different parameter, such as charge, concentration of surfactant, oil or additive, are varied.

Applying saturated MEs stabilized by $C_{10}E_4$ and saturated with various deuterated medium chain oil at 10 °C, Gradzielski et al. did observe that the particle radius increases with decreasing chain length of alkane [85]. Furthermore they calculated the sum $2\kappa + \bar{\kappa}$ of the bending constants from the polydispersity of static SANS measurements under contrast conditions. They found $2\kappa + \bar{\kappa}$ independent of the nature of the oil (2.28, 2.32, 2.30 and 2.27 kT for decane, octane, heptane and hexane, respectively), concluding that the elastic properties of the surfactant layer seem to be dominated by the properties of the amphiphile, the hydrocarbon having only a minor effect thereof.

Our aim in this study is to investigate the consequences of their findings on the exchange kinetics of ternary, nonionic surfactant system. Ten years ago Rharbi and Winnik described how solute exchange measurements, using pyrene probes with low water solubility, can be employed to follow the rates of micelle fusion and fragmentation [35, 86, 87]. In their experiments that where discussed theoretically by Hilczer et al. [88] they determined the rates of solute exchange in micelles formed from the surfactants Synperonic A7 and Triton-X100.

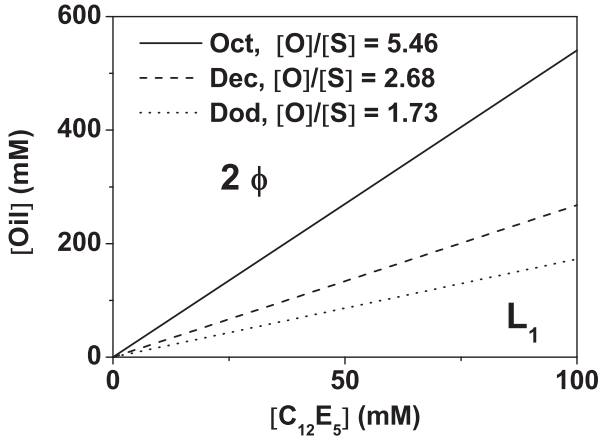

figure 3.1 partial phase diagram of the $C_{12}E_5$/oil/water system at constant molar ratio oil-to-surfactant for three different alkanes at the solubilisation boundary at 25 °C (octane: straight line, decane: dashed line; dodecane: dotted line). The phase diagram is shown as concentration of oil versus concentration of surfactant. L_1 denotes the microemulsion phase and 2Φ the two phase region

In the case of pyrene as fluorescent probe the water solubility is too high and the probe can exit from the micelle into the water phase, diffuse through the water and enter into a different micelle. In that case it is not possible to monitor solute exchange that occurs via a collision of two micelles or fragmentation of a micelle into two submicelles as could be identified for nonionic surfactants by Rharbi et al.[34]. This type of experiment is only possible if one employs a pyrene derivative with a strongly hydrophobic substituent. It is very difficult to measure the water solubility $[P]_w$ directly for molecules with low equilibrium water solubilities. An alternative is to try to estimate water solubility based on simple group-additivity rules [82]. As has been shown by Taisne et al. the presence of

two additional CH_2 groups decreases the water solubility of simple hydrocarbon molecules by about one order of magnitude [16].

For their solute exchange measurements Rharbi et al. synthesized octyl-, dodecyl- with a theoretical water solubility between 10^{-11} and 10^{-32} M. In this way, they estimated the exit rate, k^- of the probes according to

equation 3.1

$$k^- = \frac{k^+ \cdot [P]_w}{[n]}$$

where k^+ is the re-entry rate constant (which corresponds to the diffusion controlled rate constant k_{DC}) and [n] the average number of solutes per aggregate at the solubility equilibrium. Accordingly Rharbi et al. calculated theoretical exit rates in the order of 10^{-1} to 10^{-22} s^{-1}. These values are substantially lower than those of the first order exchange rate and the probe can be regarded as suitable for this experiments. Accordingly we ascertained that similar conditions pertain in our experiments so that the exchange dynamics can reliably be deduced.

In the nonionic system with $C_{12}E_5$ the influence of HM-polymers has been investigated. Starting with the work of Wang [89], who introduced HM-polymers, these molecules were used for a number of study as they are of great practical importance, for example, to enhance monolayer stability, to achieve desired rheologically properties and to simulate biologically membranes specifically. The changes in phase behavior for O/W [90-93], W/O [94, 95] and bicontinuous [62] microemulsion (ME) by addition of HM-(telechelic) polymers have been studied intensively. Models have been introduced to elucidate the interactions between polymer and surfactant layer, e.g. by de Gennes [45, 96] and [97].

Assuming uniform polymer segments, the latter authors discriminate three contributions to the adsorptions free energy: (a) a contact term, due to attractive interactions between chemically identical, hydrophilic chains of the HM-polymer and the surfactant, (b) an osmotic term, due to repulsion between adsorbed polymer chains, and (c) a fluctuation term, which is negligible. The first two terms are comparable in absolute value and have opposite sign [97], so the interactions can be directly tuned by changing the length of the hydrophilic and hydrophobic chains of the HM-polymers and the surfactant, respectively.

Quellet et al. [98] were the first to propose the formation of a transient network or core-shell nanodroplets in a W/O-ME depending on the molar ratio of hydrophilic (A) to hydrophobic (B) chains of the ABA block copolymer adsorbing into the surfactant layer; a finding which has been confirmed experimentally also by others [99-102]. In a W/O-ME the addition of an ABA block copolymer leads to the formation of a transient network (gel) or nanodroplets, when M_A/M_B <1 or > 1, respectively. For O/W-MEs reversed behavior is assumed. Experiments confirmed that the addition of telechelic polymer leads to a substantial enhancement of the viscosity without changing the size of the microemulsion droplets as observed from light scattering [96] and small angle neutron scattering experiments [96, 103]. This means that the effect of telechelic polymers on structure and rheological properties have been investigated to some extent. In contrast, much less is known about the effect of telechelic polymers on the kinetics of microemulsions and how their dynamic properties are affected by the presence of such polymers. However, for many applications of microemulsions these dynamic properties are similarly relevant as the static properties.

These studies are here further extended by introducing a charge to the stabilizing surfactant film through the addition of a small amount of ionic surfactant [104]. By this procedure, we obtained additional long-range screened Coulomb forces.

3.2 Results and Discussion

3.2.1 Influence of chain length of solubilised alkanes and temperature

3.2.1.1 Microemulsion characterization

For our experiments three single-phase MEs were prepared with octane, decane and dodecane at 25 °C with a volume fraction kept aroung 0.06 (sample composition given in table 3.1). From DLS measurements we calculated the hydrodynamic radii which are proportional to [O]/[S] (corrected with the cmc) as it was predicted (see A figure 9.1). All MEs were diluted with water up to a mixing ratio of 1:9 to ensure applicability for kinetic measurements. The droplet size was basically independent of the concentration of ME aggregates (see A figure 9.2), an observation that has been reported earlier [84].

Values of the droplet concentration were calculated determining N_{agg} from

equation 3.2

$$N_{Agg} = \frac{4 \cdot \pi \cdot (R_{th})^2}{a}$$

with R_{th} from the solution composition

equation 3.3

$$R_{th} = 3 \cdot l_S \left[1 + \frac{\Phi_O}{\Phi_S} \right]$$

where R_{th} is the theoretical radius according to the composition (calculated values of the three MEs are displayed in A figure 9.1), l_S the length of the surfactant molecule ($l_S(C_{12}E_5)$ = 1.54 nm [105]), Φ_O and Φ_S the volume fractions of the oil and the surfactant respectively. Value for the head group area $a(C_{12}E_5)$ was 46.8 $Å^2$ and taken from ref. [105]. Division of [TDMAO] by N_{agg} gave [Agg].

In order to study the dynamics of solute exchange between ME droplets the fluorescent water insoluble compound pyrene butyric acid stearyl ester was synthesized and used as fluorescent probe. In figure 3.2 a) the static fluorescence spectra of ME octane as solute containing ~ 4 molecules of pyrene ester per aggregate (straight line) is displayed. Apart from the monomer emission bands at lower wavelength ((0,0) at 378 nm), a broad excimer band at around 470 nm can be observed.

a)

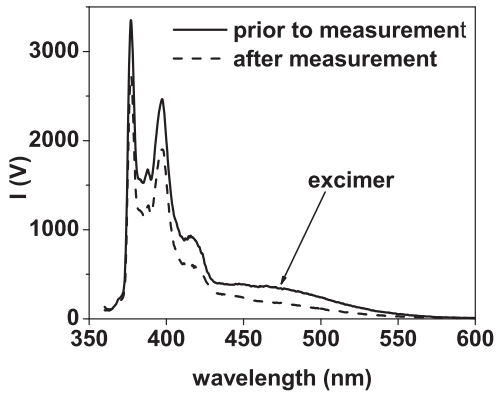

b)

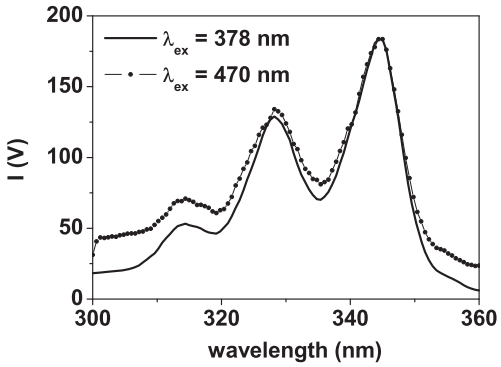

figure 3.2 a) Emission spectra (λ_{ex} = 350 nm) of pyrene ester solubilised in a ternary microemulsion (57 mM $C_{12}E_5$/ 276 mM cot/ water, 43.53 μM P.Ester). In the spectrum labeled "Prior to exchange", [P] = 43.53 μM. The spectrum "After measurement" refers to the solution obtained by mixing the original solution with an equal volume of ME without probe. b) Excitation spectra of pyrene ester in the ternary ME ([P] = 43.53 μM) with λ_{ex} = 350 nm (monomer) compared to the spectrum with λ_{ex} = 470 nm (excimer)

In figure 3.2 b) we show that the excitation spectra of the ME monitored at the emission wavelength of the monomer and that of the excimer superimpose. These spectra have essentially identical features with the monomer excitation spectrum of this pyrene ester in ethanol from which we conclude that it does not form aggregates in the ternary MEs. The excimer intensity decreases correspondingly when this ME is diluted with equal amounts of a ME containing no fluorescence probe representing the final state of a stopped-flow mixing procedure.

table 3.1 Concentration of components of the samples, total volume fraction, Φ, values of [O]/[S], concentration of ME aggregates [Agg] (calculated from the theoretical radius according to equation 3.3) and hydrodynamic radius, R_H (calculated from DLS measurements) of the three ternary surfactant systems with $C_{12}E_5$ as surfactant and octane, decane and dodecane as oil

	c(O) (mM)	**c(S) (mM)**	**Φ**	**[O]/([S]-cmc)**	**[Agg] (μM)**	**R_H (nm)**
Oct	275.50	56.98	0.0663	4.84	10.23	12.3
Dec	161.02	60.13	0.0549	2.68	20.86	8.80
Dod	134.68	78.02	0.0622	1.73	34.64	7.49

3.2.1.2 Exchange experiments and temperature dependence

From theoretical considerations applying simple group-additivity rules already discussed in the introduction of this chapter the pyrene ester can be identified as eligible probe if the observed relaxation rates in the experiments exceed 10^{-1} s^{-1}. From fluorescence decay studies of micellar solutions with pyrene triglyceride, Rharbi et al. showed that the probe is characterized by a Poisson distribution in aqueous solutions of nonionic micelles. We assume similar behavior for our pyrene derivative [34] and performed stopped-flow fluorescence measurements for mixing two otherwise identical MEs, one with the fluorescent dye (solution 1) and one without (solution 2), and monitored the decrease of the excimer signal, due to dilution, with time.

In the following we used the terms $[Agg]_0^I$ and $[Agg]_0^{II}$ for the concentration of aggregates in the solution 1 with the fluorescent probe and solution 2 without (we did not take into account the fraction of probe-free aggregates in solution 1 according to the Poisson distribution); thus

equation 3.4

$$[Agg] = \frac{1}{2}\left([Agg]_0^I + [Agg]_0^{II}\right)$$

is than the total concentration of aggregated in equilibrium (after the mixing process). The average number of probe molecules per ME aggregate was kept between 2 and 4 (less probe was necessary in smaller MEs to achieve the same excimer intensity than in bigger MEs where the aggregate was loaded with ~ 4 probe molecules; this is due to the variation of the pyrene concentration in the ME droplets as a function of size). All decay profiles from stopped-flow measurements fit well to an exponential form. Experiments were carried out at 25.0, 25.5 and 26.0 °C, to obtain information on the temperature-dependence of the kinetics. Each experiment was repeated 10 – 25 times, depending on the magnitude of the excimer intensity and the average of these runs was fitted with a mono-exponential function of the form already introduced with equation 1.2. Determination of k_{obs} at different temperatures, applied to Arrhenius´ equation, gave an apparent activation energy E_a of the kinetic process

As already established by Fletcher and Clark, the exchange kinetics of ME stabilized by nonionic surfactants is characterized by the collision-exchange-separation mechanism [23, 83, 84]. The experimentally observed coalescence rate can be described by equation 3.5.

equation 3.5

$$k_{obs} = k_{exit} + k_{fr} + k_2[Agg]_0^{II}$$

equation 3.6

$$k_{obs} = k_1 + k_2[Agg]_0^{II}$$

where k_{exit} and k_{fr} are first-order rate constants. The first one describing the exit of a pyrene molecule from the ME aggregate and the second one the break-up of the normal-sized excimer-bearing ME into two sub-microemulsion aggregates containing

single pyrene molecules, followed by growth of these sub-microemulsion aggregates either by fusion with empty ME or by interaction with surfactant monomers (fragmentation-growth mechanism; k_{fr} was therefore assigned as k_1) [35]. The relaxation rate k_2 is the second-order rate constant for the collision-exchange-separation mechanism, which corresponds to coalescence. The process described by k_{exit} is negligible because of the insolubility of pyrene ester and therefore just one first-order constant k_1 is employed (r.h.s of equation 3.6). The first- and second-order processes can be separated because they exhibit different kinetic rate laws [35].

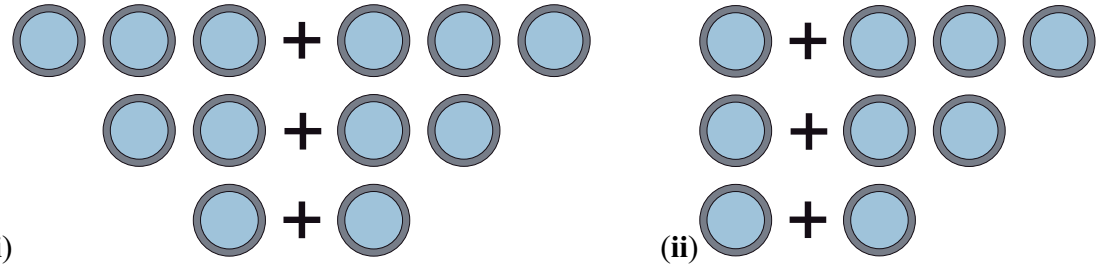

chart 3.1 The two mixing procedures employed in this work to study the exchange of oil between microemulsions in the ternary system $C_{12}E_5$/oil/water

In the following we will present results of two different mixing experiments:

(**i**) the 1:1 mixing of two identical MEs, one containing the fluorescent probe,

(**ii**) the 1:1 mixing of the ME with the lowest concentration containing the probe and increasing concentration of the second ME.

Both mixing procedures (displayed in chart 3.1) were performed for the three different oils (octane, decane and dodecane with [O]/[S] = 4.84, 2.68 and 1.73 respectively) and for a concentration series with oil volume fractions, Φ_O, of 0.0043, 0.0109, 0.0175 and 0.0304 (and 0.0432 for octane).

The normalized fluorescence intensity curves and the corresponding relaxation rates, k_{obs} for procedure (**i**) versus [$C_{12}E_5$] are displayed in figure 3.3. In a) a slowing down of the exchange kinetics for $C_{12}E_5$/decane/water with decreasing surfactant concentration (square: 60 mM $C_{12}E_5$ to crosses: 8 mM $C_{12}E_5$ with the corresponding amount of decane) can be observed.

As can be seen clearly in figure 3.3 b), k_{obs} is linearly dependent on the surfactant concentration for octane, decane and dodecane and ranges between 1.6 and 23.4 s^{-1}. These values are much higher than the maximum rate for diffusion-controlled reactions. We conclude, that k_{obs} measured with the stopped-flow fluorescence method represents the fusion-fission-process established for nonionic surfactants.

a)

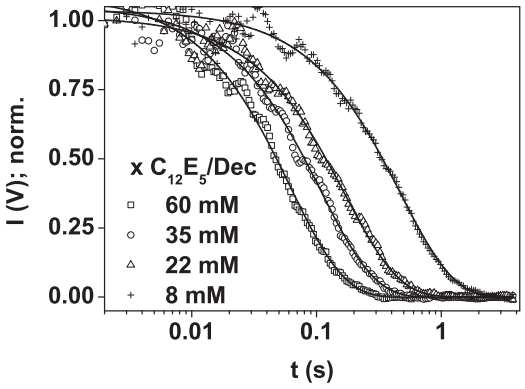

b)

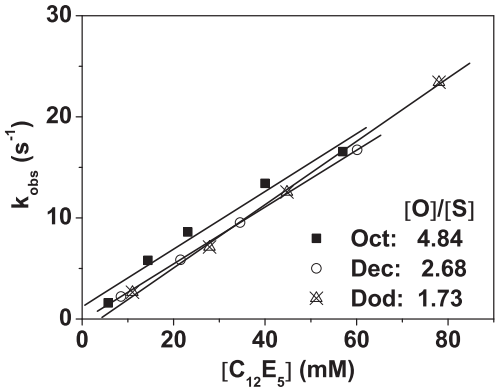

figure 3.3 a) Stopped-flow fluorescence measurements: 1:1-mixing of two identical MEs with $C_{12}E_5$ and decane in water and the fits (mono-exponential function) at 25 °C: normalized excimer intensity versus measurement time for various concentrations of surfactant. b) apparent first-order rate constant k_{obs} for octane (square), decane (circle) and dodecane (triangle) calculated from the fits of the data from individual stopped-flow experiments plotted versus the concentration of the surfactant $C_{12}E_5$. These decays were monitored at λ_{em} = 435 – 600 nm with λ_{ex} = 350 nm. Lines denote the linear fits to the data

Furthermore, in order to analyze the influence of the alkyl chain length of the alkane on the exchange kinetics, the experimental relaxation rates were plotted against $[Agg]_0^{II}$ according to equation 3.6 (see A figure 9.4). The slope in the k_{obs}-$[Agg]_0^{II}$-plot corresponds to the fusion-fission rate constant, k_2 for mixing procedure (**i**). Values of k_2 are presented as open squares in figure 3.4 b and decrease from $175.7 \cdot 10^4$ for octane to $81.08 \cdot 10^4$ and $70.54 \cdot 10^4$ $M^{-1} \cdot s^{-1}$ to decane and dodecane.

table 3.2 Calculated first- and second-order rate constants, k_1 and k_2 from the plot k_{obs} versus $[Agg]_0^{II}$ according to equation 3.6 for mixing event (**i**) (see A figure 9.4) and (**ii**) (see figure 3.4) for the three ternary systems with octane, decane and dodecane. The intercepts for the solutions with decane and dodecane in procedure (i) were not reliable in the fits and put to zero. Therefore the slope was calculated from the fit through the origin

	(i)			**(ii)**		
k_{obs} versus $[Agg]_0^{II}$	**Oct**	**Dec**	**Dod**	**Oct**	**Dec**	**Dod**
k_1 (s^{-1})	-	-	-	0.6750	1.0661	1.481
k_2 ($10^4 \cdot M^{-1}s^{-1}$)	175.7	79.80	65.51	90.86	39.32	27.86

The apparent activation energies (= $E_{a,Arrh}$), derived from Arrhenius´ plot exhibit high positive values for all mixing events (see A figure 9.3). The values range between 135 and 447 kJ/mol for octane, 229 and 346 kJ/mol for decane and between 241 and 290 kJ/mol for dodecane, but not showing any systematic trends, which is presumably due to the relatively large experimental error contained. Fletcher et al. report high activation energies of 70 - 110 kJ/mol as well, that increase with increasing droplet size [23]. We found no direct correlation between $E_{a,Arrh}$ and the droplet, but one has to take in mind the increasing experimental error from octane, decane to dodecane, due to the increasing size and therefore decreasing amplitude of the excimer signal. Furthermore, increasing the temperature corresponds to an increased distance from the solubilisation boundary where the exchange kinetics where to be investigated originally.

In summary, we found a linear dependence of the coalescence rate in the ternary system $C_{12}E_5$/octane/water on the concentration of the surfactant. The curves as function of the

surfactant concentration superimpose when octane is replaced by decane and dodecane, respectively. The second-order relaxation rate for the fusion-fission mechanism increases linearly with increasing molar ratio of oil/surfactant.

3.2.1.3 First- and Second-Order Contributions

In equation 3.6 the participation of the first- and second-order kinetics of the observed relaxation rate proposed by Rharbi et al. is described. As already discussed above we have a first-order (k_1) and a second-order process (k_2), where the latter depends on the concentration of aggregates (equation 3.6). By performing mixing experiments as described in procedure (ii), we were able to derive values for k_1 and k_2 for the ternary system with octane, decane and dodecane. The observed relaxation rates (filled symbols) for all three alkanes versus $[Agg]_0^{II}$ are displayed in figure 3.4 a.

We found a linear dependence of k_{obs} (filled symbols) on $[Agg]_0^{II}$ as proposed for ternary systems of nonionic surfactants exhibiting fusion-fission kinetics. It is clearly visible from figure 3.4 b, that changes of $[Agg]_0^{II}$ have a much bigger effect on the coalescence with octane (squares) as solute than for decane (circles) and dodecane (triangles). Increasing $[Agg]_0^{II}$ from 1 to ~ 10 μM, k_{obs} for octane increases by ~ 10 s^{-1}, whereas for decane it is only half the value.

Data were fitted with a linear function, exhibiting a linear dependence of k_1 (0.675, 1.066 and 1.481 s^{-1} for octane, decane and dodecane respectively) with increasing alkyl chain of the hydrocarbon while k_2 decreases from $90.86 \cdot 10^4$ to $39.32 \cdot 10^4$ and $27.86 \cdot 10^4$ $M^{-1} \cdot s^{-1}$ (see A figure 9.5). The first-order relaxation rate decreases with decreasing alkyl chain length, i.e. increasing size of the aggregates, but the magnitude of the change is relatively small; an observation that was reported by Rharbi et al. [34] several years earlier as well. Obviously the contribution of the first-order kinetics is only marginal and exchange of oil mainly procedes via a second-order process.

The second order rate constant decreases with increasing alkyl chain length of the oil solubilised inside the surfactant core and the evolution of this parameter is displayed in

figure 3.4 b (empty circles). This trend is identical to the one of k_2 measured for mixing procedure (**i**), but the absolute values are only half of the fusion-fission rate calculated from (**ii**).

a)

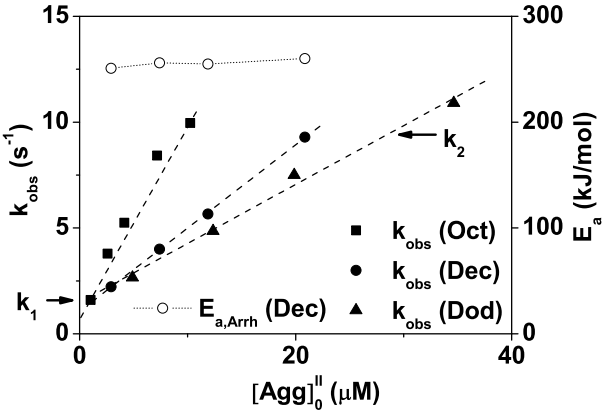

b)

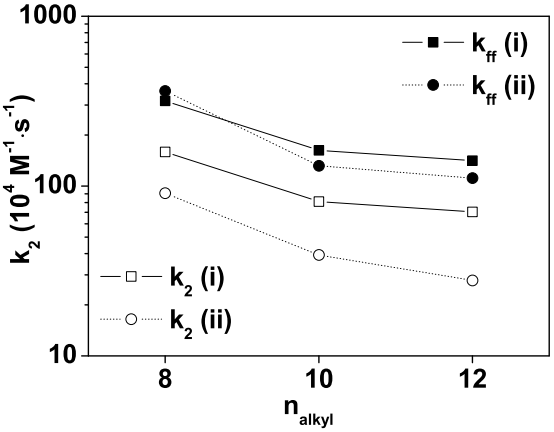

figure 3.4. a) Observed relaxation rates (filled symbols) and Arrhenius´ activation energy for octane (squares), decane (circles) and dodecane (triangle) versus the concentration of unloaded ME aggregates. b) second-order relaxation rates, k_2 as function of the alkyl chain length of the hydrocarbon from the plot k_{obs} versus concentration of probe-free aggregates (empty symbols) and k_{obs} versus the total concentration of aggregates (correction by taking into account the frequency factors for the corresponding exchange mechanism from equation 3.9 explained in detail in the discussion; filled symbols). Dashed lines denote linear fits to the data, straight and dotted lines to guide the eye

The Arrhenius energies for the mixing procures with decane are presented as empty squares in figure 3.4 a) and show only a minor increase with increasing concentration of unloaded aggregates. The absolute values of 251 - 260 kJ/mol are 13 times larger than the activation energy for the diffusion-controlled mechanism, 20 kJ/mol, calculated from the Arrhenius plot of $\ln(k_{DC})$ versus 1/T at 25.0, 25.5 and 26.0 °C.

From the plot of k_2 versus n_{alkyl} in figure 3.4 b, it can be seen clearly that fusion of two droplet is faster the bigger the ME aggregates, which is the case for shorter oils. Apparently the coalescence process becomes easier with flatter the surface of the fusing particles. If every encounter between droplets resulted in solubilisate exchange, k_2 should be comparable with the collision frequency of droplets [23]. The diffusion-controlled rate constant, k_{DC}, is given by the Smoluchowski equation:

equation 3.7

$$k_{DC} = \frac{8 \cdot R \cdot T}{3 \cdot \eta}$$

where R is the gas constant, T is the absolute temperature and η is the solvent viscosity. For water at 25 °C, $\eta = 8.904 \cdot 10^{-1}$ kg/m·s and hence k_{DC} is ~ $0.74 \cdot 10^{10}$ $M^{-1} \cdot s^{-1}$. Comparison of k_{DC} with k_2 show that 1 in 81, 190 and 264 encounters (for octane, decane and dodecane, respectively) results in solubilisate exchange. This implies the presence of an energetic barrier to the fusion process, ΔE_{eff}, which can be estimated from the ratio of the rate constant for exchange relative to the value of k_{DC} which corresponds to the value expected in the absence of an energy barrier:

equation 3.8

$$\frac{k_2}{k_{DC}} = exp\left(-\frac{\Delta E_{eff}}{k \cdot T} \right)$$

Values for ΔE_{eff} for mixing experiments (**i**) increase linearly from 42.1 to 44.1 kJ/mol with decreasing R_H (see table 3.4) a finding which was already reported by Fletcher some years ago [83]. The rather constant values for ΔE_{eff} agree with the idea that this activation process is governed by the bending energy as characterized by $2\kappa + \bar{\kappa}$, which is also

rather constant (for saturated MEs of a given surfactant C_iE_j with hydrocarbons of medium chain length [85]).

In addition we calculated the energy barrier for the first mixing experiment from k_2 presented in table 3.2. Fletcher et al. postulated that exchange by coalescence should be insensitive to the specific nature of the particular solute [22, 23]. Comparing the change of k_2 with increasing alkyl chain length of the hydrocarbon in our experiments, we conclude, that the increase of k_2 is not caused by the nature of the oil but by the size which is a consequence thereof. In the above mentioned work, it was postulated that coalescence occurs via a transition state involving the formation of highly curved regions of monolayer (hour-glass shape) [22]. In this experiment, at constant elasticity of the surfactant interface, droplets of smaller size have to proceed through a transient state of higher curvature than bigger sized droplets. As a consequence higher energy is required to overcome this barrier, which is reflected by our data directly.

3.2.2 Influence of HM-polymer

Oil-in-water MEs can take up at least 10 wt% of HM-polymer without changing their size but this incorporation is accompanied by a drastic increase of the zero-shear viscosity of 10^5 orders [93, 96, 106]. For kinetic investigations applying the stopped-flow method for viscosity reasons only the low concentration range is applicable. Antil and Rewopal, mainly differ in the length of the ethoxy chain of this end-capped polymer. Therefore we added the polymers to the system $C_{12}E_5$/decane/water in a manner that for both cases statistically 27 molecules are contained per ME droplet. The normalized fluorescence intensity curves are displayed in App fig. 6 a. The evolution of the excimer intensity for the sample without polymer and with Antil is identical, whereas a pronounced shift to slower relaxation is observed with increasing polymer content. The calculated coalescence rate event according to procedure (**i**) decreases from 2.23 s^{-1} for the pure ME only marginally to 2.02 s^{-1} for Antil but by a factor of 4 to 0.52 s^{-1} for Rewopal.

In table 3.3 the first- and second-order relaxation rate, k_1 and k_2, from stopped-flow fluorescence measurements performed according to procedure (**ii**) are displayed (see also

A figure 9.5 b). The addition of 27 molecules of Antil (the shorter HM-polymer) has only a marginal impact on the exchange kinetics of the ternary ME; the rate of droplet fragmentation decreases slightly from 1.07 to 0.87 s^{-1}, whereas the fusion rate remains constant at ~ $40 \cdot 10^4$ $M^{-1} \cdot s^{-1}$. In case of Rewopal, k_1 and k_2 both decrease by a factor of 4 to 0.25 s^{-1} and $9.5 \cdot 10^4$ $M^{-1} \cdot s^{-1}$. The reason for the more distinctive effect of Rewopal compared to Antil, comes from the longer EO-unit, which leads to steric stabilization of the droplet and provides an entropic and hydration barrier to close contact of the ME cores. Both polymers exhibit the same alkyl chain length of the B-block (the double bond in Rewopal should have only marginal effect upon the kinetics), therefore their effect on the core is identical. The reason for the much higher effect of Rewopal in slowing down exchange kinetics is thus caused by the three times longer EO chains of Rewopal.

table 3.3 First- and second-order relaxation rate, k_1 and k_2, from stopped-flow fluorescence measurements in the system $C_{12}E_5$/decane/water and calculated values for the effective activation energy, ΔE_{eff} compared to the diffusive process and the additional activation energy due, E_{add} to the additive. Rates were calculated from the mono-exponential fit of the excimer intensity decay with time (HM-polymers: A figure 9.6 b; DTAB: A figure 9.7 c). The concentration of the HM-polymers corresponds to the weight fraction of the solution, whereas the concentration of DTAB corresponds to the weight fraction of cationic to nonionic surfactant

	k_1 (s^{-1})	k_2 (10^4 $M^{-1} \cdot s^{-1}$)	ΔE_{eff} (kJ/mol)	E_{add} (kJ/mol)
pure ME	1.07	39	22.3	-
0.226 wt% Antil	0.87	40	24.4	0.2
0.500 wt% Rewopal	0.25	9.5	27.9	3.6
1.00 wt% DTAB	0.10	1.2	33.0	6.7

We also determined the Arrhenius´ activation energy for the kinetics with the HM-polymers. Compared to the values of the pure ME system of 251 - 260 kJ/mol, the activation energies for the polymer containing systems are similar and vary from 227 - 248 and 185 - 243 for Antil and Rewopal, respectively. As already mentioned above, the Arrhenius activation energy is obviously a much more complex value and does not solely represent the energy required during the coalescence of ME droplet.

According to equation 3.8, we determined the effective activation energy compared to the diffusional process for ME + polymer, which should give a much more realistic value for the free energy barrier to inter-droplet exchange. For Antil and Rewopal, we calculated ΔE_{eff} = 24.4 and 27.9 kJ/mol. The identical values for pure ME and ME + Antil reflect that no change in the kinetics could be observed. The increase of ΔE_{eff} for Rewopal describes the slowing down of the kinetics. From the decrease of k_2 due to the presence of the polymers compared to the pure ME, we calculates an additional activation energy ΔE_{add} of 0.2 for Antil and 3.5 kJ/mol for Rewopal (as simply derived from equation 3.8 comparing $k_{obs,Polymer}$ with k_{obs} of the pure ME).

We calculated the additional activation energy for the first- and second-order step to be able to separate both contributions to oil exchange in MEs with Antil and Rewopal to be 0.5 and 3.6 kJ/mol for k_1 and 0 and 3.5 kJ/mol k_2. Values for both exchange rats for one polymer are nearly identical indicating equal energetic contributions of the additive on the fragmentation-growth and the fusion-fission-step.

3.2.3 Influence of charge

In another variation of our system we varied the electrostatic conditions by admixing up to 2 wt% DTAB were added to the ternary ME $C_{12}E_5$/decane/water and stopped-flow fluorescence measurements were performed. The low concentration on DTAB, is supposed to let the ME structure and size unchanged (A figure 9.7 a), hence only additional long-range Coulomb forces are introduced into the surfactant monolayer. The evolution of k_{obs} as function of the concentration of charge is presented in figure 3.5. The observed relaxation rate decreases by a factor 10^3 as the amount of DTAB increases from 0 to 2 wt%. The exchange of decane between droplets is slowed down considerably as to be expected due to the electrostatic repulsion between the ME aggregates. From the dilution series at 1 wt% DTAB we determined k_1 and k_2 which are presented in table 3.3.

The rate constant for fission decreased drastically by a factor of 10; the one for fusion decreases even more drastically by a factor of 32. This corresponds to an effective activation energy of 33.0 kJ/mol. This value is substantially higher than ΔE_{eff} for the

amphiphilic polymers (0.266 and 0.500 wt% for Antil and Rewopal), keeping in mind that the concentration of ionic additive is defined as fraction to nonionic surfactant and not to the amount of solution.

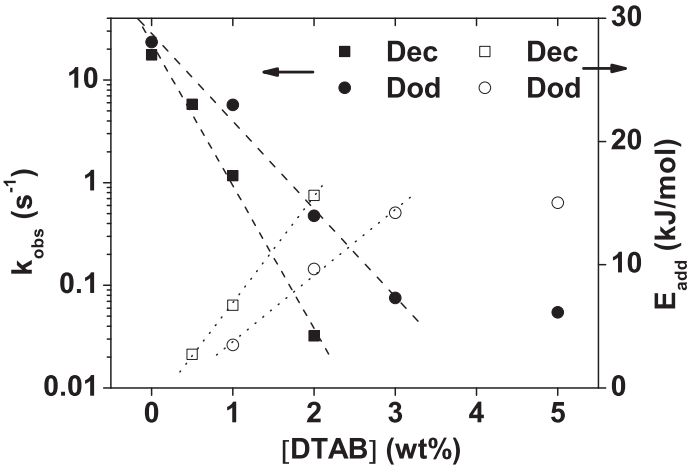

figure 3.5. Observed relaxation rates (filled symbols) from the mono-exponential fits and additional activation energies (empty symbols) from stopped-flow fluorescence measurements at 25°C (see A figure 9.7 b) of the mixing of equal MEs $C_{12}E_5$/oil/water with increasing concentration of ionic additive DTAB (wt% ionic to nonionic surfactant); squares and circles denote values for the ternary ME with decane and dodecane; dashed and dotted lines correspond to the linear fit of k_{obs} and E_{add}, respectively

From the dilution series at 1 wt% DTAB we determined k_1 and k_2 which are presented in table 3.3. The rate constant for fission decreases drastically by a factor of 10, i.e., the fission is apparently suppressed by the increased charge density; the rate constant for fusion decreases by a factor of 32. This corresponds to an effective activation energy of 33.0 kJ/mol. This value is substantially higher than ΔE_{eff} for the HM-polymers (0.266 and 0.500 wt% for Antil and Rewopal), keeping in mind that the concentration of ionic additive is defined as fraction to nonionic surfactant and not to the amount of solution.

Coulombic interactions appear to be much more effective at preventing close ME aggregate approach than the steric hindrance caused by the EO of Antil and Rewopal. However, one has to keep in mind the higher molar fraction per ME aggregate of ionic surfactant compared to the polymers. The additional activation energies due to the

presence of the ionic surfactant are displayed as circles in figure 3.5. Already 2 wt% DTAB (per g $C_{12}E_5$) lead to an increase of the activation energy by 15.6 kJ/mol.

It is also interesting to note that this effect levels off for higher addition of ionic surfactant, an effect that may be explained by the fact that around such a value of 3 - 5 mol% content of ionic surfactant counterion condensation should set-in, keeping the effective charge on the surface of the microemulsion droplets constant [57]. The additional activation energy for the first- and second-order step for oil exchange was calculate to be 5.8 and 8.6 kJ/mol for k_1 and k_2. By simply comparing these two activation energy it seems that the fusion-step is even more disfavored by the presence of the ionic surfactant than the fragmentation of droplets, which means that there is a substantial electrostatic stabilization both against fission and fusion.

The trend is the same in the O/W-ME containing dodecane, although the k_{obs} decrease slower and reach constant values at c = 5 wt% (circles in figure 3.5). Recalculating k_{obs} for the number of charges per ME droplet, the oil exchange in the bigger aggregates with decane is slowed down by a factor of 20 more compared to the one with dodecane at the same amount of surface charge density. In consistency with k_{obs}, the additional activation energy due to the charge is twice as high.

The stronger retarding effect of solute exchange in MEs with decane can be explained be the smaller interparticle distance between the aggregates. Repulsion due to Coulombic forces is much more efficient the nearer the charges between neighboring ME droplets which is true for the bigger aggregates with decane.

3.3 Discussion

As already mentioned before, the exchange of oil between the ME droplets should proceed with the same mechanism of collisional exchange. Therefore the corresponding rate constant should be identical independent of the mixing procedure applied. In the following we will discuss the deviating values (by a factor of two) of k_2 in detail.

Based on the work of Rharbi and Winnik (who studied the exchange dynamics on micelle solutions), Hilczer et al. gave a theoretical analysis of the stopped-flow fluorescence time-scan method presented on the basis of the stochastic model of solubilisation. Depending on the experimental condition in the stopped-flow mixing two limiting cases were postulated: for monodisperse micelles at low concentration exchange occur via collisional one-particle hopping, whereas in concentrated micellar solutions multiparticle hopping between the fused micellar compartments becomes possible [88]. The latter process becomes especially important for microemulsions where the transient state is rather long-lived due to sticky collision of two aggregates as it is also the case in the experiments of Rharbi and Winnik. Hilczer et al. suggested the correction of the calculated relaxation rates k_1 and k_2 in the experiment of Rharbi and Winnik by taking into account the corresponding frequency factors for both mechanisms.

Therefore it is more appropriate to rewrite equation 3.5 as follows:

equation 3.9

$$k_{obs} = k_{fr} + \frac{1}{2} k_{ff} [Agg]$$

The first term on the right-hand side of corresponds to the fragmentation-growth mechanism and the corrected rate-constant is given by

equation 3.10

$$k_{fr} = k_1 - k_2 [Agg]_0^I$$

where $[Agg]_0^I$ is the concentration of the initially present aggregates containing the fluorescent probe (with k_1 and k_2 from the experimentally measured linear dependence of k_{obs} versus $[Agg]_0^{II}$). The second term on the right-hand side of corresponds to the fusion-fission mechanism with $k_{ff} = 4k_2$ and a factor of ½, which corresponds to the frequency factor of the slowest possible exchange process. The factor of 4 arises from the normalization of the transition probability and describes the number of different micelle pairs (in terms of the probe occupancy) which can be created after fusion-fission of two aggregates [88].

In the experiments of Rharbi et al., the second order rate constants were calculated from the dependence on $[Agg]_0^{II}$ (see equation 3.6). However, it is obvious from our experiments, that values for k_2 from this plot differ when taken from different mixing experiments. Hence, we recalculated the relaxation rate for the fusion-fission mechanism as postulated from Hilczer et al. (equation 3.9).

In table 3.4 the calculates data for fusion-fission and the second-order rates from the k_{obs}-[Agg]-plot for the exchange of solute (k_{ff}, k_2) are listed. Values for the exchange via fragmentation-growth mechanism (intercept) were negative for decane in (**i**) and (**ii**) and for dodecane in (**ii**). Consequently, the two relaxation rates were calculated from the linear fit through the origin.

table 3.4 Fusion-fission and second-order relaxation rates calculated according to Hilczer [88] for two different mixing events (**i**): $[Agg]_0^I = [Agg]_0^{II}$ and (**ii**): $[Agg]_0^I \leq [Agg]_0^{II}$. ΔE_{eff} calculated from k_2 compared to the diffusion-controlled reaction (eq. 3.8)

	(**i**)				(**ii**)		
k_{obs} versus $[Agg]$	**Oct**	**Dec**	**Dod**		**Oct**	**Dec**	**Dod**
k_{ff} (10^4 $\cdot M^{-1}\cdot s^{-1}$)	317	162	141	**k_{ff} (10^4 $\cdot M^{-1}\cdot s^{-1}$)**	363	132	111
k_2 (10^4 $\cdot M^{-1}\cdot s^{-1}$)	79.5	40.5	35.3	**k_2 (10^4 $\cdot M^{-1}\cdot s^{-1}$)**	90.9	32.9	27.9
ΔE_{eff} (kJ/mol)	42.1	43.7	44.1	**ΔE_{eff} (kJ/mol)**	41.7	44.2	44.7

Finally the solute exchange rates from the k_{obs}-$[Agg]_0^{II}$-plot in figure 3.4 b (empty symbols) where replaced by the corrected values of k_{ff} for mixing procedure (**i**) and (**ii**) (filled symbols) according to Hilczer et al.. The fusion-fission rate increases with decreasing alkyl chain length of oil from e.g. $111\cdot10^4$ to $363\cdot10^4$ $M^{-1}\cdot s^{-1}$ for (**ii**).

From this detailed analysis we can conclude that the first-order contribution to solute exchange is negligible for both mixing events. As would be expected for MEs with a nonionic surfactant as dispersant, collisional exchange is the dominant mechanism.

Constistently, values for ΔE_{eff} are nearly identicall for both mixing procedures and are listed in table 3.4 (recalculated for the corrected values of k_2) The fusion-fission-rates are in very good agreement within experimental error. Obviously, determination of the relaxation rate of solute via collision of two ME aggregates can be detected independent of the mixing procedure applied.

3.4 Conclusion

The exchange rate of octane, decane and dodecane in O/W-microemulsion droplets stabilized by $C_{12}E_5$ occurs with a rate that is slower than the diffusion-controlled limiting value. We calculated the corresponding free energy barrier to this fusion-fission process which is much smaller for bigger droplets. The observed coalescence rate for the mixing of identical MEs at the solubilisation boundary depends linearly on the concentration of oil and superimpose for all three hydrocarbons as function of the concentration of surfactant. From dilution series we determined the first- and second-order rate constant for all three microemulsions. The first-order relaxation rate decreases with increasing size of the aggregates. At the same time k_2 increasing exponentially with increasing R_H. At constant values for $2\kappa + \bar{\kappa}$, the effective activation energy for coalescence compared to the diffusional process decreases with increasing droplet radius, which is in accordance with the faster exchange of solute.

Upon addition of the two dioleyl-polyethyleneoxides, Antil and Rewopal, which only differ in the length of the ethoxy chain in the mid-section of this BAB-triblock polymer, the observed relaxation rate decreases by a factor of ~ 0 and 4, when ~ 27 molecules per ME droplet are present. The first- and second-order rate constants are affected to the same degree by the retarding influence of the polymers.

Finally we added cationic surfactant to the nonionic ME to introduce small amounts of charges on the droplet surface and to obtain additional long-range screened Coulomb forces. Only 2wt% of ionic surfactant decreased the observed relaxation rate by a factor of 10^3. The addition of such small amounts of additive should have no influence on the sum $2\kappa + \bar{\kappa}$ of the bending constants.

In summary we may state that our experimental kinetic results are important evidence of the relations between the molecular structure of a given amphiphilic system and the bending moduli and dimension of the corresponding monolayer which have been described only in static experiments in the literature before. Moreover we could prove that the second-order relaxation rate of the exchange of solubilisate in nonionic MEs is independent of the mixing procedure.

4 Kinetics of the equilibration of microemulsions and the exchange of oil in a quaternary surfactant system

Graphical Abstract

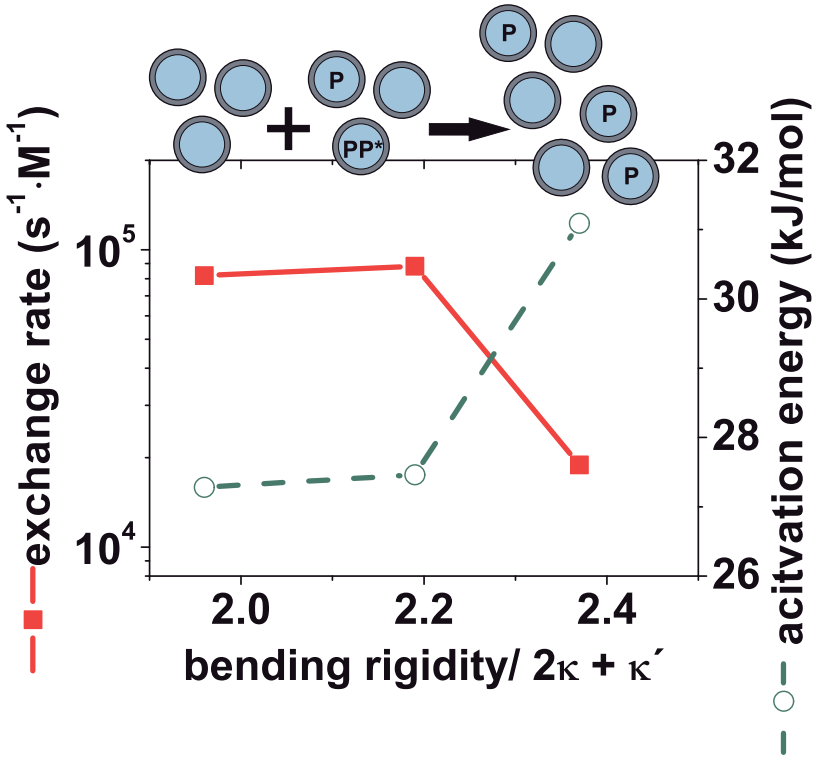

Abstract

The formation and the inter-droplet exchange rates of (o/w) microemulsions in the quaternary system tetradecyldimethylamine oxide/1-hexanol/n-decane/water has been investigated. The aim of the study was to test whether there is a correlation between the measured rates and the interfacial rigidity (expressed as the sum $2\kappa + \bar{\kappa}$), the charge introduced into the surfactant layer, the temperature and the amount of solubilised oil. Stopped-flow measurements were performed to follow the fast kinetics by means of three different detection methods (fluorescence, turbidity, SAXS). Essentially all three methods detect the same process but in a different fashion so they yield complementary kinetic information and lead to a more comprehensive picture. Furthermore it is possible to choose the desired methods according to the experimental conditions. Both the formation and the exchange mechanism involve transient oil droplet coalescence and separation. There is a linear correlation between the logarithm of the rate of formation and the difference of the droplet concentration. The logarithm of the rate of exchange of solubilisate is directly proportional to the droplet concentration. The activation energy for this step was found to be linearly dependent on $2\kappa + \bar{\kappa}$ of the microemulsions.

4.1 Introduction

In the previous chapter the dynamics of the exchange of oil between classical ternary systems of nonionic MEs has been presented. However for practical application often multicomponent systems are used. Accordingly a comprehensive study on the exchange dynamics and the equilibration of MEs in the quaternary system TDMAO/1-hexanol/decane/water is presented. In the first part of this chapter exchange dynamics will be conducted in the same manner as in the previous chapter, i.e. by monitoring the decrease of the excimer signal over time by mixing of identically sized droplets with one of the mixing partners containing a fluorescence label.

In the second approach the equilibration of two differently sized MEs to yield a final ME of intermediate size was followed via turbidity, fluorescence and SAXS measurements. By applying these complementary methods we expect to gain detailed information about the mechanism of equilibration and to see how the different detection techniques pick up this process. In these experiments we varied the temperature (in order to access the Arrhenius activation energy) and also addressed the question of having a charged surfactant present during the process of ME formation (as introduced by admixing an ionic surfactant). This then allows us to see how electrostatic interactions affect this process.

In this chapter various kinetic experiments on the chosen quaternary microemulsion will be reported with the aim of obtaining a consistent picture with respect to the parameters that govern the solute dynamics in such systems. This will be correlated with the typical parameters characterizing the microemulsions present such as for instance the size of the aggregates, amount of charge in the interface and temperature. Here the influence of the number of aggregates and second-order relaxation rate k_2 of the formation of MEs and the amount of decane on k_2 of the exchange of MEs will be of particular interest. We will also show the correlation of the sum $2\kappa + \bar{\kappa}$ of the bending constants on the activation energy in the latter case.

Experiments from the previous chapter show that the stopped-flow technique is very suited for studying coalescence processes in droplet microemulsions and allows discerning in detail effects of the amphiphile composition. Therefore the findings in this

chapter are of fundamental interest for a better understanding of the dynamic aspects of microemulsions but they are also of central importance for all solubilisation processes. The dynamics of solubilisation in micellar systems and microemulsions is one of their key applications but is so far still only poorly understood, a situation which by our findings and further application of this method shall be improved substantially.

4.2 Experimental

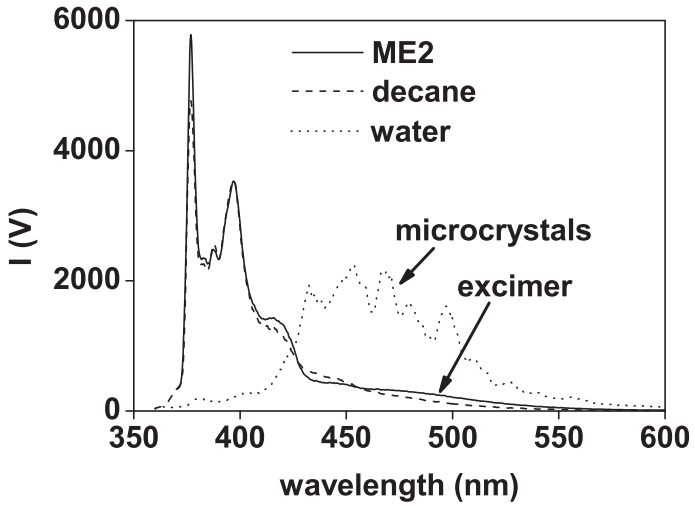

figure 4.1 Fluorescence emission spectra (λ_{exc} = 350 nm) of the pyrene butyric acid stearyl ester in ME2 (straight line), in decane (527 μM) (dashed line) and in water (434 μM) (dotted line). The dye is not soluble in water and only microcrystals can be observed (intensity multiplied by a factor of 10). In the quaternary ME the pyrene ester forms excimers ([n] = 1.3; this corresponds to [P]/[Dec] ~ 1 : 4600) and a broad emission intensity at higher wavelength than the monomer emission can be detected

We chose the fluorescent probe pyrene butyric acid stearyl ester whose water solubility should be between that of dodecylpyrene and the triglyceride derivative. From that we can identify the pyrene ester as suitable probe if the observed relaxation rates in our experiments exceed 10^{-1} s^{-1}. Upon excitation the pyrene ester emits a blue "monomer" fluorescence in MEs that contain only a single probe. In ME aggregates that contain two (or more) probe molecules, pyrene excimer contributes a broad excitation band between 450 and 550 nm (figure 4.1). From fluorescence decay studies of micellar solutions with pyrene triglyceride, Rharbi et al. showed that the probe is characterized by a Poisson distribution in aqueous solutions of nonionic micelles. We assume similar behavior for our pyrene derivative [34] and performed stopped-flow fluorescence measurements for mixing two identical MEs, one with the fluorescent dye and one without, and monitored the decrease of the excimer signal, due to dilution, with time (chart 4.1, *Scheme I*).

The average number of probe molecules per ME aggregates, [n] was kept between 1.1 and 1.3 and the intensity decay curves were fitted with a mono-exponential function to yield the apparent first order rate constant, k_{obs}. MEs containing three (or more) probe molecules require multiple exchanges with empty aggregates to produce MEs containing a single dye. This results in multiple exchange and would complicate the kinetics formalism describing the state of the system during this exchange [35]. The intensity decay curves could than not be fitting with a mono-exponential. Therefore kinetic curves exhibiting mono-exponential decays give confidence about the adjustment of experimental parameters.

4.3 Results and Discussion

4.3.1 Phase behavior

In the introduction the phase diagram of the quaternary system 100 mM TDMAO/hexanol/decane/water was described in detail already (figure 1.1). The blue region denotes the extended isotropic channel of O/W-ME. This L_1-phase contains ME droplets of spherical shape with a maximum size and perfect sphericity at the upper solubilisation limit (emulsification boundary). The concentration of ME droplets from the ternary system at 36 mM decane to the maximum solubilisation capacity at 130 mM hexanol and 1200 mM decane ranges from 1064 - 15 µM. Values of the droplet concentration were calculated determining N_{agg} from the radii calculated from SANS measurements published by Gradzielski et al. [61] with equation 3.2; division of [TDAMO] by N_{agg} gave [Agg].

Because of this change of concentration over two orders of magnitude the quaternary system TDMAO/hexanol/decane/water is very suitable for studying the kinetics of formation of MEs. An additional task was to study the influence of charge introduced in the system. It has been reported before [57, 107], that the size and shape of quaternary MEs based on TDMAO remain constant over the whole existence region of the L_1-phase

upon the substitution of small amounts of up to 5 mol% of the nonionic surfactant by the cationic surfactant TTAB. The influence of the amount of solubilised oil and added charge introduced into the system on the solubilisation kinetic will be discussed in detail in the following.

table 4.1 Composition of the samples in water employed for kinetic measurements investigated by turbidity, fluorescence and SANS experiments, volume fraction Φ (surfactant, cosurfactant, hydrocarbon) radii of the ME aggregates (radii of ME1 and ME2 determined with d_{22}-decane in D_2O [61], radius of ME3 extrapolated from the linear dependence of the radii in [61] versus the concentration of decane), the concentration of microemulsion droplets [Agg] and the sum $2\kappa + \bar{\kappa}$ of the bending constants, where κ is the mean bending modulus and $\bar{\kappa}$ the Gaussian modulus from Ref. [61]

	[TDMAO] (mM)	**[hexanol] (mM)**	**[decane] (mM)**	**Φ**	**R (nm)**	**[Agg] (μM)**	$2\kappa + \bar{\kappa}$
ME1	100.0	82.30	248.1	0.0652	6.33	136.8	2.37
ME2	100.0	105.0	400.5	0.0888	8.93	66.76	2.19
ME3	100.0	115.1	600.0	0.1193	12.8	30.33	1.96

4.3.2 Kinetics of the exchange of oil between microemulsions

4.3.2.1 Influence of amount of solubilised oil and temperature

In the first part of this work we will present results addressing the question of how fast the exchange of oil occurs between identically sized and composed (except for the fluorescence probe) microemulsion aggregates, i.e., the oil exchange as it occurs under equilibrium conditions. Subsequently we will discuss a possible correlation between the resistance to droplet coalescence and the monolayer properties. In chart 4.1 (*Scheme I*) a sketch of the stopped-flow experiment performed in fluorescence mode is given. By adding 1.1 - 1.3 molecules pyrene ester per aggregate to the solutions of ME1, ME2 and ME3, the exchange of the fluorescence probe (and thereby indirectly that of decane)

between the aggregates was monitored over time at 25, 26 and 27 °C. Due to the experimental conditions a pseudo-first order reaction can be seen and the fluorescence curve were fitted with a mono-exponential function to give observed relaxation rates k_{obs} of 3.626, 8.221 and 3.819 s^{-1} (at 25 °C) for ME1, ME2 and ME3 respectively. We estimated the exit rates for the pyrene ester between $4 \cdot 10^{-4}$ - 10^{-22} s^{-1}. This value for the monomer diffusion of probe through the water phase is lower than the exchange rates determined for the quaternary MEs. We conclude, that k_{obs} is indeed represents the exchange of solute due to fusion of two microemulsion aggregates.

a) *Scheme I*

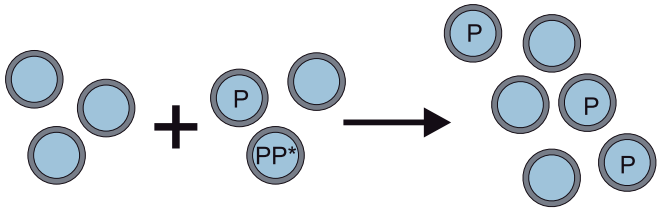

b) *Scheme II*

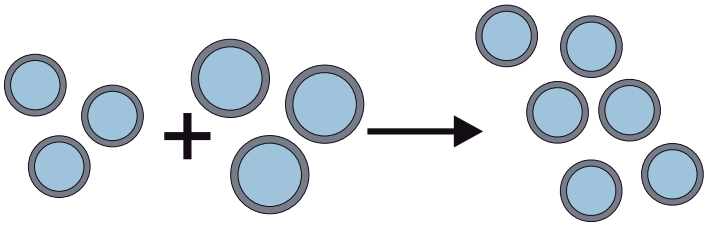

c) *Scheme III*

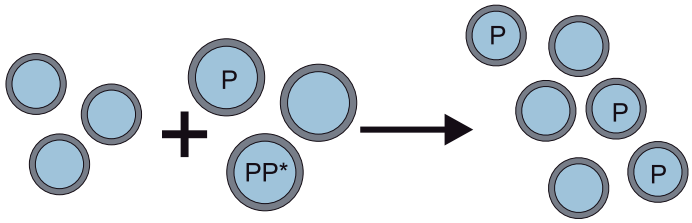

chart 4.1 Schematic drawing of the mixing processes employed in this chapter: a) *Scheme I*: stopped-flow fluorescence measurements as in b) but for mixing identically composed and sized microemulsion droplets with one sample containing a fluorescent probe P therefore exhibiting an excimer (PP^*) intensity at longer wavelength than the monomer signal. b) *Scheme II*: stopped-flow fluorescence measurement of the equilibration of MEs, 1:1 mixing of O/W microemulsions of different concentration of cosurfactant and oil and therefore different size fluorescence probe as in a); c) *Scheme III*: stopped-flow transmission/SAXS measurements with identical mixing process as in b) without fluorescence probes; this is only a schematic drawing monitoring the most important mixing step naturally followed by a cascade of additional steps

The coalescence rate k_2 was obtained by division of k_{obs} with the concentration of aggregates bearing no fluorescent probe. This concentration is the sum of [Agg] from solution 2 and the fraction of MEs in solution 1 containing no probe molecules according to the Poisson distribution. Theoretical considerations were discussed in detail in Ref. [35]. For the current experimental conditions in the quaternary MEs the fraction of probe-free aggregates was estimated to be ~ 40%. The corrected values for k_2 are presented in figure 4.2 b (filled squares) as function of sum $2\kappa + \bar{\kappa}$ of the bending constants. As would be expected, the k_2 is lowest for ME1, being the smallest ME, exhibiting therefore the biggest resistance against fusion. By increasing the size of the aggregates, thereby decreasing $2\kappa + \bar{\kappa}$, the coalescence rate increases continuously from 2.9 to $12.3 \cdot 10^4$ $s^{-1} \cdot M^{-1}$. This trend reflects nicely the effect of the increasing hindrance to fusion caused by the decrease of cosurfactant content. The more cosurfactant in the ME aggregate, the softer the interface and the less energy is required to produce on encounter pair.

If every encounter between droplets resulted in solubilisate exchange, k_2 should be comparable with the collision frequency of droplets [23]. The diffusion-controlled rate constant, k_{DC}, is given by the Smoluchowski equation (equation 3.7). Comparison of k_{DC} with k_2 show that 1 in 60 000 – 280 000 encounters results in solubilisate exchange. This implies a rather high barrier to the fusion process and a free energy barrier to inter-droplet exchange ΔE_{eff} can be estimated from the ration of the rate constant for exchange relative to the value of k_{DC} from equation 3.8 which corresponds to the value expected in the absence of an energy barrier. Values for ΔE_{eff} are given as triangles in figure 4.2 and increase from 26.8 and 32.3 kJ/mol with increasing $2\kappa + \bar{\kappa}$. The higher the resistance against fusion, the more encounters are necessary for one successful collision. Consequently ΔE_{eff} is higher for the smaller ME with the stiffer interface.

a)

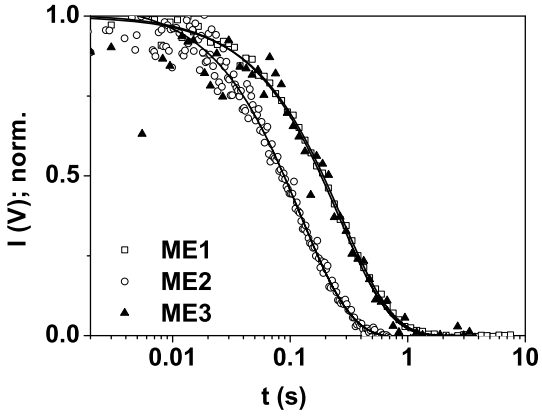

b)

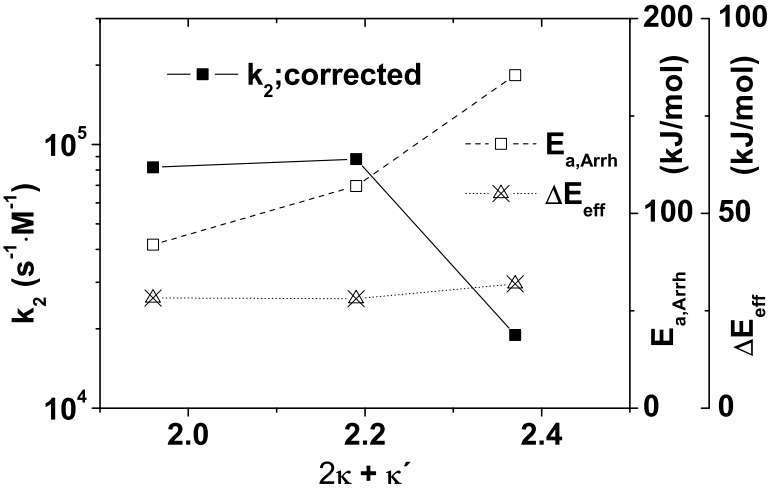

figure 4.2 a) Stopped-flow fluorescence measurements of the exchange of solubilisate between ME1, ME2 and ME3 with [n] = 1.1 - 1.3 at 25 °C. b) Second-order relaxation rates of the exchange of solubilisate between ME1, ME2 and ME3 as function of $2\kappa + \overline{\kappa}$. Rate constants (filled squares) were obtained from the mono-exponential fit of the pseudo-first order reaction displayed in a) and corrected by the fraction of aggregates in solution 1 bearing no probe molecule according to the Poisson distribution [35]. SF-fluorescence curves were derived according to chart 4.1 (*Scheme III*) monitored at λ_{em} = 435 - 600 nm with λ_{ex} = 350 nm. Arrhenius´ activation energy $E_{a,Arrh}$ (empty squares) was derived from measurements at three different temperatures (25, 26 and 27 °C). The effective activation energy ΔE_{eff} (triangles) was calculated comparing k_2 with the theoretical diffusion controlled relaxation rate

The activation energy $E_{a,Arrh}$ calculated from the temperature dependence of the rate constant increases similarly with decreasing droplet size (figure 4.2). This decreasing activation energy with increasing cosurfactant content may be explained by the different composition of the amphiphilic monolayer and the corresponding different spontaneous curvature. With increasing concentration of the cosurfactant the amphiphilic monolayer does not only become more flexible, as evidenced by the reduced value of $2\kappa + \bar{\kappa}$ (table 4.1, A figure 9.9), but also favors a less curved interface. Both should facilitate passing intermediate states in the fusion processes required for exchange of oil by a coalescence mechanism. In comparison one has also observed before in micellar kinetics that the presence of alcohols as cosurfactant leads to speeding up of the micellar kinetics [23, 108].

4.3.2.2 Influence of charge

All three MEs were charged with tetradecyltrimethylammonium bromide/TTAB by replacing 0.5, 1.0, 1.5 and 2.0 wt% of the zwitterionic surfactant with the ionic one. As was verified from the static SANS spectra (A figure 9.8), no influence of the charge to the size was detected in this range of charged system.

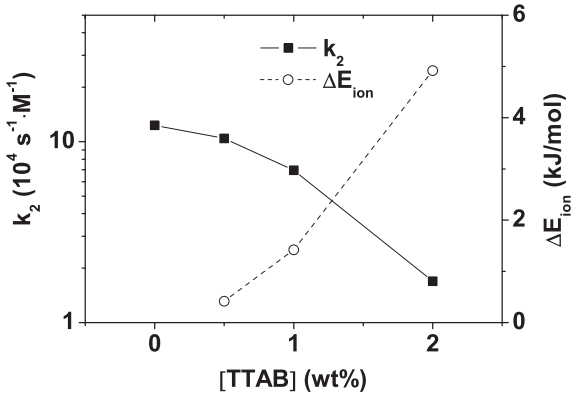

figure 4.3 Observed relaxation rates (squares) of the exchange of solubilisate of ME2 for various degrees of ionic substitution (chart 4.1, *Scheme I*). Additional activation energy (circles) due to electrostatic repulsion during the process of formation as function of charge introduced into the system (A table 9.2)

ME2 was modified with up to 2 wt% TTAB and stopped-flow fluorescence measurements were performed (*Scheme I*). The evolution of k_2 as function of the concentration of charge is presented in figure 4.3. The logarithm of the observed relaxation rate decreases by nearly on decade as the amount of TTAB is increases from 0 to 2 wt%. The exchange of decane between droplets is slowed down considerably as to be expected due to the electrostatic repulsion between the ME aggregates. This corresponds to an additional activation energy ΔE_{ion} of 0.4 kJ/mol for 0.5 wt% TTAB to 4.9 kJ/mol for 2.0 wt% TTAB (2.5 kT/wt% ionic surfactant) due to the electrostatic repulsion incurred by the presence of the ionic surfactant (as simply derived from the Arrhenius equation).

4.3.3 Kinetics of the equilibration of microemulsions

4.3.3.1 Influence of amount of solubilised oil and temperature

The second part of our kinetic study deals with the exchange of oil between differently sized and composed microemulsion droplets. Here we address the question: How does the difference in composition and the charge influences the solubilisation kinetics? As we showed above the quaternary system 100 mM TDMAO/hexanol/decane/water is quite suitable to study the kinetic of the equilibration of microemulsions. A very easy method is to choose MEs of different concentration and therefore different size along the isotropic channel and to study the kinetic of the 1:1 - mixture with time as illustrated in chart 4.1, *Scheme II* for transmission and *Scheme III* for fluorescence measurements. During the experiments in fluorescence mode the ME with the bigger particle size was loaded with 1.1 - 1.3 molecules of pyrene ester per aggregate.

The stopped-flow fluorescence measurement of the 1:1 mixing of the smaller ME1 with the bigger ME2 at 25 °C (*Scheme II*) is presented in figure 4.4 a). The excimer intensity value is ~ 1.31 V at t = 0 and decreases to a plateau of 1.20 V within one second. Due to

the experimental conditions a pseudo-first order reaction can be seen and the fluorescence curve was fitted with a mono-exponential function to give an observed relaxation rate k_{obs} of 5.69 s^{-1}, which is well above the maximum value for the diffusion of the pyrene ester through the water phase which we discussed earlier. The employed fluorescent probe does not leave the microemulsion aggregate and is therefore suitable to monitor the process of formation of MEs. Division of k_{obs} with the concentration of unloaded MEs (137 μM, which is in all cases [Agg] of the smaller ME) gave the second-order rate constant k_2 as $4.16 \cdot 10^4$ $M^{-1} \cdot s^{-1}$. From additional measurements at 26 and 27 °C an activation energy $E_{a,Arrh}$ of 82 kJ/mol was calculated by employing Arrhenius` equation.

Values of k_2 and E_a from the mixing of all three MEs, one against the other, are presented versus the difference of concentration of aggregates, $[Agg]_1$ - $[Agg]_2$ of the initial MEs are presented as filled circles in figure 4.4 d) (index 1: bigger ME; index 2: smaller ME). The logarithm of k_2 for the formation of middle-sized O/W-MEs in fluorescence mode shows an approximately linear dependence $[Agg]_1$ - $[Agg]_2$. In contrast, no direct correlation between $E_{a,Arrh}$ and $[Agg]_1$ - $[Agg]_2$ is observed. The experimental error for E_a of the three MEs is less than 10%, but one has to keep in mind, that every change in temperature will induce a shift in the phase diagram and therefore change the L_1-phase.

In figure 4.4 b, we present SF-transmission measurements (see chart 4.1, *Scheme I*) of identical mixing processes discussed in the paragraph above. Transmission curves were fitted with a second-order fit function as would be expected for this coalescence process. Division with the sum of $[Agg]_1$ and $[Agg]_2$ gave the coalescence rate constant k_2 (filled squares in figure 4.4). Just as k_2 from the fluorescence measurements, the relaxation rates shows a linear dependence on $[Agg]_1$ - $[Agg]_2$, thereby starting from a higher value at low differences in [Agg] and reaching identical values for high differences in [Agg]. The higher the distance of the initial MEs in the phase diagram the higher values of $[Agg]_1$ - $[Agg]_2$. During coalescence e.g. one small ME1 fuses with one bigger ME3. As [Agg] of ME1 is four times higher than for ME3, a high number of aggregates are left over after the first coalescence step. Hence, several steps of coalescence have to take place to build the final, middle-sized microemulsion aggregates. Obviously k_2 represents this increasing number of steps with increasing distance of the MEs to each other.

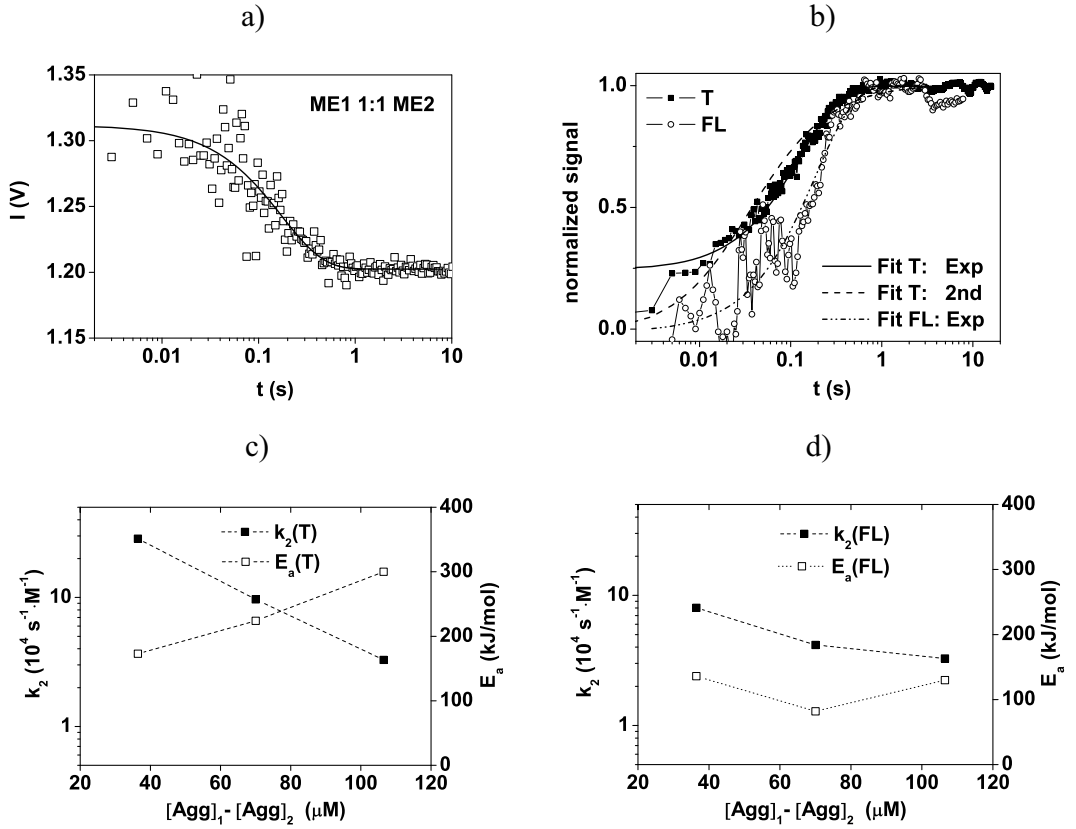

figure 4.4 a) Stopped-flow fluorescence measurements: 1:1-mixing of ME4 and ME2 (*Scheme II)* and the fit of the mono-exponential function at 25 °C. b) calculated second-order relaxation rates k_2 (filled symbols) and activation energies (empty symbols) of the formation of MEs from SF-transmission (squares) and –fluorescence (circles) measurements versus the difference of the concentration of aggregates, $[Agg]_1$ - $[Agg]_2$ of the initially present MEs, where the index 1 relates to the MEs with the lower concentration of decane and higher concentration of aggregates. Activation energy were derived from the relaxation rates at three different temperatures: for fluorescence measurements at 25, 26 and 27 °C, transmission measurements at 23, 25 and 27 °C

The same conclusion holds for the activation energy of the SF-transmission measurements. E_a also shows a linear dependence on $[Agg]_1$ - $[Agg]_2$. As would be expected, E_a is higher for the mixing of MEs whose starting point in the phase diagram is far away from each other when more steps of coalescence are required to reach equilibrium. Surprisingly E_a of both detection methods differ the more the higher the value of $[Agg]_1$ - $[Agg]_2$. For the mixing of M4 with ME3 the activation energy in transmission mode is even three times higher than for fluorescence.

4.3.3.2 Influence of charge

As we were interested in the effect of electrostatics on the formation of MEs we also performed SF-transmission and -fluorescence measurements in the system presented so far in which up to 2 wt% of the nonionic TDMAO was replaced by the cationic TTAB. In addition SF-SAXS measurements were carried out to gain more information about the structural changes during the mixing.

Stopped-flow fluorescence and transmission measurements

The experiment described in 3.3.1 was repeated according to *Scheme II* and *III* while increasing the amount of charge in the system. Fluorescence intensity decay and transmission curves were fitted with a first-order and second-order fit function, respectively, as described above and the resulting coalescence rates (squares for transmission, circles for fluorescence) as function of charge introduced into the system are presented in figure 4.5 a).

The relaxation rate in transmission mode decreases exponentially from $9.65 \cdot 10^4$ $M^{-1} \cdot s^{-1}$ for the non-charged system to $2.68 \cdot 10^4$ $M^{-1} \cdot s^{-1}$ with 2 wt% TTAB (squares in figure 4.5 a). As already depicted in the exchange kinetics, the introduction of charge into the ME shell has a great impact on the kinetic in our ME system. In case of the formation process the electrostatic repulsion leads to a slowing down of the formation by a factor of 4 accompanied by an additional activation energy ΔE_{ion} of 0.9 - 3.2 kJ/mol (1.5 kT/wt% ionic surfactant) (squares in figure 4.5 b) calculated with equation 3.8.

The activation energy from transmission measurements at 23, 25 and 27 °C show no systematic trend. E_a with 2 wt% TTAB is 216 kJ/mol; this value is nearly identical to 224 kJ/mol found for the uncharged coalescence process. The energy derived from temperature dependent measurements is obviously a much more complex value that might e.g. include slight changed in [Agg] and does not solely represent the energy required during the coalescence of ME droplet. For that purpose we employ ΔE_{ion} as the more meaningful factor describing the influence of the charged surfactant layer on the coalescence process.

a)

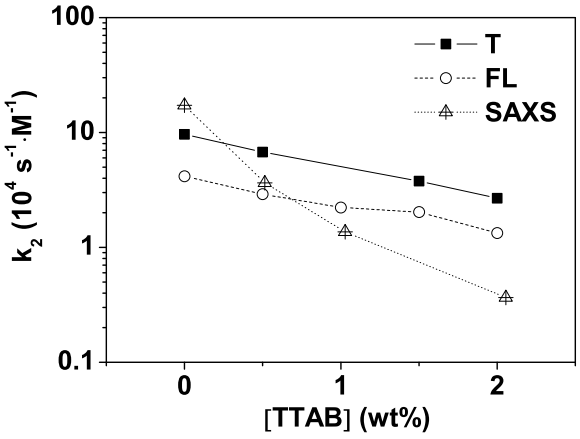

b)

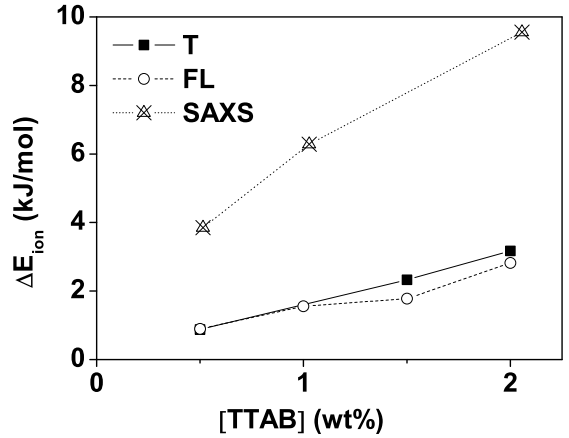

figure 4.5 Comparison of SF-measurements with different complementary methods of detection; transmission = square, fluorescence = circle, SAXS = triangle a) observed relaxation rates of the formation of MEs from the mixing of ME1 1:1 with ME2 for various degrees of ionic substitution. b) Calculated additional activation energy due to electrostatic repulsion during the process of formation

Stopped-flow fluorescence measurements gave relaxation rates k_2 and additional activation energies presented as circles in figure 4.5 a and b. Coalescence rate k_2 exhibits the same tendency as observed with transmission measurements, apart from a symmetric shift of k_2 to lower values, meaning the process of formation is a little bit faster for transmission measurements. This could very well be due to the difference kind of change

in signal of both methods. The excimer intensity in fluorescence measurements decrease only if the solubilisate between both aggregates exchange. This means that two MEs have to diffuse towards one another, the interfaces must stick together and form a channel through which the oil can exchange. For transmission measurements the turbidity increases earlier, i.e. in the moment both ME aggregates touch.

Nevertheless values of ΔE_{ion} are identical within experimental error for both detection modes. From this comparison we conclude that the influence of charge on the process of the formation of MEs, can be detected either with fluorescence or with transmission spectroscopy. Concerning k_2, both methods detect the same event during the process of formation of quaternary microemulsions and now it is possible to choose the more advantageous detection depending on the properties of the aggregates. In principle it is easier and less time-consuming to perform stopped-flow transmission measurements. In cases of high charges on the surface or low radii of the MEs, the amplitude increases dramatically and no kinetic data can be obtained. In that case the (nearly) identical parameter can be achieved by stopped-flow fluorescence measurements.

Stopped-Flow SAXS measurements

Small angle X-ray scattering experiments are a useful tool to obtain insight into structural transitions during kinetic investigations. We performed stopped-flow SAXS measurements on the same system discussed in the passage above and compared the parameters obtained with the two other detection methods. The scattering is best depicted by plotting $I(q)\cdot q^2$ versus q, as done in figure 4.6. The scattering pattern right after the closure of the hard stop (filled squares) is that of very polydisperse spheres with a smeared minimum at $q \sim 0.8\ nm^{-1}$. At $t = 0.015\ s$ the minimum becomes more pronounced indicating the particles size becomes much more well-defined. Between 0.239 and 9.127 s the minimum at mid-q-range becomes much more pronounced, indicating increasing monodispersity of the spherical aggregates present (due to the formation of a homogeneous size distribution after starting from two differently size populations (*Scheme III* in chart 4.1).

It is difficult to see changes in the intensity during the measurement. Therefore the evolution of the normalized scattering intensity at low q (q = 0.07973 nm^{-1}) as function of time is presented in figure 4.7 a) and fitted with a second-order function. The observed relaxation rate from the second-order fit was 35.1 s^{-1} for the uncharged system (ME2 1:1 ME1). By division with the sum of $[Agg]_1$ and $[Agg]_2$ we calculated a coalescence rate of $17.2 \cdot 10^4$ $M^{-1} \cdot s^{-1}$. By increasing the amount of charge in the system to 2 wt%, the kinetic is slowed down considerably. The normalized intensities at low q are displayed in figure 4.7.

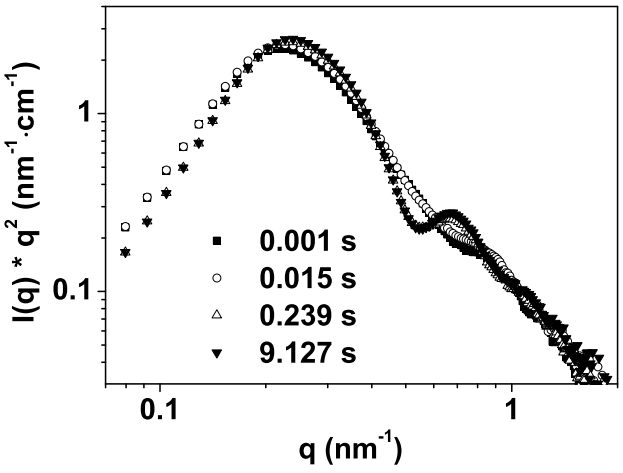

figure 4.6 Plot of $I(q) \cdot q^2$ versus q for the SAXS patterns taken at various times after mixing ME1 1:1 with ME2 (at 25 °C)

The calculated relaxation rates and additional energies due to the charge for the process of formation are illustrated as triangles in figure 4.5 a) and b) respectively. Between 0 and 2 wt% TTAB k_{obs} decreases by a factor of 10 and thus much faster than deduced from the fluorescence and transmission measurements. Accordingly ΔE_{ion} derived from SAXS exhibits higher values and increases more strongly than for the two other detection methods. In general, relaxation rates derived from turbidity and SAXS measurements should represent identical processes during the formation of MEs. In contrary, values for k_{obs} are different in fluorescence mode. The reason why relaxation rates from turbidity and SAXS deviate for his quaternary system could be just due to different experimental conditions (flow rate, slight changes in sample composition, etc.).

The mixing of ME1 with ME2 is finished within a minute and the radii of the initially present MEs are quite similar. For this reason it is difficult to obtain any structural information of the coalescence process. Nevertheless, by fitting the SAXS curves in figure 4.7 a) with a model for spheres with a homogeneous size distribution for the fusion of two solutions with different particle size *(*one population with smaller and one with bigger particle size) we obtained the evolution of the polydispersity index, PDI with time (see figure 4.7 b). The PDI reaches a plateau at 0.16, indicating the formation of relatively monodisperse spherical aggregates of intermediate size. The relaxation rate for the PDI is 30.16 s^{-1}, a value nearly identical to k_{obs} obtained from the intensity at low q-range, which is 35.1 s^{-1}.

a)

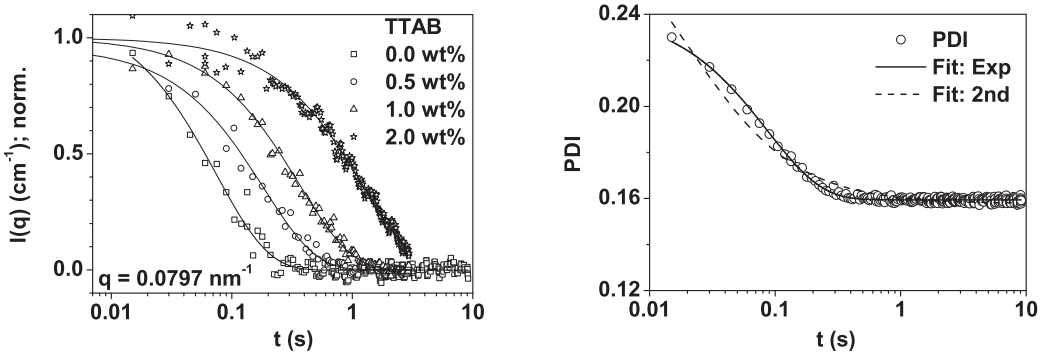

figure 4.7 a) normalized intensity at q = 0.07973 nm^{-1} over time for the 1:1-mixing of ME1 and ME2 and the fits of the mono-exponential function for various degrees of ionic substitution: squares, circles, triangles, stars correspond to 0.0, 0.5, 1.0 and 2.0 wt% TTAB. b) Evolution of the polydispersity index with time from a) from the fitting of the SF-SAXS curve with a model for homogeneous spheres (with two size populations)

In conclusion, we have presented arguments that by performing either stopped-flow fluorescence, transmission or SAXS measurements we receive relaxation rates and additional activation energies due to ionic repulsion in the same order of magnitude for all three detection methods when introducing charge into the system by replacing up to 2 wt% of TDMAO with TTAB.

4.4 Conclusions

In this chapter the dynamics of oil exchange in the quaternary O/W microemulsion system TDMAO/1-hexanol/decane/water as a function of the composition (and therefore droplet size) and for the case of introducing electrostatic repulsion into the originally uncharged system has been investigated. This was done by fast mixing experiments by means of the stopped-flow method. By this method two types of experiments were done; one in which identically composed and sized droplets were mixed and where the exchange of a fluorescence marker was followed, and the other where differently sized droplets were mixed to yield droplets of intermediate size and this process was followed by fluorescence, turbidity, and small-angle x-ray scattering (SAXS).

The latter two see basically the same process but SAXS allows following the exchange process with corresponding structural detail. In contrast the fluorescence experiment follows a pseudo first-order reaction and monitors the elementary exchange process, which is more directly related to the individual coalescence process, as due to the low solubility of decane in water the exchange has to occur via coalescence of microemulsion droplets.

The corresponding kinetic rate constants were determined for the three different detection methods for differently composed microemulsions and various mixing schemes. Conducting mainly stopped-flow fluorescence and transmission measurements we found very similar coalescence rates, k_2, in the order of $2.7 - 29 \cdot 10^4$ $M^{-1} \cdot s^{-1}$ for both processes. From that we conclude that the formation of MEs as well as the inter-pool exchange is based on the same mechanism: the fusion of two droplets to from a transient, droplet dimer followed by a break down into two separate droplets with randomization of solubilisates between aggregates, i.e, by coalescence processes.

By varying the concentration of solubilised oil, thereby varying the size of the microemulsion aggregates, we could show that the logarithm of k_2 depends linearly on the difference in droplet concentration of the two initial MEs during the formation process. This means that the exchange process is the slower the further away in the phase diagram the two starting solutions are located. The determination of the activation energy

from the temperature dependence of the rate constant gave a linear dependence on $[Agg]_1$ - $[Agg]_2$ as well. This demonstrates that for this process a multi-step exchange has to occur to yield the final new size distribution of microemulsion droplets.

For the case of exchange between identically sized droplets from the comparison to a diffusion controlled exchange reaction we find that only 1 out of 60 000 - 280 000 encounters leads to and effective exchange of oil of the aggregates. From this we can calculate the effective activation energy to be 27 - 32 kJ/mol for all MEs investigated. This activation energy becomes smaller with increasing content of the cosurfactant. However, with increasing cosurfactant content also the spontaneous curvature of the microemulsion is reduced as well as the bending rigidity of its amphiphilic monolayer. Apparently this correlates with the reduced activation energy and it is interesting to note that the change in activation energy is quantitatively very close to the formerly observed reduction of the bending energy of the monolayers. Apparently the resistance of the surfactant monolayers is the main component controlling the coalescence process required for droplet exchange.

Addition of charge by replacing up to 2 wt% of TDMAO with the cationic TTAB leads to a slowing down of both coalescence processes by about one order of magnitude. Apparently the coalescence of MEs is substantially hindered already by the presence of small amounts of ionic surfactant. This corresponds to an additional activation energy ΔE_{ion} of 1.5 - 2.5 kJ/mol due to the electrostatic repulsion incurred by the presence of 2 mol% of the ionic surfactant. From Arrhenius plots activations energies were determined both for the process of equilibration and the exchange of solubilisate. We obtained higher values for the first mechanism which we found quite reasonable since the former not only involves interpool-exchange of solubilisate but also a major redistribution of the surfactant monolayers from both different MEs.

In summary, experiments show that the stopped-flow technique is very suited also for studying coalescence processes in multicomponent systems. The main parameter determining the exchange rate is apparently the bending rigidity of the amphiphilic monolayer. Incorporation of an ionic surfactant slows down the kinetics of the inter-droplet exchange of solubilisate due to the higher activation energy caused by the electrostatic repulsion between the aggregates.

5 The kinetics of solubilisate exchange in a zwitterionic microemulsion on addition of hydrophobically end-capped poly(ethylene oxide)

Graphical Abstract

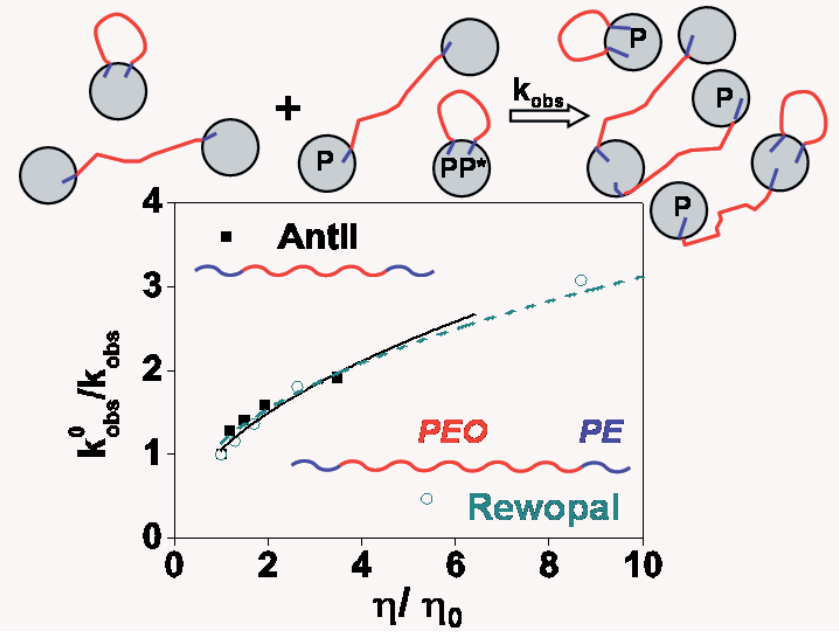

Abstract

We report the slowing down of the oil exchange kinetics of a zwitterionic microemulsion by addition of telechelic polymers of different length measured by stopped-flow fluorescence in which the disappearance of excimer was monitored over time. The employed additives are the hydrophobically-modified polymers Antil and Rewopal.

The exchange rate of solute for the pure microemulsion is 8.2 s^{-1} and decreases for both polymers to 2.932 s^{-1} and 2.67 s^{-1} when 1.6 wt% Antil and 0.5 wt% Rewopal (i.e. ~ 27 HM-polymers per aggregates) are added. At the same time, addition of the telechelic polymer to the microemulsion leads to a substantial increase in viscosity of one order of magnitude for Antil and two orders of magnitude for Rewopal (although the number of linking molecules is larger in the case of Antil). We attribute the slowing down to the steric hindrance of the mobility of the droplets due to the formation of a polymer network.

5.1 Introduction

In the previous chapter the influence of temperature, amount of oil and charge on the dynamics of oil exchange between ME droplet has been studied. In chapter 3 the retarding effect on the coalescence of HM-polymers on MEs in the ternary system with $C_{12}E_5$/oil/water has already been observed. In this chapter first the influence of the added polymer on the structure of the equilibrium solution of MEs presented in chapter 0 at various concentrations will be discussed. To obtain a so-called transient network, we will start from a monodisperse O/W-ME of a quaternary surfactant system and add amphiphilic polymers whose extremities will preferentially fix to the droplets. As amphiphilic polymers dioleyl- and distearyl-polyethyleneoxide compounds (R-EO_x-R) Antil and Rewopal with a length of the polyethylene oxide (EO) part of x = 55 (Antil) or 150 (Rewopal) were employed. Then we study the kinetic of the exchange of solubilisate between ME droplets by applying the stopped-flow fluorescence method. Finally a quantitative model will be presented based on the assumption of a network with finite mesh size, ξ that inhibits the diffusion of the microemulsion droplets and therefore the exchange of solubilisate.

5.2 Results and Discussion

5.2.1 Viscosity measurements

The addition of very small quantities of telechelic polymer to the microemulsion leads to a substantial increase in viscosity (see figure 5.1) of one order of magnitude for Antil and two orders of magnitude for Rewopal although the number of linking molecules is larger in the case of Antil. It has been reported that the ratio of molecules bridging two droplets depends on the ratio between the end-to-end distance of the hydrophilic part of the polymer and the interdroplet distance [109]. This ratio is larger in the case of Rewopal and consequentially the ratio of bridges for the same number of polymers per droplet will be also larger (table 5.1).

table 5.1 Molecular formulas and lengths of the ethoxy chain, L of the polymers used, calculated according to the Flory-Huggins-theory ($<R_{ee}^2> = 2PL$; $P_{EO} = 3.8$ Å) [110]

polymer	**structure**	$\langle R_{ee}^2 \rangle^{1/2}$ **(nm)**	$\langle R_{ee}^2 \rangle^{1/2} / R_{d-d}^{surf}$
Antil	$C_{18}EO_{55}C_{18}$	5.75	0.78
Rewopal	$C_{18}EO_{150}C_{18}$	9.5	1.29

The contribution of loops and bridges to the increase of viscosity is different. In the range of polymer concentration that we studied we assume that both configurations will be present. The increase of the viscosity due to the decoration of the droplets is due to an increase on the effective volume fraction and it depends linearly with the concentration. On the other hand, in the case of bridged droplets the viscosity increases due to the formation of a network and it is expected to grow exponentially with the concentration. Antil, the shorter polymer, will be preferentially forming loops and a bigger component of a linear increase with the concentration is observed. In the case of Rewopal it is rather an exponential dependence with the concentration.

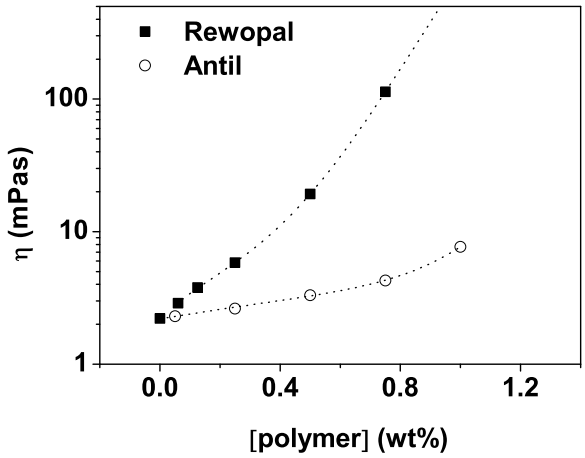

figure 5.1 Zero - shear viscosity as a function of the concentration for the Antil (circles) and Rewopal (squares) system at 25 °C

5.2.2 Kinetic of the exchange of solubilisate

In our kinetic study we performed stopped-flow fluorescence measurements of two identical ME, one with 1 molecule of pyrene ester, the other without the fluorescent probe. Increasing concentrations of Rewopal and Antil were added to the ME in each case. Due to the very fast increase of the zero-shear viscosity we were able to add 0.5 wt% Rewopal and 1.6 wt% Antil at a maximum. During stopped-flow measurements the intensity of the excimer over time was monitored; the intensity decay curves were fitted with a mono-exponential function to yield the apparent first order rate constant, k_{obs}. In figure 5.2 the intensity over time for the ME with 0.00 (square), 0.75 (circle) and 1.60 wt% (triangle) Antil are displayed. It can be seen clearly that the kinetic is considerably slowed down by increasing the polymer concentration. Straight lines denote the mono-exponential fitting curves which overlap the data very well.

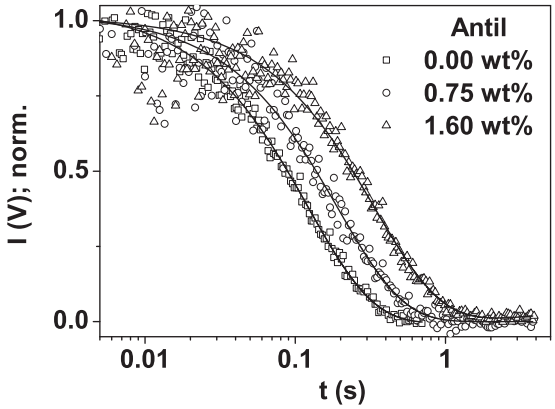

figure 5.2 SF-fluorescence normalized intensities of two identical ME (ME2: 100 mM TDMAO/105 mM Hexanol/400.5 mM decane) with 0.00 (squares), 0.75 (circles) and 1.60 wt% (triangles) Antil, one containing no probe, the other containing ~ 1 probe molecules per aggregate mixed 1:1. The excimer intensity of the excimer signal was monitored over time. Lines denote the mono-exponential fitting curve

The calculated values for k_{obs} as a function of the telechelic polymer concentration are presented as squares for Rewopal and circles for Antil in figure 5.3 a). The exchange rate for the pure ME is 8.2 s^{-1} and decreases for both polymers to 2.932 s^{-1} and 2.67 s^{-1} when 1.6 wt% Antil and 0.5 wt% Rewopal are added. Rewopal causes the same shift of k_{obs} with only one third of added mass. As this two telechelic polymers are identical in the nature of the A and B block and the length of the hydrophobic part, the difference observed in the kinetic measurements must be due to the length of the ethoxy chain that builds the water soluble middle block. From theoretical considerations discussed elsewhere [111] we can identify the pyrene ester as an eligible probe if the observed relaxation rates in our experiments exceed 10^{-1} s^{-1}.

From fluorescence decay studies of micellar solutions with pyrene triglyceride, Rharbi et al. showed that the probe is characterized by a Poisson distribution in aqueous solutions of nonionic micelles. We assume similar behavior for our pyrene derivative [34]. Values of k_{obs} exceed the minimum value by at least one order of magnitude and therefore give confidence that the decrease of the excimer intensity is the direct result of solute exchange through collision of two ME aggregates and not of monomer diffusion through the water phase.

a)

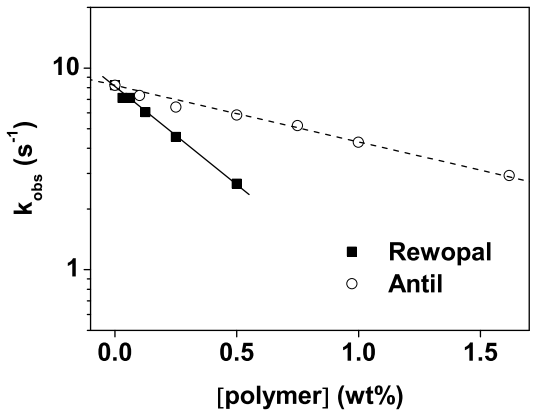

b)

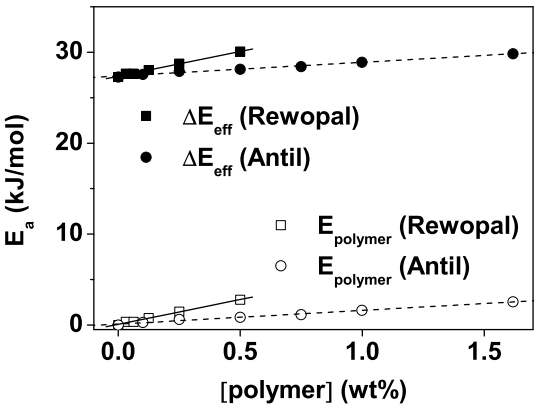

figure 5.3 a) observed relaxation rates of the exchange of solubilisate of the MEs with Rewopal (square) and Antil (circle). Relaxation rates were obtained from fitting SF fluorescence curves fitted with a mono exponential function. For the experiment identical volumes of a ME one without and one with probe were mixed in the stopped-flow device and the excimer intensity was measured at a function of time. b) Calculated effective activation energies (filled symbols) compared to the diffusion-controlled process and additional activation energies (empty symbols) due to the presence of the polymer in the ME. Lines denote the linear fit of the data (straight: Rewopal, dashed: Antil)

From temperature-dependent measurements at 25, 25.5 and 26.0 °C we calculated the activation energy, $E_{a,Arrh}$ for the particular exchange conditions. $E_{a,Arrh}$ for the pure ME is 114.4 kJ/mol. In the case of ME + Antil and Rewopal values range erratically between 80.3 - 134.2 and 74 - 114.4 kJ/mol and show no direct correlation to the polymer concentration.

The coalescence rate k_2 was obtained as k_{obs} /[Agg] with [Agg] = 66.7 μM for the ME. The exchange rate decreases from $12.3 \cdot 10^4$ $M^{-1} \cdot s^{-1}$ to $4.00 \cdot 10^4$ $M^{-1} \cdot s^{-1}$ for Rewopal and $4.39 \cdot 104$ $M^{-1} \cdot s^{-1}$ for Antil. This trend reflects nicely the effect of the increasing hindrance to fusion caused by the presence of the polymer. These values are substantially lower than the diffusion-controlled rate constant, $k_{DC} = 7.419 \cdot 10^9$ $M^{-1} \cdot s^{-1}$, calculated from the Smoluchowski equation (already presented as equation 3.3), which should be observed if every encounter between droplets resulted in solubilisate exchange. Comparison of k_{DC} with k_2 show that 1 in 169 000 - 185 000 encounters results in solubilisate exchange. This implies a rather high barrier to the fusion process and a free energy barrier to inter-droplet exchange ΔE_{eff} can be estimated from equation 3.5.

Values for ΔE_{eff} are given as filled symbols in figure 5.3 b) for Rewopal (squares) and Antil (circles) and increase from 27.28 kJ/mol for the pure ME to 29.84 with 1.6 wt% Antil and to 30.07 kJ/mol with 0.5 wt% Rewopal. Addition of Rewopal leads to a much steeper increase of ΔE_{eff} which would be expected since the hydrophilic block is more than twice as long as in the case of Antil. Hence, ΔE_{eff} represents the activation energy required for the coalescence of two ME aggregates much better than the values calculated from Arrhenius´ equation.

Comparing the energies for the exchange process from the system without and with additive, we calculated an additional activation energy, $E_{a,polymer}$ due to the presence of the telechelic polymer again calculated from Arrhenius´ equation and adapted like for the electrostatic case:

equation 5.1

$$\frac{k_{polymer}}{k_{obs}} = \frac{\tau_{obs}}{\tau_{polymer}} = exp\left(-\frac{E_{a,polymer}}{k \cdot T}\right)$$

In figure 5.3 b) values are presented as open symbols. At approximately equal ratio of polymer per ME, e.g. 0.25 wt% Antil and 0.50 wt% Rewopal, $E_{a,polymer}$ is 2.79 kJ/mol for Rewopal. This value is 4.5 times higher than that of Antil.

5.3 Discussion

It is expected that the polymer molecules adsorb onto the surfactant monolayer with their hydrophobic block (sticker). At shorter ethoxy chain length and longer interparticle distance, both ends stick to one ME and loops should be formed. At longer ethoxy chain length and the same interparticle distance (as would be true in our experiment), there is a possibility that the stickers form a bridge between two ME droplets, which would correspond to a single bond if we visualize the ME aggregates as "atoms" and the polymers as "bond" [93]. Accordingly at higher polymer concentration also multiple bonds are formed and the viscosity increases rapidly due to the fast formation of a transient network. The longer ethoxy chain of Rewopal with 150 EO-units does not only cause more steric repulsion due to the longer sticker chain length at similar number density but also form bridges between the ME droplets faster than in the case of Antil.

The effect of viscosity on the kinetics has been reported before. Schlarb-Ridley et al. [112] studied the reaction between cytochrome *f* and plastocyanin and the impact of low and high molecular mass viscogens. They observed a strong dependence of the rate of reaction on solvent viscosity. According to Stokes´ law, the diffusional rate constant is inversely proportional to viscosity and the reaction therefore should be slowed down with increasing η. By applying the stopped-flow method they found a strong increase of the relative second-order rate constant, k_2/k_2^0 with increasing relative viscosity, η^0/η with a slope greater than 1 which has been observed by some authors before [113, 114]. A feature that was attributed to an activation controlled-process according to Kramers´ theory [115] as opposed to the diffusional-case where the slope would yield a value of 1. Schlarb-Ridley obtained almost identical curves for the three low-molecular mass viscogens glycerol, ethane diol and sucrose. The other two compounds, ficoll 70 and dextran 70, had no influence on in k_2/k_2^0 within the observed range of concentration by increasing the viscosity to a similar extent. In the first case they concluded that k_2 of the reaction between cytochrome *f* and plastocyanin depends on two processes occurring in series which proceed activation-controlled. In the latter case they suggested non-uniform solutions of bulk solution due to associated thickeners and free solution, where the reacting protein molecules could diffuse unhindered.

equation 5.2

$$\frac{k_{obs}^{0}}{k_{obs}} = A\left(\frac{\eta}{\eta^{0}}\right)^{x}$$

In the present case, such a plot (figure 5.4) also gives a slope greater than 1, which is according to Kramers´ theory corresponds to an activation-controlled process [115]. This is in correspondence to our calculated value of an effective activation energy that has to overcome because of the non-diffusional behavior. Fitting the results to equation 5.2 gives a value for x = 0.44 for Antil and 0.50 for Rewopal an observation which has been reported before in protein reactions [116, 117] and which was attributed to a partial shielding from the frictional effects of solvent by the protein matrix [112, 116, 117].

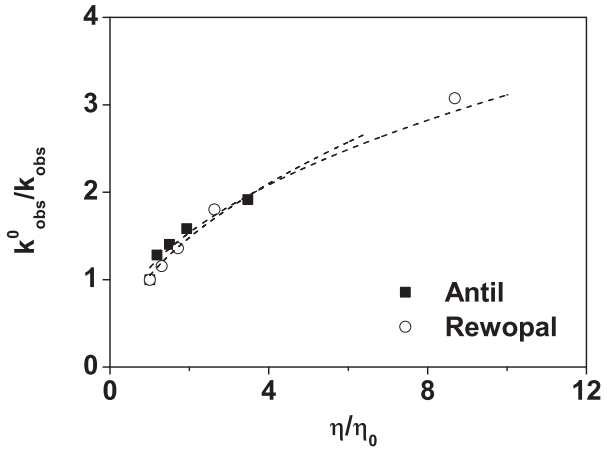

figure 5.4 Effect of the reciprocal relative viscosity of the solution on the relative observed rate k_{obs} for Antil and Rewopal (squares and circles). The experimental data were fitted to equation 5.2. Dashed lines are fits to the data

The main problem of this approach is that equation 5.2 comes from the Smoluchowski equation assuming that the viscosity of the medium is no longer the viscosity of the solvent but the viscosity of the polymer matrix. Another theoretical approach is to consider the slowing down of the diffusion of the droplets due to steric hindrance as proposed by de Gennes [118, 119] who stated that the retardation factor should obey a scaling law:

equation 5.3

$$\frac{D}{D_0} = exp\left[-\left(\frac{d}{\xi}\right)^{\delta}\right]$$

where d is the size of the droplets and ξ is the mesh size and δ is 2 for non cross-linked systems. Assuming that the correlation length scales as $\xi \sim N^{-1/2}c^{-1/2}$, the decrease on the kinetic rate constants should scale as d^2Nc.

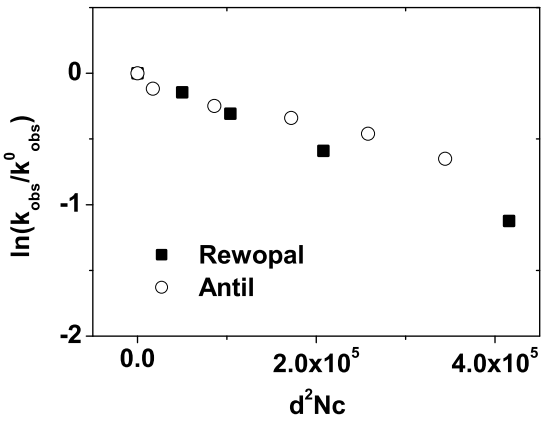

figure 5.5 Natural logarithm of k_{obst}/k^0_{obst} as a function of d^2Nc

In contrary to the assumption of Schlarb-Ridley of a non-uniform solution and in agreement with earlier publications we propose the existence of a transient, homogeneous network [109] with a polymer-induced transition from randomly to locally ordered droplet arrangements [94] for all types of thickeners independent of their nature and chain lengths. Accordingly, to our opinion the rate constant is only affected by the ratio of hydrophilic polymer chain length and interparticle distance.

If multiple bridging between aggregates is permissible, the homogeneous solution consists of "cubes", where the A-blocks of the HM-polymers form the edges and the ME droplets the corners. At high polymer concentration the distance between MEs is equal to the chain length of the EO-chain, L; at lower concentrations the edge length, d is bigger than L.

In that case, the viscosity experienced by the ME droplet is low and the exchange of oil is fast. From geometrical consideration the following relation holds:

equation 5.4

$$d = \xi = \sqrt{\frac{3 \cdot m_{polymer}}{L \cdot \rho_{polymer} \cdot \Phi_{polymer}}}$$

where $m_{polymer}$ is the mass of the polymer per "cube", $\rho_{polymer}$, the density of the and $\Phi_{polymer}$, the volume fraction of polymer in the ME solution. Visualizing the diffusion of the droplets within the polymer cage, the edge length, d would correspond to a mesh size, which we donate as ξ and which should be correlated to the kinetic rates.

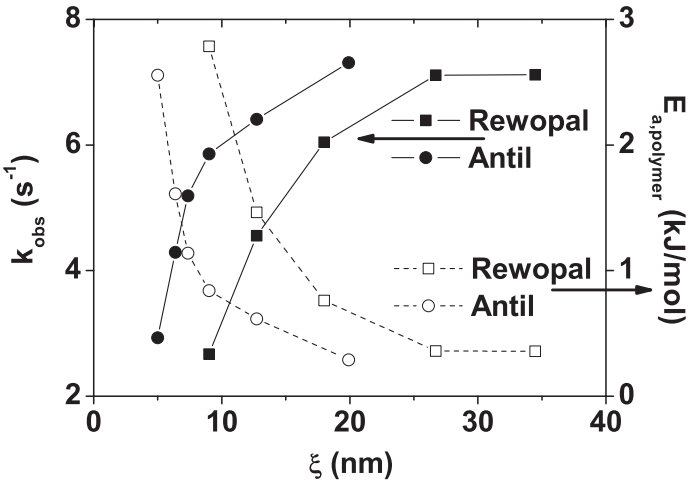

figure 5.6 Observed relaxation rates of the exchange of oil (filled symbols) and additional activation energies (empty symbols) due to the presence of Antil (square) and Rewopal (circle) in the quaternary ME with TDMAO/hexanol/decane/water at 25 °C versus the mesh size of the polymer network

In figure 5.6 k_{obs} and $E_{a,polymer}$ are displayed as function of the estimated mesh size. Both parameters show the same trend and absolute values are quite similar but do not superimpose as we would have expected. At identical values of ξ, Rewopal is slower and consequentially more energy is required for the coalescence of two ME droplets.

5.4 Conclusion

In chapter 4 the kinetics of the exchange of oil between microemulsion aggregates of the quaternary system described in chapter 3 are presented as function of added telechelic polymers measured by stopped-flow fluorescence in which the disappearance of excimer was monitored over time. The employed additives are amphiphilic polymers Antil and Rewopal. Increasing the concentration of additive up to ~ 27 molecules per aggregate, the exchange rated decreased from 8.2 s^{-1} for the pure microemulsion to 2.932 s^{-1} and 2.67 s^{-1} when Antil (1.6 wt%) and Rewopal (0.5 wt%) were added.

At the same time, addition of the telechelic polymer to the microemulsion leads to a substantial increase in viscosity of one order of magnitude for Antil and two orders of magnitude for Rewopal, although the number of linking molecules is larger in the case of Antil. Therefore the existence of a transient, homogeneous network with a polymer-induced transition from randomly to locally ordered droplet arrangements was proposed for all types of thickeners independent of their nature and chain lengths The slowing down was attributed to steric hindrance of the mobility of the droplets due to the polymer network. It was shown that the rate constant for oil exchange is only affected by the ratio of hydrophilic polymer chain length and interparticle distance.

In the previous three chapters the dynamics of the exchange of oil and the formation in ternary and quaternary ME system were studied with respect to temperature, length of the alkyl chain of the hydrocarbon and the concentration of solubilisate. In addition the effect of additives, i.e. charge and polymer, resulting in a pronounced slowing down of the coalescence has been studied in detail.

6 Solubilisation of different medium chain esters in zwitterionic surfactant solutions – effects on phase behavior and structure

Graphical Abstract[1,2]

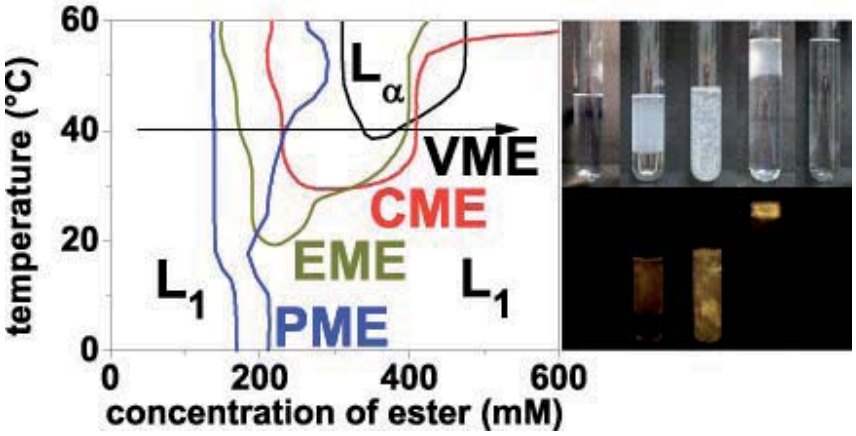

[1] Parts have been published in modified form as: A. Barth, I. Grillo, M. Gradzielski, Tenside Surf. Det. 2010, 47, 300

[2] parts have been published in modified form as: A. Barth, S. Prevost, J. Popig, M. Dzionara, G. Hedicke, M. Gradzielski Journal of Colloid and Interface Science; accepted

Abstract

The effect of solubilisation of methyl esters with different chains of medium length into the binary surfactant system tetradecyldimethylamine oxide/water was studied at a constant surfactant concentration of 200 mM. As esters we employed valeric, capronic, enanthic, and pelargonic methyl ester, thereby decreasing the polarity. Always a phase sequence L_1-L_α-L_1 is observed with increasing ester concentration, where the L_α-phase increases in extent and goes to much lower temperatures with increasing chain length of the ester. Viscosity measurements show a maximum at intermediate concentrations of additive that is independent of the type of ester. From SANS measurements detailed information about the structural changes occurring during the rod-to-sphere transition in the system of the shortest additive is deduced, which proceeds first through a pronounced rod growth. Interestingly, for the different esters an almost constant value of the volumic solubilisation capacity is observed, in agreement with the relatively constant interfacial tension. For the different esters no effect on the radius and the area requirement at the amphiphilic interface is observed at the solubilisation boundary. The microemulsions present here are spherical aggregates where the ester is partitioned between core and shell. From the SANS and interfacial tension data the effective bending constants of the surfactant monolayers were deduced and they show that the extension of the L_α-phase is directly related to a corresponding increase in the bending constants of the surfactant/ester monolayers.

6.1 Introduction

In chapter 4 the formation of zwitterionic MEs has been studied with respect to temperature, charge (introduced into the surfactant monolayer) and addition of polymer. In the following chapter the formation of bilayers, i.e. multilamellar vesicles in this case, in the ternary system TDMAO/ester/water will be investigated in detail. As already mentioned in chapter 1, one of the key properties of surfactants is their capacity to solubilise hydrophobic compounds such as oils, a property which is for instance of central importance for their application in detergency or pharmaceutical formulations. However, they are also able to incorporate more polar substances such as medium-chain alcohols, aldehydes [120] or ketones [121], carboxylic acids [61, 122] or isosorbides [123] which are less considered to be hydrophobic solubilisates but, if polar enough, may function as cosurfactants. Such polar compounds are typically not just located in the interior of micellar aggregates but also in the palisade layer and therefore modify the sate of aggregation by shifting the packing parameter. Esters with chains of medium length are positioned somewhere between these extremes with respect to their polarity.

They are also more flexible with respect to tuning their amphiphilic properties as the alkyl chains of acid and alcohol part can be varied separately. Accordingly their phase behavior is more complex as they may possess at the same time the properties of a cosurfactant and of a solubilisate. In addition, the balance between these two characters may in depend strongly on temperature and concentration, and, of course, on their detailed molecular architecture. Typically the solubilisation capacity of aqueous surfactant solutions for oils is rather low and for most surfactants limited to a fraction of an oil molecule per surfactant molecule [124]. This applies in particular to ionic surfactants where the solubilisation capacity normally has to be raised by the addition of a cosurfactant in order to form microemulsions [125-127]. In contrast, for nonionic surfactants often one observes much larger solubilisation capacities that can be tuned by changing the temperature [54, 55, 128].

The solubilisation of hydrocarbons leads to a rod-to-sphere transition that occurs at the higher oil concentration the shorter the chain length of the hydrocarbon [129]. For the case of hydrocarbon solubilisation it is interesting to note that also the formation of

isotropic microemulsion gels of cubic structure can be induced, which contain a molar ratio of surfactant / oil of 2-6, depending on the chain length of the oil and decreasing with shorter oil chain length [130, 131]. In contrast, the solubilisation of medium chain alcohols leads first to an elongation of the rodlike micelles and then to the formation of lamellar phases, either in the form of multi-lamellar vesicles (at lower alcohol content) or planar lamellae [132]. Just before reaching the solubilisation capacity then an L_3-phase is observed [43]. In addition, for alkylamine oxides one observes a large increase of the solubilisation capacity for conventional oils upon addition of cosurfactants but already without they can incorporate some amounts of oils [133]. This property renders them interesting surfactants not only for practical applications in detergency [134, 135] but also for a systematic study of the effect of the polarity of the solubilisate on its solubilisation properties.

Previous investigations on the zwitterionic surfactant tetradecyldimethylamine oxide (TDMAO) with respect to the solubilisation of the ester methyl heptanoate (EME) have shown that it can solubilise rather large amounts of that ester and form a low-viscous microemulsion phase at high content (molar ratio ester/surfactant $\approx$ 2:1) of EME. However, at lower ester content (for a molar ratio of about 1:1 of EME/TDMAO) a lamellar phase of multilamellar vesicles is formed, which is relatively sensitive to changes in temperature and vanishes for temperatures below 20 °C [136, 137]; then a microemulsion is formed. Apparently this ester shows a phase behavior in between that observed for alcohols and hydrocarbons. Very similar observations have been reported for the addition of hexylacetate or hexylmethylketone, which first behave like cosurfactants and then like hydrocarbons [74]. That interesting behavior will be generalized in this study with respect to the behavior of various esters that differ in the chain length of the acid and with respect to its relation to the bending elasticity of the amphiphilic interface.

In this chapter the effect of the polarity of the solubilisate on the surfactant system will be studied in more detail and the question of how the phase behavior and formed microemulsions are affected by that will be addressed. For that purpose, methyl esters of carboxylic acids of various chain lengths - from pentanoic to nonanoic - were employed, thereby modifying polarity and amphiphilicity of this added oil in a systematic fashion.

For these systems the phase behavior will be presented, as well as viscosity and interfacial tension measurements. These investigations were complemented by small-angle neutron scattering (SANS) experiments and measurements were performed at a surfactant concentration of 200 mM. From the systematic variation of the ester length an insight into the relation between the mesoscopic structure and the type of ester employed should be gained.

6.2 Experimental

Analysis of SANS data

Model-free analysis of SANS data

The SANS curves were first analyzed using a model-free analysis. Porod's law (equation 6.1) assumes a sharp interface at high q and was used to evaluate the incoherent scattering background I_{inc} as well as the specific interface Σ (= S/V).

equation 6.1

$$I(q) = I_{inc} + 2\pi(\Delta SLD)^2 \Sigma q^{-4}$$

where ΔSLD is the contrast (difference between the scattering length densities) between the micelles and the solvent.

Guinier's law (equation 6.2) can be applied to extrapolate the low q data (for $qR_g << 1$):

equation 6.2

$$I(q) - I_{inc} = I_0 \, exp\left(-\frac{R_g^2}{3} \cdot q^2\right)$$

For spheres $R = \sqrt{5/3} R_g$. With the help of equation 6.2, the intensity can be extrapolated to q = 0, I_0, and this value is given by:

equation 6.3

$$I_0 = \phi \langle V \rangle (\Delta SLD)^2 S(0) + I_{inc}$$

which allows to deduce the average particle volume <V> (Φ, S(0), and I_{inc} being the volume fraction, the structure factor at q = 0, and I_{inc} the incoherent background scattering, respectively).

The invariant Inv was used to check the validity of the data as explained in the following. The theoretical invariant for a system composed of two phases is given as:

equation 6.4

$$Inv = 2\pi^2 (\Delta SLD)^2 \phi (1 - \phi)$$

The experimental invariant can be calculated according to:

equation 6.5

$$Inv = \int_0^\infty I(q)q^2 dq$$

and is practically evaluated using the Guinier approximation for extrapolation between 0 and q_{min} and the Porod approximation between q_{max} and ∞. Both invariants should be equal if the two phase assumption holds and the volume fractions are correct.

Combining equation 6.4 and equation 6.5 we find a relation leading to the so-called Porod volume (or correlation volume):

equation 6.6

$$V_P = \frac{2\pi^2}{Inv}(1-\phi)\frac{I_0}{S_0}$$

The Porod volume can then be compared to the volumes gained from fits with appropriate models thereby validating the structural picture.

Modelling of SANS data

For monodisperse interacting homogeneous particles the intensity is given as [138]:

equation 6.7

$$I(q) = \phi\langle V\rangle(\Delta SLD)^2 P(q)S(q) + I_{inc}$$

with I_{inc} the incoherent scattering, ϕ the volume fraction of aggregates, Φ their volume, ΔSLD the contrast between the micelles and the solvent, the form factor P(q) with P(0) = 1 and the structure factor S(q).

In our case the form factor was represented by homogeneous micelles, either rotational ellipsoids, or polydisperse spheres (for highly swollen micelles close to the phase separation). The form factor for spheres is:

equation 6.8

$$P_{sph}(q) = \left(3\frac{sin(qR) - q\cdot R\cdot cos(qR)}{(qR)^3}\right)^2$$

For uniaxial ellipsoids with equatorial semi-axes R and rotational semi-axis $R\nu$ the form factor is given as:

equation 6.9

$$P_{ell}(q) = \frac{2}{\pi}\int_0^{\pi/2}\left(3\frac{j_1\left(qR\sqrt{\sin^2\varphi + \nu\cos\varphi}\right)}{qR\sqrt{\sin^2\varphi + \nu\cos\varphi}}\right)^2 \sin\varphi\, d\varphi$$

Where j_1 is the first order spherical Bessel function $j_1(x) = (\sin x - x\cos x)/x^2$.

For the case of polydisperse spheres we employed a Gaussian for the size distribution f(R) over the radius and evaluated the scattered intensity as:

equation 6.10

$$I_{sph}(q) = \phi\cdot(\Delta SLD)^2\cdot\int_0^{\infty} f(R)\cdot\left(\frac{4}{3}\pi\cdot R^3\right)^2\cdot P(q,R)\cdot S(q)\cdot dR$$

In all cases the analytical hard sphere structure factor S(q) according to the Percus-Yevick approximation [139] was employed. For ellipsoids the effect of ellipticity was neglected and the hard sphere radius was taken as proportional to the radius of the sphere of equivalent volume; the effective volume fraction entering the structure factor expression is given by the number density arising from the form factor.

In both cases S(q) used is the analytical expression of the solution of the Percus-Yevick equation for monodisperse hard spheres [139]. Note that S(0) is only a function of the effective volume fraction:

equation 6.11

$$S(0) = \frac{1 - 4\phi_{HS} + 6\phi_{HS}^2 - 4\phi_{HS}^3 + \phi_{HS}^4}{1 + 4\phi_{HS} + 4\phi_{HS}^2}$$

For the case of ellipsoids we used for the hard sphere structure factor the volume of the ellipsoid times a scaling factor that allows for incorporating a hydration shell into the effective hard sphere interaction. This scaling factor then went as cubic root into the hard sphere radius (as obtained for the sphere of identical volume as the ellipsoid) and was typically in the range of 1.03 - 1.07, thereby corresponding to a hydration layer of 2 - 4 Å. Above mentioned equation 6.11 was finally used to validate the reliability of our

fitting parameters (see supplementary part). The comparison of the Porod volume, V_p for all samples normalized to S(0) and the volume calculated from the fits matches well and confirms the output information of our fitting model.

6.3 Results and discussion

6.3.1 Phase behavior

The observed phase behavior for a constant surfactant concentration of 200 mM is summarized in figure 6.1 for the four different esters investigated. Generically all phase diagrams look similar but there are systematic trends that depend on the length of the alkyl chain of the ester. For the shortest chain oil (VME, figure 6.1 a) at room temperature only an isotropic L_1-phase is observed, which can incorporate up to 3.5 ester molecules per surfactant molecule. Only at elevated temperatures, i.e. above 38 °C, a birefringent vesicle phase is formed. As an example for the observed phase behavior some representative photos of samples of the VME system at 40 °C under normal light and between crossed polarizers are given in figure 6.2. For the lowest and highest concentration isotropic and clear solutions are observed. For a concentration of 350 mM VME a homogeneous and highly viscous but transparent sample (air bubbles do not rise here, i.e. the sample has a yield) is found that shows a birefringence pattern typically observed for densely packed multilamellar vesicles [10, 107, 128]. This vesicle phase borders in both concentration directions on an isotropic L_1-phase, being separated from it by a two-phase region with a turbid phase on top (figure 6.2).

Upon increasing the alkyl chain length of the ester one finds that the liquid crystalline vesicle phase is systematically shifted towards lower temperatures and lower ester concentrations (figure 6.1). For the case of EME one observes already at room temperature a separation of the L_1-phase into a lower and a higher concentration range part. For the case of PME the formation of the liquid crystalline L_α-phase becomes much more pronounced and now this vesicle containing L_α-phase separating the L_1-phase is

extending down to 0 °C while also becoming wider with respect to its concentration range.

At the same time the phase behavior is less dependent with respect to temperature. Apparently by increasing the chain length of the acid of the ester the tendency for stabilizing bilayers is substantially increased, i. e., the cosurfactant properties of the esters increase with increasing length of their alkyl chain. This is somehow similar to the case of medium chain alcohols, where the appearance of the lamellar phase is also observed the earlier the longer the chain length of the alcohol [140].

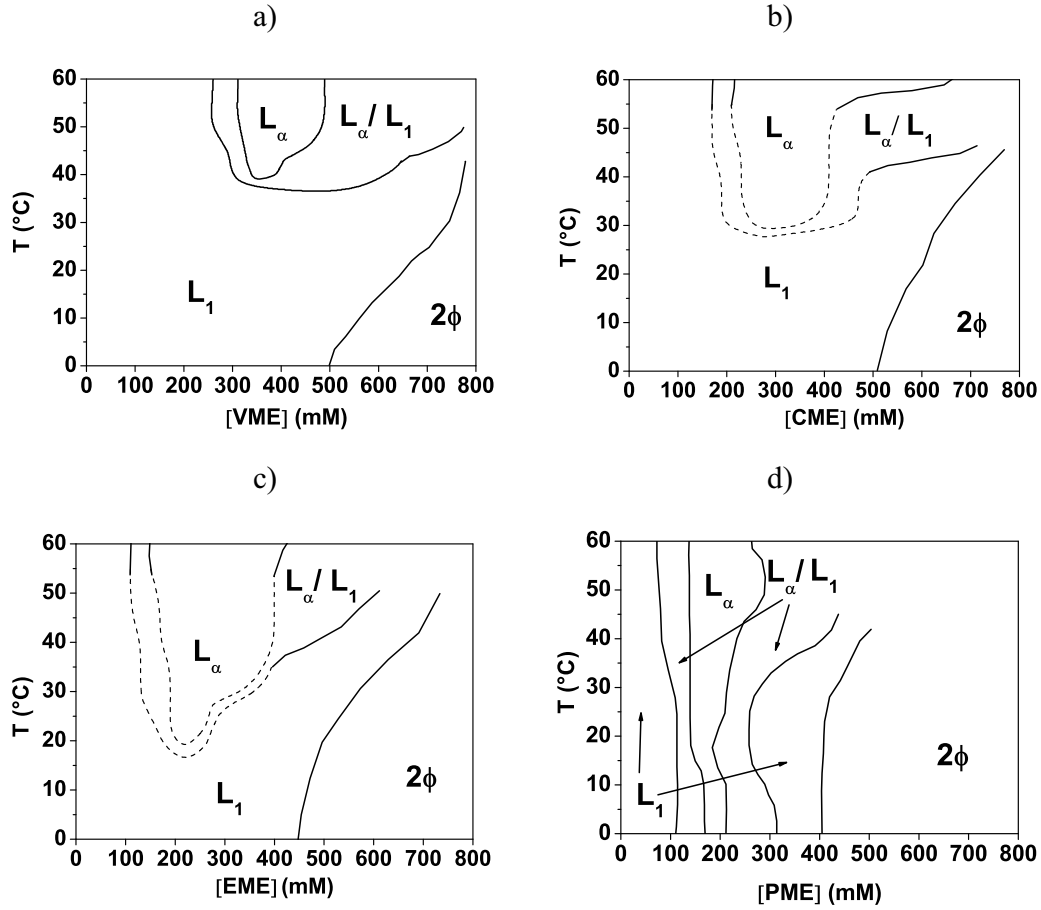

figure 6.1 Temperature-dependent phase diagrams for samples of 200 mM TDMAO as a function of the concentration of added alkyl methyl ester. a) valerian methyl ester (VME), b) capronic methyl ester (CME), c) enanthic methyl ester (EME), d) pelargonic methyl ester (PME); dashed lines in b) and c): data taken from Ref. [63]

With respect to the solubilisation capacity one finds that it is reduced systematically with respect to the number of ester molecules solubilised per surfactant molecule with increasing alkyl chain length of the ester (figure 6.3). There is roughly a linear decrease of this measure for the solubilisation capacity as a function of the alkyl chain length of the acid part of the ester, going down from almost 4 for VME to 2.2 for PME. However, if we compare the solubilised volumes of oil we obtain an almost constant value for the different esters. This means that the structural conditions of solubilisation are very similar for all esters.

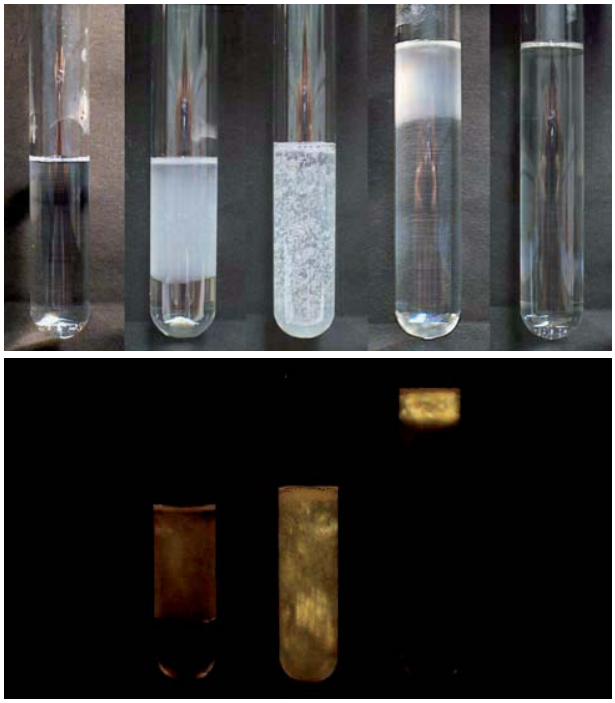

figure 6.2 Photographs of samples of the ternary system with VME at 40 °C. top: normal light; bottom: under crossed polarizers; from left to right: 100 mM , 300 mM, 350 mM, 500 mM, 650 mM ester, see figure 6.1 a

This can be explained by the fact that the solubilisation capacity in microemulsions is typically related to the interfacial tension [128, 141, 142]. For that purpose almost saturated microemulsions with the various esters were measured by means of the spinning drop-method against the pure ester at 25 °C. The interfacial tensions γ observed are relatively similar with values between 0.35 and 0.45 mN/m (see figure 6.3), showing a slight increase with increasing chain length. This explains the observed relatively

constant solubilisation capacities for the different esters, as the maximum size of the formed microemulsion droplets should be given by [85]:

equation 6.12

$$\gamma \cdot R_{max}{}^{2} = \frac{k \cdot T}{8 \cdot \pi \cdot p^{2}}$$

where R_{max} is the size of the microemulsion droplets at the solubilisation boundary, k the Boltzmann constant, T the temperature, and p (= $<R^2>/<R>^2 - 1$) the polydispersity index of the microemulsion droplets. Accordingly for similar interfacial tensions γ one would expect similar solubilisation (provided the polydispersity of the aggregates does not change much, which again would depend on changes of the bending elasticity of the amphiphilic monolayers with the different esters, which will be discussed later).

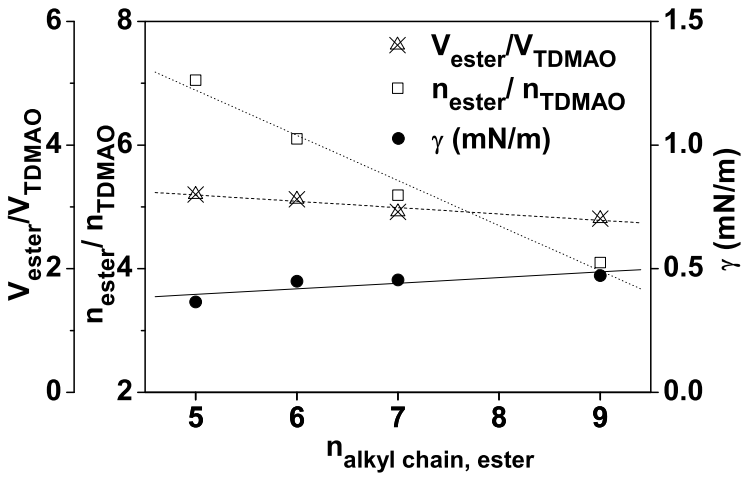

figure 6.3 Solubilisation capacity in terms of volumic (triangles) and molar (open squares) ratios between solubilised ester and surfactant, and interfacial tension (full circles) as a function of the number of carbon atoms of the acid of the ester (25 °C, 200 mM TDMAO)

As all samples were prepared by applying shear forces during the preparation process (shaking, stirring) the question arises whether the observed vesicles phase is in a thermodynamically stable or metastable state. Therefore, a way was employed to prepare

these phases without shear. One possibility to accomplish this is to bring the variable component, in this case the ester, by diffusion into the sample. For this experiment the samples with EME was prepared as follows: a micellar solution of 200 mM TDMAO was placed in a test tube. Above this solution a layer of excess EME was poured carefully to prevent the additive from mixing with the lower surfactant solution. This two-phase system was kept at rest for several months in a thermostated bath at 25 °C. It should be noted that this contact method might lead to incorrect conclusions the longer the waiting period due the possible hydrolysis of the ester.

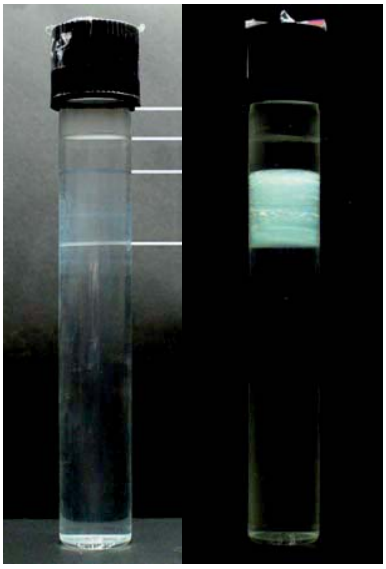

figure 6.4 Photographs of a sample where the semipolar additive EME diffused in a solution of the surfactant (at 25 °C) after several months at normal light (left) and between crossed polarizers (right)

If the pure surfactant solution is contacted with EME the additive will diffuse into the surfactant solution. According to Fick´s first law, a concentration gradient forms. At $t = 0$, no enathic methyl ester has diffused into the solution. At $t = \infty$, the ester concentration will be the same in every part of the test tube. As diffusive processes in solution are very slow, one finds at intermediate time (weeks, month) an EME gradient with highest concentration at the top near the pure ester phase and lowest concentration at the bottom of the test tube. Therefore at different heights different phases will be present formed by the diffusion process. In this way one obtains the same phase sequence in a

single tube as one would get if the ester concentration is increased stepwise as it was done for the determination of the phase diagram [135].

At the bottom of the test tube we find an extended isotropic phase, which is the micellar phase. Between crossed polarizers the second, birefringent phase can be identified as vesicle phase. At the top of the tube two additional transparent phases can be observed. The lower is the second L_1-phase (with high ester content) - the microemulsion also observed in the phase diagram -, the upper is the remaining excess of ester that did not diffuse.

From the diffusion experiment we could confirm the vesicle phase to be the thermodynamically stable phase. This is further proved by simply increasing the temperature of a TDMAO/EME solution. The sample 200 mM TDMAO/225 mM EME changes from the isotropic L_1-phase at 15 °C without any shear forces just by increasing the temperature to 25 °C and this process is totally reversible.

6.3.2 Viscosity

As the zero shear viscosity is indicative of the structures contained in surfactant solutions it was determined for constant surfactant concentration of 200 mM as a function of the amount of added ester. The obtained results (summarized in A figure 9.10) show that for all systems studied, the viscosity passes through a pronounced maximum at relatively low ester concentration of 50 – 100 mM. The viscosity maximum becomes more pronounced with increasing chain length and its position shifts to higher concentration with decreasing chain length of the ester.

This can be explained by the fact that the area required at the interface per ester molecule is very similar but their volume decreases with the chain length. Accordingly for the same molar concentration the packing parameter is correspondingly more changed by longer esters. At higher concentrations viscosity values almost as low as that of pure water are attained. Such an intermediate increase in viscosity is to be attributed to the formation of rod-like micelles as it is typically observed for the case of admixing cosurfactants to surfactant solutions [63].

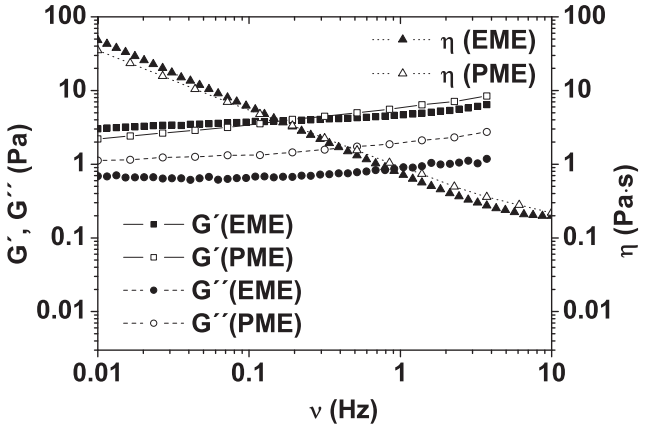

figure 6.5 Elastic and viscous modulus (squares and circles) and dynamic viscosity (triangles) of vesicles containing 200 mM TDMAO/225 mM EME (filled symbols) or 175 mM PME (open symbols) respectively

In contrast the two vesicle phases for EME and PME occurring at room temperature show a gel-like consistency and accordingly were investigated by oscillatory rheology. The storage and loss modulus (G´, G´´) are given in figure 6.5 and show rather constant values for G' and G'', a behavior typically observed for densely packed vesicles with a yield stress [10, 48, 107]. The storage modulus is higher than the loss modulus by a factor of 5.5 for EME and 3 for PME, respectively, which shows that the sample with the shorter chain ester has the more pronounced elastic properties. However, the storage modulus being almost identically in the range of 3 - 5 Pa for both systems indicates that the structure of the vesicle gel is very similar for both cases. In addition, this value is very similar and only slightly less than for the related system with 220 mM hexylacetate as additive [134].

6.3.3 Small-angle neutron scattering

In order to obtain further insight into the structural progression upon addition of the esters to the surfactant solution as well as with respect to the structural changes taking place as a function of temperature SANS experiments were performed on selected samples.

The changes occurring at 25 °C as a function of the VME concentration are given in figure 6.6. One observes that without ester and at the lowest concentration (which is still in range of relatively higher viscosity, cf. A figure 9.10) one has elongated, rod-like micelles present, which already at a concentration of 273 mM VME start becoming transformed into rather polydisperse microemulsion droplets. Close to the emulsification boundary (672 mM VME) the droplets have substantially grown and the form factor bump around q = 0.85 nm^{-1}, indicates a radius of 5.3 nm of the microemulsion droplets and that they are not very polydisperse. Due to the relatively high volume fraction of 0.147 already a weak correlation peak is seen that is described well by the hard sphere structure factor. The change of the curves when moving away from the emulsification boundary is due to the fact that spherical microemulsion droplets are only observed close to the emulsification boundary, while with increasing distance to it increasingly more anisometric microemulsion aggregates are formed [78, 143].

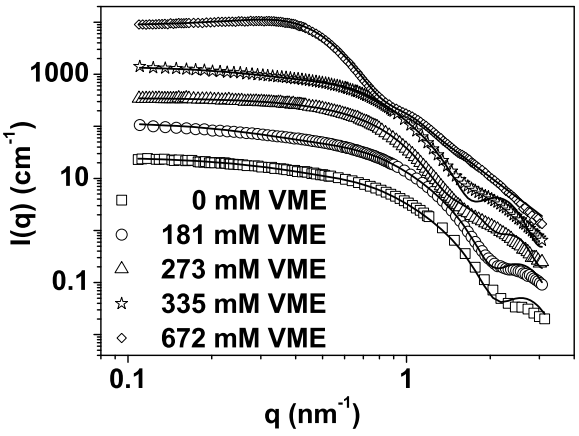

figure 6.6 SANS-measurements in the system 200 mM TDMAO/ D_2O containing 0 (squares), 181 (circles), 273 (triangles), and 672 mM (rhombs) VME at 25 °C. The sample with 0 mM VME is given in units of cm^{-1} and subsequent samples were multiplied each by a factor 3^n for better lucidity. Solid lines are fits from the model with a model of monodisperse prolate ellipsoids or polydisperse spheres (672 mM VME) (the ellipsoid form factor exhibits oscillations at high q, which arise from not having accounted for the instrumental smearing)

For the case of the VME system at ester concentrations well below the one required to observe the transition to the lamellar phase almost no effect on the scattering curves is observed when raising the temperature from 25 to 35 °C (A figure 9.11). The scattering curves are indicative of somewhat elongated micelles. Only a very slight increase in intensity at low q indicates a correspondingly small increase in elongation with rising temperature.

In contrast, for the sample containing enough VME to induce the transition to a lamellar phase a very pronounced effect on the scattering pattern is observed beyond this transition temperature. While at the temperatures in the L_1-phase the scattering pattern of spherical particles is seen, at 42.7 °C a pronounced correlation peak of the lamellar is seen (figure 6.7). It is located at q = 0.2013 nm^{-1} thereby showing a repeat distance of the lamellar stacking of 31.2 nm. By multiplying the stacking distance with the amphiphilic volume fraction, a lamellar thickness of 2.86 nm can be estimated. For further comparison the thickness can also be gained from plotting $\ln(q^2I(q))$ versus. q^2 [144], which yielded here a lamellar thickness of 2.60 nm. The latter value being more realistic as the first one does not account for the non-planar arrangement of lamellae in the vesicles nor for any fluctuations.

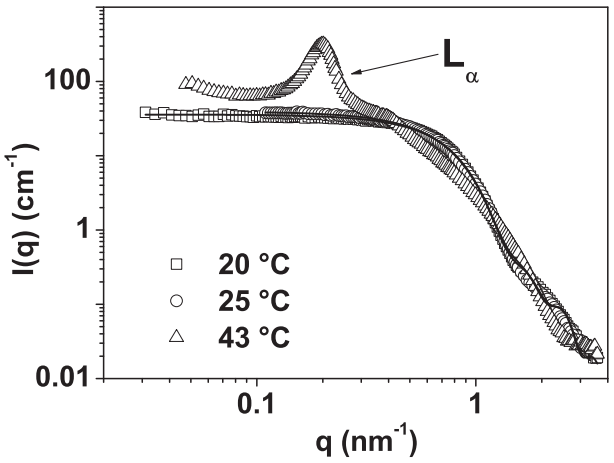

figure 6.7 SANS measurements in the system 200 mM TDMAO/ D_2O with 273 mM VME at three different temperatures. Solid lines are fits from the model with a model of monodisperse prolate ellipsoids for the sample at 20 and 25 °C

The pure surfactant solution is known to form short cylindrical aggregates [54]; while at the solubilisation boundary spherical MEs can be detected. In order to quantify the rod-to-sphere transition we fitted all data with a model of monodisperse prolate ellipsoids or, when the anisotropy went to 1, with polydisperse spheres. Similarly all microemulsions with the different esters were analyzed with the model of polydisperse spheres. The fits are given as solid lines in figure 6.6 and figure 6.8 do reproduce the evolution of the data quite well. The obtained fit parameters are summarized in table 6.1 and table 6.2.

table 6.1 Obtained particle parameters from SANS at 25 °C with a model of monodisperse prolate ellipsoids or, when the anisotropy went to 1, with polydisperse spheres: σ, the standard deviation of the Gaussian distribution; R, radius of the equatorial semi-axis; υ, the ellipticity

c(ester)	σ	R	ν
0 mM VME		2.0	5.19
181 mM VME		2.1	5.77
335 mM VME		2.5	4.50
273 mM VME		2.5	3.92
672 mM VME	1.0720	5.5	1
588 mM CME	1.1690	5.9	1
500 mM OME	1.1080	6.0	1
400 mM PME	0.9324	5.9	1

For increasing concentration of VME (figure 6.6) the ellipticity ν was calculated from the fits for ellipsoids and describes the change in shape of the aggregates. Values of $\nu < 1$ describe an oblate ellipsoid, a value of $\nu = 1$ a sphere, and $\nu > 1$ a prolate ellipsoid. We found values of $\nu >> 1$, i.e., prolate ellipsoids; with a slight increase of ν till ~300 mM VME, followed by a steady decrease of the ellipticity towards 1. At the border to the two-phase region $\nu = 1$, i.e., spherical micelles are present as to be expected (see figure 6.8).

When comparing the scattering curves for samples with the different esters but very close to the emulsification boundary at 25 °C one finds that they look rather similar (figure 6.8). One observes only a slight increase of intensity with increasing length of the ester. This demonstrates that very similarly sized microemulsion droplets are formed in these systems irrespective of the ester employed, with a slight increase in size with increasing chain length. However, looking into the region of q = 0.8 nm^{-1} one finds that the bump indicative of the monodispersity of the droplets becomes somewhat more pronounced with increasing ester chain length.

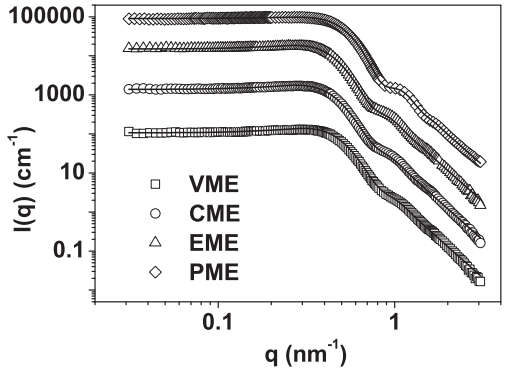

figure 6.8 SANS intensity curves for four different MEs at the solubilisation limit in the system 200 mM TDMAO/ D_2O with VME (squares), CME (circles), EME (triangles) and PME (rhombs). For the sample with VME I(q) is given in units of cm^{-1}. Subsequent samples have been multiplied each by a factor 3^n for better lucidity. Values of the intensity at q = 0 are listed in table 3. Solid lines are fits with a model of polydisperse spheres (equation 6.10)

Apparently the droplets become more monodisperse with increasing length of the ester, an effect, which could be explained by an increasing bending elasticity of the amphiphilic monolayer covering the microemulsion droplets. Similar effects on the bending elasticity have been observed for the addition of medium-chain alcohols to TDMAO microemulsions [145]. The main difference to this case here would be that in our case the ester functions at the same time as cosurfactant and solubilisate.

table 6.2 Various parameters for samples at the emulsification boundary. Volume ratio of oil to surfactant Φ_O/Φ_S, mean sphere radius <R>, polydispersity index p (taking into account the experimental smearing with a Gaussian distribution of 8% standard deviation), and values for $2\kappa + \bar{\kappa}$ calculated from p and γR^2)at 25 °C)

c(ester)	672 mM VME	588 mM CME	500 mM EME	396 mM PME
Φ_O/Φ_S	1.5175	1.5019	1.4211	1.3667
I_0 (cm^{-1})	107.7	142.2	157.0	146.7
<R> (nm)	5.46	5.88	5.99	5.75
p	0.179	0.182	0.167	0.137
$2\kappa + \bar{\kappa}$ via p (kT)	1.47	1.44	1.66	2.36
γ (mN/m)	0.34	0.45	0.45	0.47
$2\kappa + \bar{\kappa}$ via γR^2 (kT)	1.77	2.61	2.84	2.92

The experimental parameters (<R>, p, and γ) given in table 6.2 can now be used to calculate the sum $2\kappa + \bar{\kappa}$ of the bending constants, where κ is the mean bending modulus and $\bar{\kappa}$ the Gaussian modulus [64]. This sum is directly related to the corresponding experimental parameters via two independent relations [63]:

equation 6.13

$$2\kappa + \bar{\kappa} = \gamma \cdot R_m^{\,2} - \frac{k \cdot T}{4\pi} \cdot f(\Phi)$$

equation 6.14

$$2\kappa + \bar{\kappa} = \frac{k \cdot T}{8\pi \cdot p^2} - \frac{k \cdot T}{4\pi} \cdot f(\Phi)$$

with

equation 6.15

$$f(\Phi) = ln(\Phi) + \frac{1-\Phi}{\Phi} \cdot ln(1-\Phi)$$

where equation 6.13 and equation 6.14 are based either on combining the values of the mean radius of the surfactant shell (which was taken to be the outer radius of the

aggregate R_{fit} minus 1.0 nm to account for the length of the TDMAO molecule; in order to be in the middle of the surfactant monolayer) with the corresponding interfacial tensions, or alternatively to calculate the same sum $2\kappa + \bar{\kappa}$ directly from the polydispersity index p of the microemulsion droplets. The concentration dependent translational entropy of dispersion is accounted for by f(Φ) (equation 6.13). This approach has been proven to be appropriate for the description of microemulsion droplets in many cases [47, 85, 93, 146].

The values for $2\kappa + \bar{\kappa}$ obtained by the two approaches differ in absolute numbers, the ones derived from equation 6.13 always being larger, but their general increase with increasing length of the ester is the same. Here it might be noted that the values derived via equation 6.14 should be more precise and reliable as the experimental quantity with the highest error is certainly the interfacial tension (where random and systematic errors may easily be in the range of 30 - 50%, while the errors for R_m and p, should be 5 - 10% and < 5%, respectively). The trend for $2\kappa + \bar{\kappa}$ shows that the microemulsion monolayer becomes stiffer with increasing chain length of the ester and this observation is in agreement with investigations on the effect alcohols on the bending rigidity of microemulsion droplets with TDMAO [145]. This stiffening with increasing ester chain length is also in good agreement with the observation that the lamellar phase becomes more stable and extended the longer the ester (see figure 6.1).

From the Porod approximation of equation 6.1 the Porod constant $c_4 = 2\pi \cdot (\Delta SLD)^2 \cdot \Sigma$ was employed to calculate the surface area per head group (a_s) for all concentrations of VME. The surface area can be gained from the specific area, Σ by division with the surfactant concentration (corrected by the cmc). In figure 6.9 the calculated values for a_s are presented as function of Φ_{VME}/Φ_S. At low concentration of additive a constant surface area per head group of around 0.52 nm^2 was found (in very good agreement with the value of 0.51 nm^2 previously obtained by surface tension measurements [147]), which increases at $\Phi_{VME}/\Phi_{TDMAO} \sim 0.5$ to reach a plateau of ~ 0.77 nm^2.

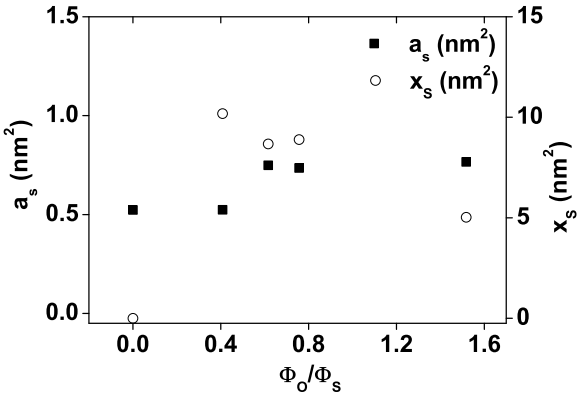

figure 6.9 Surface area per head group (squares) for different concentrations of ester calculated from the Porod plot, and surface excess (circles) calculated from the ratio S/V obtained from the fit for the system 200 mM TDMAO/VME (A figure 9.13 b)

The increase is due to the incorporation of the ester into the interfacial region and that the value afterwards remains constant indicates that further ester does not reside at the interface but instead becomes incorporated in the interior of the aggregates, thereby leading to the rod-sphere transition. From the data it can be estimated that the area required at the interface per VME molecule is 0.18 nm^2. This value is somewhat larger than the value of 0.10 nm^2 previously derived for hexanol in mixtures with TDMAO [61], which may be explained by the fact that the alcohol can substitute a solvating water molecule of the surfactant head group, which is not possible in the same way by the ester.

Accordingly the rod-to-sphere transition for VME occurs for around one third of the total amount of additive, which can be incorporated in a micellar solution of 200 mM TDMAO. From the ambivalent character of the ester the question arises whether the whole amount of ester is incorporated inside the micelle at the solubilisation boundary. From the ratio of S/V of an average aggregate (from the SANS fits) we determined the difference of surface according to the fitted value and from the known composition of the samples, expressed in equation 6.16, where σ_T is the head group area of the surfactant, σ_E the head group area of the ester, V_T and V_E the volume of surfactant and ester and N_T and N_E the number densities of TDMAO and ester, respectively. If all of the ester resides inside the micelle a value of 0 should be found.

equation 6.16

$$\frac{S}{V} = \frac{N_T \sigma_T + N_E \sigma_E}{N_T V_T + N_E V_E}$$

equation 6.17

$$\frac{S}{V} = \frac{\sigma_T + \frac{N_E}{N_T} \cdot \sigma_E}{V_T + \frac{m_E \cdot M_T}{M_E \cdot m_T} \cdot V_E} = \frac{\sigma_T + x_S}{V_T + \frac{m_E \cdot M_T}{M_E \cdot m_T} \cdot V_E}$$

If the ester partitions between the core and the shell, the surface excess x_S, which corresponds to an excess area per micelle, is different from 0 (equation 6.17, where m_T and m_E are the masses and M_T and M_T the molar masses of surfactant and ester, respectively). In figure 6.9 the surface excess for increasing concentration of VME in a 200 mM micellar solution of TDMAO can be seen. At low concentration the ester behaves as a cosurfactant and the surface excess is > 0. At the solubilisation limit ($\Phi_{VME}/\Phi_S = 1.52$) the excess has not dropped down to 0. Hence there is still some larger amount of VME left in the shell, as observed before from the calculation of a_s. The same calculations were done for the other esters and a surface excess for VME, CME, EME and PME of 11.1, 10.2, 10.0 and 11.6 nm^2, respectively, is obtained. The surface excess is obviously independent of the nature of the ester.

6.4 Conclusion

In this chapter the phase diagrams of the ternary system of 200 mM tetradecyl-dimethylamine oxide in aqueous solution and various esters of intermediate polarity have been presented. With increasing alkyl chain length valerian (VME), capronic (CME), enanthic (EME) and pelargonic methyl ester (PME) were employed. In all cases an L_1-L_α-L_1-transition with increasing concentration of additive is observed, where its location depends on the temperature, being higher in temperature the shorter the ester. From viscosity and SANS measurement in the system with VME, the concentration at which the rod-to-sphere transition occurs was estimated to be around one third of the maximum concentration solubilised in the surfactant solution. This means that up to this concentration a growth of rodlike micelles occurs as it is typically observed upon addition of a cosurfactant and which explains the increase in viscosity. However, unlike the case of alcohols as cosurfactants, where this growth of rods is followed by the formation of bilayers, here further addition of the ester at room temperature results in the solubilisation of the additional ester for short esters, while only the longer ones form a vesicle phase. However, upon further addition also these vesicles solubilise the ester into the interior of the aggregates thereby leading to microemulsions, which is clearly different from the case of alcohols. Thereby either a rod-to-sphere or a rod-to-lamellae-to-sphere transition takes place in which microemulsion droplets are formed.

However, the phase behavior is strongly temperature dependent and an L_1-L_α-transition can also be induced by simply increasing the temperature. For the shortest additive VME a continuous L1-phase is found at room temperature. Already for the longer CME the transition moves close to room temperature, for EME it occurs at room temperature, and for the longer PME the lamellar phase extends then down to 0 °C. The minimum ester concentration and the temperature at which this transition occur decrease with increasing alkyl chain length of the ester and is therefore influenced by the polarity of the additive. Apparently the longer esters behave more like straight chain alcohols and therefore are able to form bilayer structures at room temperature. It is interesting to note that neither the volume of solubilised oil at the emulsification boundary nor the maximum viscosity is affected by the chain length.

A SANS study yielded a more refined structural information regarding the growth of the rods, the formation of bilayers in the form of multilamellar vesicles and to gave a quantitative analysis of the rod-to-sphere transition. At the solubilisation limit for all four esters we found spherical microemulsions of similar size of 5 - 6 nm radius with a decreasing polydispersity with increasing chain length of the additive. The obtained structural parameters together with the relatively constant interfacial tension (that increases slightly with increasing ester chain length) were used to calculate the sum $2\kappa + \bar{\kappa}$ of the bending constants of the amphiphilic monolayer, which is increasing with increasing chain length of the ester. This then explains well the enhanced stability of the lamellar phase with increasing ester length as one can expect the rigidity of the monolayer to scale similarly as that of the corresponding bilayer. The absolute values are also smaller than the corresponding ones for alcohols of similar chain length [62], which explains why the alcohols do form stable bilayer systems whereas the esters with their softer interface prefer the path to forming a microemulsion.

Apparently there is a clear correlation between the mesostructure of the microemulsion and the phase behavior of the whole surfactant/ester system. By looking at the bending energy one is able to have a self-consistent understanding for both. The addition of semi-polar additives like esters is an interesting way of formulating amphiphilic systems as their flexible polarity and their character, which is in between that of a typical cosurfactant and that of a solubilisate allows for tuning structures and properties over a large range. Furthermore such types of compounds are frequent additives in practical formulations as perfumes, modifiers and stabilizers. Observations from this chapter should therefore have a profound impact on the general understanding of such mixed amphiphilic systems and allow for a more rational design of them based on properties requested.

7 Solubilisation of medium chain esters in zwitterionic surfactant solutions - kinetics of solubilisation

Graphical Abstract

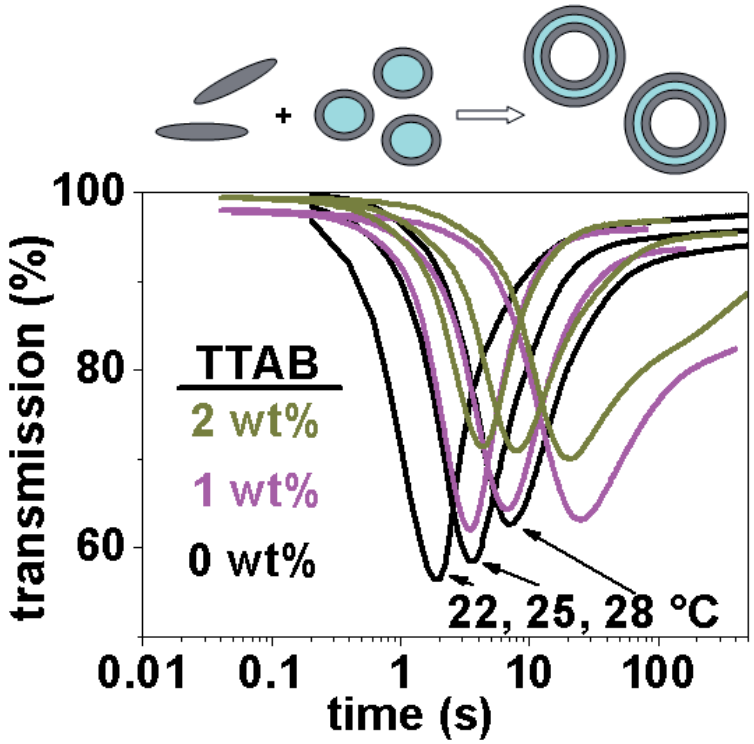

Abstract

Stopped-Flow transmission and conductivity measurements have been performed to investigate the formation process of multilamellar vesicles in a ternary surfactant system. Two pathways to reach the vesicle phase were employed: a) mixing of two microemulsions and b) mixing of a micellar solution with a microemulsion. The results show the presence of two relaxation processes for both mixing procedures characterized by the relaxation times τ_1 and τ_2. Both relaxation times depend linearly on temperature and non-linearly on charge. A fitting model using the sum of two stretched exponential functions is presented to account for these two processes. The kinetic rates increase by factor of 4-5, i.e. the dynamic of the formation process scales roughly with the distance between the starting composition and the final composition, which means it depends on the amount of material that has to be redistributed during the equilibration process. Additional stopped-flow small angle X-ray and dynamic light scattering experiments were performed to gain structural information. It is shown that the available experimental data can be qualitatively explained by assigning τ_1 to the formation of mixed aggregates. We found a characteristic time for vesicles formation of $\tau_2 \sim 30$ s. On a timescale of ~ 400 s reorganization processes occur.

7.1 Introduction

In the previous chapter the phase behavior of the ternary system TDMAO/alkyl methyl ester/water has been studied intensively with respect to the alkyl chain length of the esters employed. Due to the highly symmetric vesicle phase in the phase diagram with EME it was possible to study the kinetics of the formation process depending on the distance between the starting composition and the final composition. A roughly linear dependency could be found. Accordingly the time constant observed is related to the concentration difference in EME between the two isotropic solutions that are mixed. Comprehensive studies on the micelle-to-vesicle transition demonstrated that vesicle size and kinetic rate depend on the total amphiphile concentration and on the ionic strength of the solution. Therefore the question of having charged amphiphilic mono- and bilayers present during the process of vesicle formation (as introduced by admixing an ionic surfactant) was addressed. This then allows learning how electrostatic interactions affect this process.

In this chapter stopped-flow measurements with complementary detection methods, i.e. turbidity, conductivity, SAXS and DLS will be presented and the formation of multilamellar vesicles in the ternary surfactant system with respect to changes of temperature and charge will be discussed.

7.2 Experimental

Stopped-Flow studies were carried out using a Bio-Logic SFM400/S stopped-flow instrument described in 0 with simultaneous detection of the transmission and conductivity signal. For transmission detection, the wavelength was adjusted at 546 nm. For conductivity measurements with the MCS-200 the optimum frequency (chosen from the impedance spectra) of υ = 4833 kHz. The device was operated at a voltage of 50 mV, which results in currents of 1 µA to 1 mA for the investigated samples. The conductivity κ was detected as function of time. Under these conditions and using a FC-15 flow cell for the transmission and conductivity detection, at 14 ml/s the dead time was 2.6 ms.

equation 7.1

$$T = T_\infty + A_1 \cdot exp\left(-\left(\frac{t}{\tau_1}\right)^\beta\right) + A_2 \cdot exp\left(-\left(\frac{t}{\tau_2}\right)^\gamma\right)$$

Stopped-Flow transmission measurements were fitted with the sum of two stretched exponential functions according equation 7.1, where T is the measured transmission, T_∞ the transmission at infinite measurement time, A_1 and A_2 the amplitudes of the two relaxation times. Two exponential functions were necessary as we have two opposing effects present in our kinetic data (figure 7.3). In equation 7.1, the kinetic behavior is described by two characteristic time constants τ_1 and τ_2, while the exponents β and γ are characteristic for the spread of the relaxation process (being 1 for a mono-exponential relaxation). Stopped-Flow conductivity measurements were fitted with one stretched exponential function.

7.3 Results and Discussion

7.3.1 Phase behavior

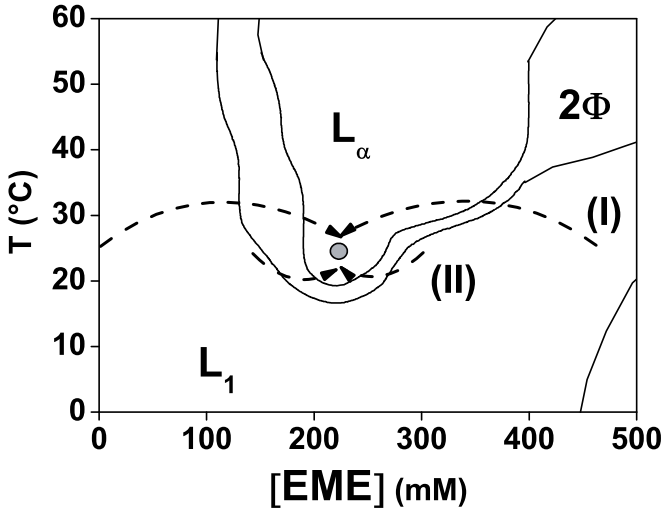

figure 7.1 Temperature-dependent phase diagrams for samples of 200 mM TDMAO as a function of concentration of added enanthic methyl ester (EME). Dashed lines demonstrate two possibilities of mixing isotropic microemulsions to reach the birefringent vesicle phase at 225 mM EME

The observed phase behavior for a constant surfactant concentration of 200 mM depending on the concentration of added EME is summarized in figure 1 and has been described in detail in chapter 6. At temperatures lower than 18 °C only an isotropic L_1-phase is found, which can incorporate more than 2 ester molecules per surfactant molecule. For intermediate EME concentrations ([EME]/[TDMAO] ~ 1) a phase of multilamellar vesicles has been observed, which splits the L_1-phase into a lower concentration and a higher concentration part can be observed. The birefringent vesicle phase is separated by a two-phase region from the L_1-phase.

7.3.2 Influence of charge

In the next step the influence of the charge to the system was studied. Therefore 1 wt% and 2 wt% TDMAO respectively were replaced by TTAB, a cationic surfactant exhibiting the same alkyl chain length than the primary surfactant.

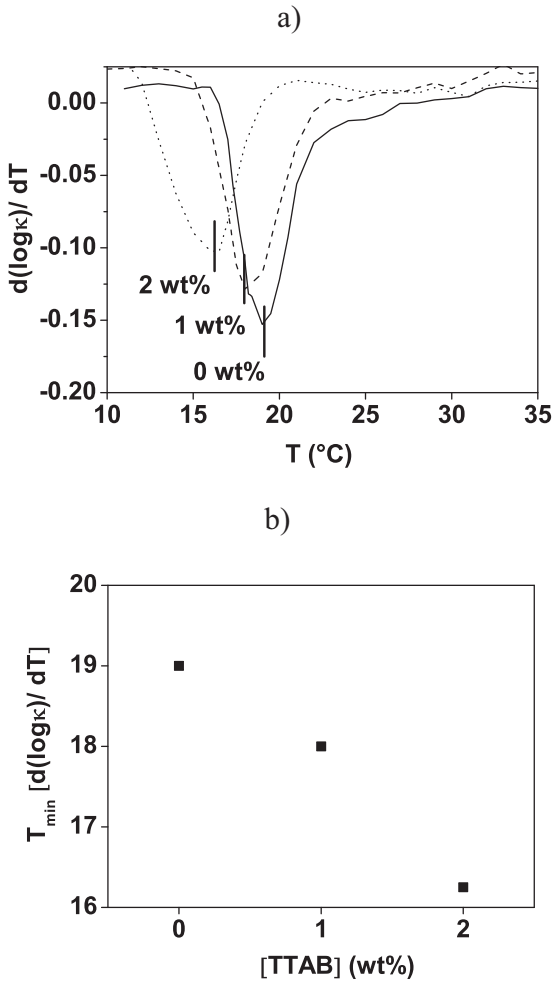

figure 7.2 Conductivity measurements of the vesicle phase 200 mM TDMAO/ 225 mM EME (see A figure 9.14); phase transition from O/W-ME to vesicle displayed by a) the deviation of (log κ) with temperature; decrease of the transition temperature visible with increasing charge (0 wt% TTAB: solid line; 1 wt% TTAB = dashed line; 2 wt% TTAB = dotted line) and b) the minimum temperature of the deviation depending on the amount of charge in the system

A sample of 200 mM TDMAO and 225 mM EME would exhibit a microemulsion phase at temperatures below 18 °C. Increasing the temperature to e.g. 40 °C, conductivity should decrease passing the two-phase region to reach the vesicle phase. In figure 7.2 a) the derivative of the logarithm of the specific conductivity as a function of temperature for the system with 0 (solid line), 1 (dashed line) and 2 (dotted line) wt% TTAB is shown. The representation of the conductivity as the derivative of the logarithm enables to differentiate between the microemulsion and vesicle phase. The former can be found on the left side of the minimum, the latter on the right hand side. We wanted to quantify the influence of the charge to the ternary system. In figure 7.2 b) the temperature at the minimum of the derivative is given for all three concentrations of TTAB. We find that the transition L_1-to-vesicle decreases roughly linear with increasing charge. So regarding the phase behavior of the system 200 mM TDMAO/ EME, the vesicle phase is shifted to lower temperatures by 3 °C when charging the system with 2 wt% TTAB

7.3.3 Dynamics of spontaneous formation of vesicles – stopped-flow measurements

The presence of a vesicle phase embedded in an L_1-phase in TDMAO/EME mixtures (see figure 7.1) is an intriguing phenomenon as it allows the formation of a liquid crystalline vesicle phase by mixing two isotropic L_1-phases, one with an ester content below and one above of the concentration required for the vesicle phase. Thereby one is able to study an interesting morphological transition as well as the redistribution of solubilized EME. Accordingly we decided to study this transition by means of stopped-flow experiments that allow following the evolution of the vesicle phase as a function of time after rapid mixing of the two starting components. In that context we were interested in the effect of charging the initially present micelles or microemulsion droplets (by admixing cationic surfactant) and also how the location of the starting solutions in the phase diagram affects the dynamics of vesicle formation and the redistribution of EME.

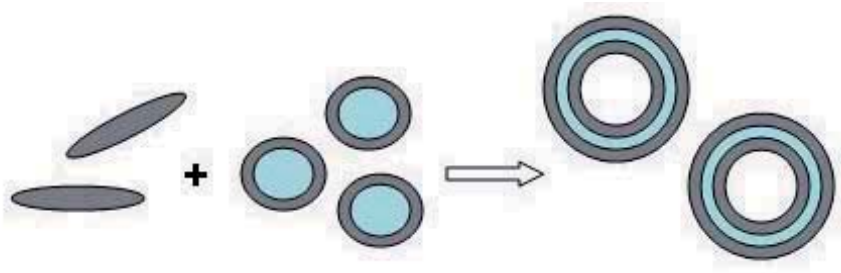

chart 7.1 Schematic drawing of the mixing processes presented in this work: 1:1-mixing of a micellar solution or microemulsion with a microemulsion of higher concentration, yielding multilamellar vesicles

For that purpose we employed two different mixing procedures to reach the liquid crystalline vesicle phase of composition: 200 mM TDMAO/225 mM EME at 25 °C.

(**I**) 1:1-mixing of the micellar solution of the surfactant with the isotropic microemulsion at 200 mM TDMAO/450 mM ester (see also chart 7.1).

(**II**) 1:1-mixing of isotropic solutions of 200 mM TDMAO/150 M and 200 mM TDMAO/300 mM EME.

The third way is the mixing of the micellar solution with the pure ester to give a final concentration of 200 mM TDMAO/225 mM EME. In the present work the kinetics of the first two possibilities are presented.

7.3.4 Transmission measurements

As the vesicle phase is significantly more turbid than the starting L_1-phases, stopped-flow transmission measurements were performed in order to follow their formation process. The obtained time-dependent transmission curves for the mixing process of method a) at 25 °C are shown in figure 7.3 for various amounts of substituted TTAB. At $t \sim 0$ the transmission is nearly 100%, which corresponds to the values of the two isotropic starting solutions.

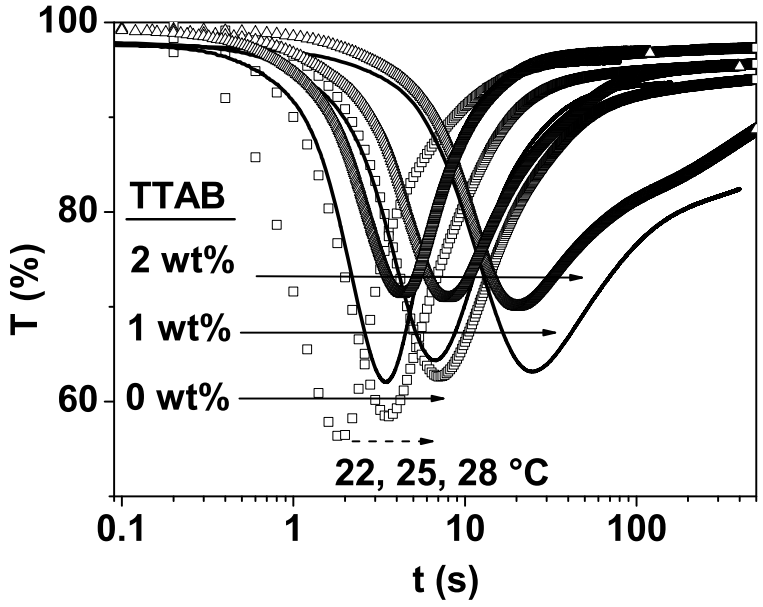

figure 7.3 SF-transmission measurements at 22, 25 and 28 °C (curves from right to the left) at 546 nm: mixing of a micellar solution with a microemulsion (200 mM TDMAO 1:1 450 mM EME/ 200 mM TDMAO) (procedure **I**) to reach vesicle phase; replacement of TDMAO with 0, 1 and 2 wt% TTAB is displayed as squares, straight line and circles. The thickness of the cuvette was 1.5 mm

For the case of no ionic TTAB present in the surfactant mixture, the transmission decreases to 58 % within the first 3 s, but afterwards increases substantially again. At the end one has a relatively transparent case where one has increasingly more transparent samples with increasing TTAB content, which is explainable by the electrostatic repulsion of the bilayers and the correspondingly increased degree of ordering. Obviously the kinetics of the structural reorganisation is at least a two-step process that requires for completion several minutes. For the samples containing TTAB the general behaviour of the transmission curves is similar but shifted to longer times with increasing TTAB content and the decrease of transmission is increasingly less pronounced. The overall form of the transmission curves is not surprising as one may expect that during the transformation process, in which micelles and microemulsion droplets form multilamellar vesicles (see chart 7.1), one has a structurally rather ill-defined situation.

This means that the fluctuations in the structural organisation are very large. Accordingly one expects a high osmotic compressibility of the system and therefore a large scattering intensity (corresponding to a low transmission). At longer times this disorder is reduced again, multilamellar vesicles are formed, and, in a still slower process, will become more organised and well-defined still.

table 7.1 amplitudes, relaxation times and stretching factors for the formation of the vesicle phase according to step (**I**) (figure 7.1); stopped-flow transmission measurement at 25°C, total volume = 151 µl, flow rate = 14 ml/s

[TTAB]	A_1	τ_1	β	A_2	τ_2	γ	T_∞
0 wt%	0.554	2.06 s	2.13	-0.526	8.90 s	1.26	0.947
1 wt%	0.562	3.89 s	1.95	-0.521	12.3 s	1.20	0.83
2 wt%	0.356	4.24 s	2.20	-0.315	23.8 s	1.25	0.81

The structural transformation has to proceed via a substantial growth of the originally small micelles and microemulsion droplets. This growth might initially proceed unidimensionally and lead to the formation of elongated micelles that then grow bidimensionally until they become so large that their closure is no longer unfavoured by the bending energy of the bilayers. As we have two opposing effects present in our kinetic data (figure 7.3) the experimentally observed transmission curves were quantitatively described by equation 7.1, in which two stretched exponential functions were employed in order to describe the two opposite effects on the transmission.

For the case of the formation of the uncharged vesicles for the two relaxation times values of 2.06 s and 8.90 s, respectively, are found, i. e. the processes observed are relatively slow compared to simple micellar transformations. The effect of charging the aggregates was studied by admixture of the cationic surfactant TTAB. The stopped-flow transmission curves of the corresponding mixing processes are included in figure 7.3. Apparently the electrostatic repulsion leads to a slowing down of the formation process while at the same time the minimum transmission becomes much higher.

The relaxation times more than double when going from 0 to 2 wt% TTAB (see A table 9.5) and a logarithmic decrease of the relaxation rates with increasing concentration of charge can be observed (see figure 7.4). This corresponds to an additional activation energy ΔE_{ion} of 1.8 - 2.4 kJ/mol due to the electrostatic repulsion incurred by the presence of 2 mol% of the ionic surfactant (as derived from equation 3.6.

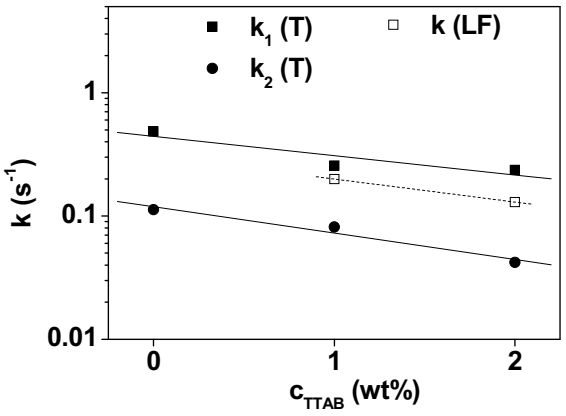

figure 7.4 Relaxation rated k_1 and k_2 for the formation of the vesicle phase at 200 mM TMDAO/ 225 mM EME according to mixing procedure (**I**) for SF-transmission measurements (filled symbols) and relaxation rate k for SF-conductivity measurements (empty symbols). Lines are linear fits of the data to guide the eye

The stretching factors, β and γ, remain similar und independent of the charging. As they indicate the width of the relaxation rate of the structural transformation it shows that this structural feature remains unaffected by the incorporation of the ionic surfactant. For all cases β is much larger than γ. This demonstrates that the first process has a much wider distribution of relaxation rated compared to the second process that apparently exhibits a much more homogenous kinetics, being relatively close to a mono-exponential process. As shown above the vesicle phase at 200 mM TDMAO/225 mM EME can also be reached according to mixing procedure (**II**). In figure 7.5 the temperature dependent stopped-flow transmission measurements identical to that of procedure (**I**) are displayed. The starting solutions were two isotropic L_1-phases of the composition of 200 mM TDMAO/150 mM EME and 200 mM TDMAO/300 mM EME respectively. The data were again fitted with the sum of two stretched exponential functions. Fitting results are

listed in table 7.2. At first, values of the final transmission, T_∞ for both mixing steps are compared. In the uncharged system for 22, 25 and 28 °C, T_∞ is 0.947, 0.957 and 0.975 for procedure (**I**) and 0.935, 0.948 and 0.973 for procedure (**II**). Evidentially, the same phase is present during the mixing process in both mixing events.

table 7.2 Relaxation times and activation energies from SF-transmission measurements in figure 7.5 according to procedure (**II**); mixing of two microemulsions (200 mM TDMAO/ 150 mM EME 1:1 300 mM EME/ 200 mM TDMAO) to reach vesicle phase; total volume = 151 µl, flow rate = 14 ml/s

	A_1	τ_1 (s)	β	A_2	τ_2 (s)	γ	T_∞
22 °C	0.283	0.90	1.907	-0.237	22.6	0.636	0.935
25 °C	0.213	0.44	1.884	-0.178	2.26	1.167	0.948
28 °C	0.137	0.14	1.237	-0.165	1.06	0.577	0.973
E_a (kJ/ mol)		***225***			***378***		

Compared to procedure (**I**) the kinetics is faster by a factor of 4-5 and at the same time the minimum of transmission is reduced by a factor of 2. This means that the kinetics of the formation process scales roughly with the distance between the starting composition and the final composition, i.e., the amount of transferred EME. In both cases the kinetic of the whole reorganization process is mostly controlled by the exchange and equilibration of the inbalance of the EME concentration. As the difference in EME between the two isotropic solutions that are mixed is three times higher for (**II**) a direct relation to the time constant observed can be found.

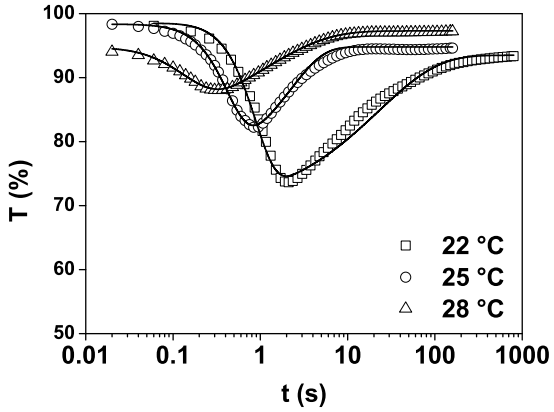

figure 7.5 SF-transmission measurement; mixing procedure (**II**) (200 mM TDMAO/ 150 mM EME 1:1 200 mM TDMAO/ 300 mM EME) to reach vesicle phase at three different temperatures (22°C: squares, 25°C: circles, 28°C: triangles). Straight lines are the fits from the sum of two stretched exponential functions (equation 7.1)

7.3.5 Conductivity measurements

During the process of formation of vesicles from micellar solutions or microemulsions a significant amount of solvent, that is water in this experimental setup, will be entrapped inside the vesicle resulting in a decrease of the conductivity. For that reason stopped-flow conductivity measurements were done to monitore the formation process. In figure 7.6 the formation of vesicles depending on temperature (22, 25, 28 °C as squares, circles and triangles) and charge (1 and 2 wt% TTAB as empty and crossed symbols) are displayed. Just as the transmission curves all kinetics in conductivity mode exhibit a distinct plateau at the start of the measurement. Followed by a relatively fast decay in the conductivity signal a second plateau is reached after approximately 10 - 1000 s. All kinetic curves were analyzed with single stretched exponential function (see table 7.3 where A is the amplitude, τ the relaxation time, β the stretching factor and κ_∞ the conductivity at infinity). It was not possible to gain a consistent result for the system without charge, which might be due to the low value of 0.014 mS/cm, measured under static conditions.

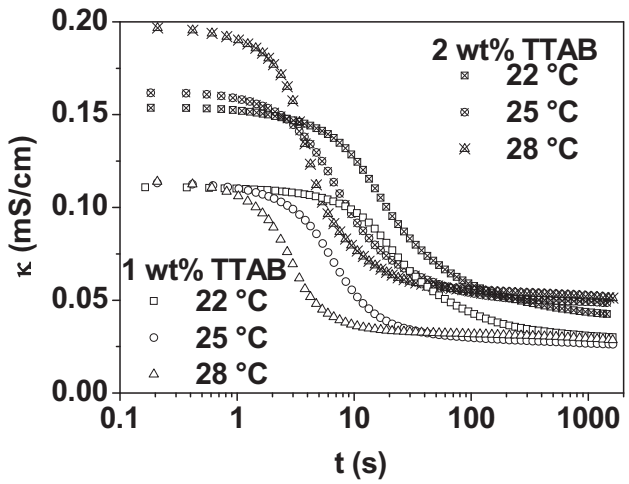

figure 7.6 SF-conductivity measurements at 22, 25 and 28°C (square, circles and triangles): mixing of 2 isotropic L_1-phases [(200 mM TDMAO + x TTAB) 1:1 (200 mM TDMAO/ 450 mM EME + x TTAB)] to reach vesicle phase; replacement of TDMAO with 1 (open symbols) and 2 (crossed symbols) wt% TTAB; total volume = 151 µl, flow rate = 14 ml/s

At 25 °C and substitution of TDMAO with 1 wt% TTAB, the relaxation time $\tau = 5.02$ s. This value ranges between the two relaxation rates found in the SF-transmission measurements and supports the idea of a three step process, first the mixing of the aggregates, second the closure of the amphiphilic film to form vesicles and third the reorganization of the aggregates. Increasing the amount of charge to 2 wt% TTAB, τ increases to 7.70 s. At ~ 1000 s the conductivity reaches a plateau in all cases of $\kappa_\infty = 0.026$ and 0.049 mS/cm (at 25 °C) for charging of the system with 1 and 2 wt% TTAB; values that were also found under static conditions and that confirm the formation of the particular vesicle phases. In figure 7.4 the evolution of the relaxation rates for the formation according to procedure (**I**) are displayed for both detection methods (filled symbols: SF-transmission, empty symbol: SF-conductivity). Obviously, all three relaxation rates exhibit identical charge-dependence of the formation of vesicles in this ternary system.

table 7.3 Relaxation times and activation energies from SF-conductivity measurements in figure 7.6 for the formation of the vesicle phase according to step (**I**) (figure 7.1); total volume = 151 µl, flow rate = 14 ml/s; in addition the value for the conductivity of the vesicle phase under static conditions, k_{stat} is given

1 wt% TTAB	**A (mS/cm)**	**τ (s)**	**β**	**κ_∞ (mS/cm)**	**k_{stat} (mS/cm)**
22 °C	0.088	27.6	0.638	0.030	
25 °C	0.083	5.02	0.584	0.026	0.026
28 °C	0.092	1.99	0.738	0.029	
E_a (kJ/ mol)		***57.4***			
2 wt% TTAB					
22 °C	0.124	20.9	0.609	0.046	
25 °C	0.125	7.70	0.570	0.049	0.049
28 °C	0.160	4.31	0.778	0.051	
E_a (kJ/ mol)		***22.7***			

Likewise, temperature dependence was observed and values for Arrhenius´ activation energies (table 7.3) could be calculated from the measurements at 22, 25 and 28 °C. For the loading of the initially presents aggregates of 1 and 2 wt% TTAB, 57.4 and 22.7 kJ/mol were calculated for the one-step process observed in conductivity mode, values that are substantially lower than those found in transmission measurements. From that we can only assume that the intermediate state prior to the vesicle structure is only marginally influenced by a change of the temperature.

7.3.6 Small angle X-ray measurements

Until now several information about structural changes during the formation of vesicles were obtained from stopped-flow transmission and conductivity measurements. As can be seen clearly both methods detect different transitions in the kinetics of the vesicle formation. The decays in the detection signal occur on different times scale and therefore correspond to different steps in the process of formation. To gain further information and to assign the different relaxation times to the appropriate kinetic steps stopped-flow SAXS measurements were carried out.

For procedure (**I**) SAXS scattering curves at various times after mixing were monitored (see A figure 9.15). After a few seconds the appearance of a minimum in the range $q = 0.08 - 0.09$ nm^{-1} is observed (triangles), which is characteristic for the presence of vesicles (of a radius of 35-40 nm). It shifts to lower q thereby indicating that the vesicles become somewhat larger. This is in accordance with the change of the slope at larger q. Depending on the dimensionality of the aggregates, I(q) shows a dominant q^{-D} dependence in the double-log plot where D = 0, 1 and 2 denote globular micelles, cylinders and bilayers respectively [144]. With increasing time after the mixing, a change of the slope from 0.55 at 0.44 s to 1.69 at 2.80 s is observed, which can be attricuted to a decrease of the bending of the surfactant layer. In this range the formation of mixed aggregates of cylindrical micelles and slightly prolate microemulsion droplets is assumed. Shortly after the first minimum, several additional minima appear at larger q that are shifted to higher scattering vektor as well.

The observed changes in the scattering pattern seem to be quite complicated and an explanation could be the overlap of the particle structure and form factors of the aggregates present during vesicle formation. If the initial structure, cylindrical micelles and slightly prolate microemulsion droplets, form mixed aggregates than each of them would contribute with its own form and structure factor to the scattering pattern. A separation of these effects is not feasible. Unfortunately it is not possible to receive further information about the structural changes occurring during vesicle formation.

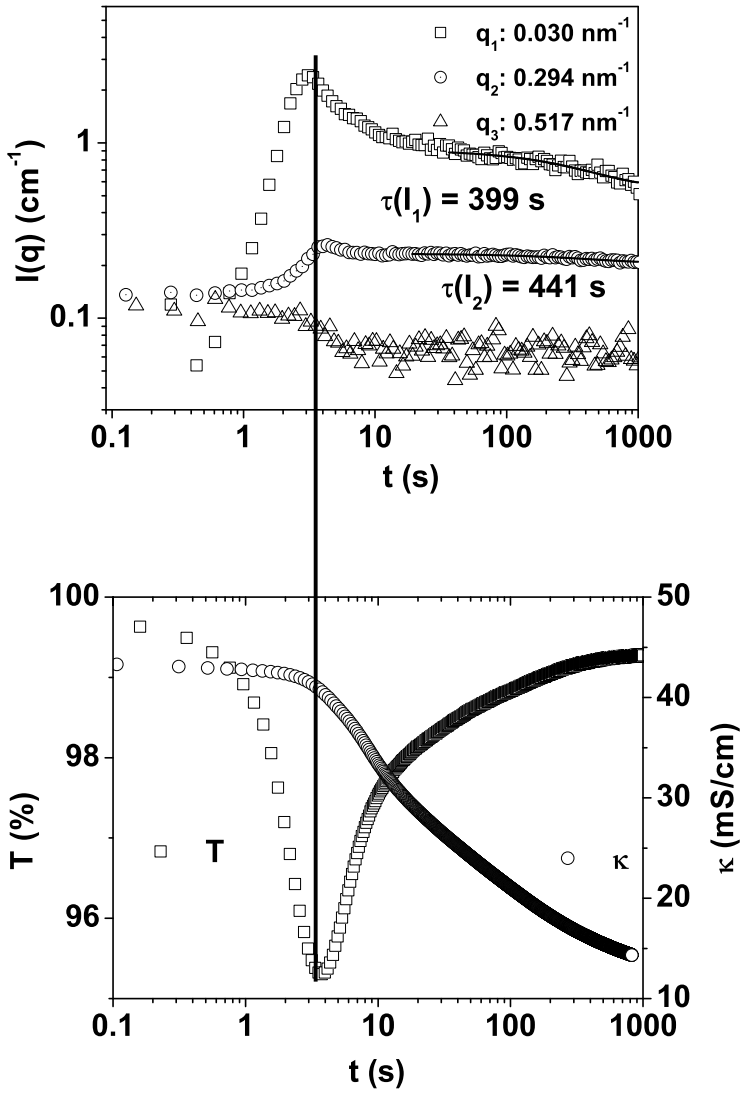

figure 7.7 Top: evolution of the intensity at different scattering vectors. Bottom: transmission and specific conductivity of identical mixing procedure like in the upper graph. The SAXS intensity patterns correlate with the minimum in the transmission signal, indicating the presence of large objects or fluctuations. The evolution of the intensity at high q shows the same time dependence than the decrease of the conductivity, which correlated to the closure of the surfactant monolayer to form bilayer structures. Note that SAXS measurements were performed at 6.67 ml/s and transmission and conductivity measurements at 3 ml/s

However, in order to gain characteristic time constants from the SAXS measurements, intensities at different q-values were displayed as function of time in figure 7.7. The curves at q_1 = 0.030 nm^{-1} (squares) and q_2 = 0.294 nm^{-1} (circles), the range where

changes at long and medium distances in the system are observed, both show the same prominent peak at ~ 4 s, i.e., at the same time as it was observed for the turbidity measurements. Within 3 - 4 s the intensity increases by two orders of magnitude at q_1, indicating the formation of big (= mixed) aggregates, which is in accordance with a value of D > 2 already discussed above. At t > 4 s a decrease of the intensities q_1 and q_2 is observed, accompanied by a sudden increase of the transmission. At the same time a decrease of the conductivity occurs, which was delayed during the first aggregation process. The decrease of the conductivity represents the initial formation of vesicles because part of the solvent is entrapped inside the vesicle. Intensity at q_3 = 0.517 nm with a relaxation rate of 4.3 s with a stretching factor of 3 that is even higher than for β in transmission measurements. This rate is in the same order of magnitude than 1 for q_1 and q_2 that exhibits values of 2.2 s and 3.2 s (β (q_1) = 3.8 and β (q_2) = 3.7), respectively.

In all curves presented in figure 7.7 a slight break at t > 10 s can be observed. Obviously the system undergoes at least one additional process after the closure of the bilayers, which can be attributed to an ordering phenomenon. Nevertheless we found a characteristic time for vesicles formation of ~ 30 s. On a timescale of ~ 400 s reorganization processes occur.

7.3.7 Dynamic light scattering measurements

In a first attempt to study the size and structure of the reorganization process (1 min - 2 h) with DLS was not successful due to the very high concentration of TDMAO and EME in the vesicle phase, leading to multiple scattering. Therefore we performed stopped-flow measurements with a home-built DLS set-up to be able to resolve the initial states during vesicles formation and to gain some size information.

Shortly after the mixing of equal volumes of 200 mM TDMAO 1:1 200 mM TDMAO/ 450 mM EME a fast decay in the autocorrelation function with a relaxation rate of $\tau_1 \sim 0.3$ ms is observed, indicating the presence of very small particles, e.g. micelles or microemulsions. After only a few second a slow mode (τ_2), which can be attributed to

slower, bigger particles, appears that is shifted to higher τ within 100 s. Hence, the autocorrelation functions were fitted with the sum of two exponentials and the evolution of the fast and slow mode, τ_1 and τ_2 are displayed in figure 7.8. The fast mode decreases with a relaxation rate of 21 s; at the same time, the slow mode increases with τ_2 = 63 s.

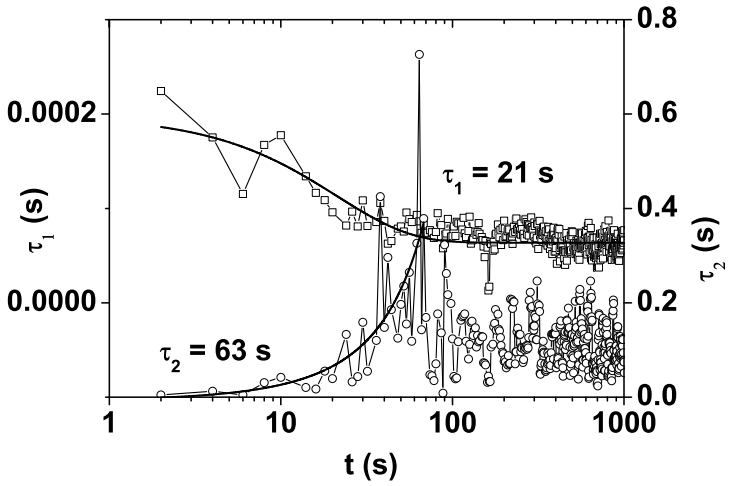

figure 7.8 Evolution of the fast (1) and slow (2) decay time gained from stopped-flow DLS measurements (at 25°C, 532 nm, 90° angle): 200 mM TDMAO 1:1 200 mM TDMAO/ 450 mM EME. DLS curves were accumulated every 2 s and fitted with the sum of two exponential functions

Obviously the increasing decay times of τ_2, indicating increasing particles size is accompanied by decreasing radius of the smaller aggregates. However it was not possible to resolve the range of the reorganization process at longer timescale for the second mode due to the multiple scattering of the sample. At ~ 100 s the decay of τ_2 corresponds no longer to an exponential profile. This might be due to the presence of a local network (e.g. entangled long cylinders) inside the sample. We do not anticipate finding similar relaxation rates, as we expect these processes to take place simultaneously. Obviously the mixing processes described in this chapter are characterized by a sequence of several reorganization steps that could not be resolved within these experiments.

7.4 Conclusion

In this last chapter the phase diagram of the ternary system tetradecyl dimethyl amine oxide (TDMAO) / enanthic methyl ester (EME) / water at a constant surfactant concentration of 200 mM was employed to study the formation of vesicles with stopped-flow measurements in transmission, conductivity, small-angle X-ray and dynamic light scattering mode.

First the case under static condition was discussed where smaller amounts of the nonionic TDMAO are exchanged by the cationic surfactant tetradecyl trimethyl ammonium bromide (TTAB). Always a phase sequence of L_1(micellar) - vesicle - L_1(microemulsion) as a function of EME concentration is found, which strongly depends on temperature, where below a certain temperature the vesicle phase vanishes. The incorporation of the charged TTAB leads to a reduction of this vesicle-to-L_1 transition, the more so the higher the amount of incorporated TTAB. This increased tendency for vesicle formation can be explained by the reduction of the Gaussian bending modulus $\bar{\kappa}$ due to electrostatic interaction that favours the formation of vesicles.

Due to the symmetry of the phase diagram, kinetic measurements were possible, where one can form a phase of multilamellar vesicles by mixing two isotropic L_1-phase solutions. Accordingly this vesicle phase can be obtained by mixing a micellar solution with a microemulsion containing EME as solubilisate, where the difference in composition (given by the concentration difference of EME) between the two samples can be varied.

Stopped-flow transmission measurements were employed as a suitable tool to follow the kinetics of the formation process. It is observed that the formation of multilamellar vesicles is a two step process where first a pronounced decrease of the transmission signal in the range of 0.44 - 2.06 s is observed, which is followed by a slower increase of the transmission with a time constant between 2.26 and 8.90 s, finally yielding a rather transparent vesicle phase. Apparently two processes with opposite effects on the transmission signal occur during this process. The first one can be identified with the disorganisation of the originally present micelles and microemulsion droplets while the second one is the formation and organisation of the multilamellar vesicles.

The kinetics of vesicle formation depends strongly on the amount of incorporated cationic surfactant TTAB and is slowed down by a factor 4 - 5 when 2 wt% surfactant is replaced by TTAB. Apparently the coalescence of amphiphilic domains, which is required in the process of forming multilamellar vesicles starting from micelles and microemulsion droplets, is substantially hindered already by the presence of small amounts of ionic surfactant, which indicates that presumably they are located in the domains of such aggregates that have to fuse in order to form the finally present multilamellar vesicles, i.e. in the rims of the amphiphilic structures. In summary, our experiments show that the stopped-flow technique is very suited for studying complex reorganisation processes in amphiphilic systems and allows discerning in detail effects of initial composition and content of ionic surfactants on the kinetics of the formation process of multilamellar vesicles. Stopped-flow small angle X-ray scattering and dynamic light scattering experiments confirmed these two steps. However it was not possible to gain any further structural information of the intermediates.

From stopped-flow conductivity measurement a third, intermediate step during vesicle formation could be identified, which corresponds to the closure of the amphiphilic layer to form bilayers and which is accompanied by a pronounced decrease of the conductivity. The calculated relaxation rates of the charge-dependent measurements range in between and parallel to those two observed in transmission mode.

Compared to the first procedure (mixing of micellar solution and microemulsion) the kinetics is faster by a factor of 4 - 5, when two microemulsions are mixed. This means that the kinetics of the formation process scales roughly with the distance between the starting composition and the final composition, i.e., the amount of transferred EME.

8 Conclusion and Outlook

Final conclusion

This thesis deals with the dynamics in amphiphilic system. The first task was to study the exchange of solubilisate between microemulsion aggregates applying classical ternary and one quaternary system. The latter one was employed to study the kinetics of the equilibration of microemulsions. For both approaches the coalescence of two microemulsion droplets is required. Therefore the coalescence dynamics were investigated by changing several parameters, i.e. temperature, composition, hydrocarbon chain length, amount of charge in the amphiphilic layer and amount of amphiphilic polymer.

For all kinetic measurements the stopped-flow method was employed which is a versatile method to study fast kinetics after a rapid mixing process with a time resolution of down to 1 ms, and was coupled to different detection systems, e.g. transmission, conductivity, fluorescence, dynamic light, small-angle x-ray or neutron scattering.

Spherical O/W microemulsions of the ternary system $C_{12}E_5$/oil/water were employed to study the exchange of oil under equilibrium conditions. Stopped-flow fluorescence measurements were performed and the decrease of the excimer intensity of a hydrophobic pyrene ester was monitored over time. The concentration of microemulsion droplets and the alkyl chain length of the oil solubilised inside the surfactant layer were varied systematically. The second-order rate constant was found to increase exponentially with increasing hydrodynamic radius of the droplets. At constant values for the sum of the bending constants $2\kappa + \bar{\kappa}$, the effective activation energy for coalescence compared to the diffusional process decreases with increasing droplet radius, which is in accordance with the faster exchange of solute. Due to different mixing procedures reported in the literature, the exchange of oil was studied for the 1:1-mixing of (**I**) identical concentration of microemulsion droplets and (**II**) for a constant and low concentration of the first solution containing the fluorescent probe mixed with increasing concentration of `empty` droplets.

It was proven that the second-order relaxation rate of the exchange of solubilisate in nonionic microemulsions is independent of the mixing procedure. The crucial factor is the proper treatment of the data according to the mixing process or rather the concentration jump applied.

O/W microemulsions of the more complex quaternary system TDMAO/ 1-hexanol/decane/water were utilized to study the dynamics of the exchange of decane and the formation of microemulsions as a function of the composition (and therefore droplet size). The corresponding kinetic rate constants were determined for the three different detection methods for differently composed microemulsions and various mixing schemes. Finally dynamics were studied for the case of introducing electrostatic repulsion into the originally uncharged system.

Stopped-flow fluorescence measurements were performed for a detailed analysis of the exchange kinetics. By increasing the size of the aggregates, thereby decreasing $2\kappa + \bar{\kappa}$, the coalescence rate increases continuously. This trend reflects nicely the effect of the increasing hindrance to fusion caused by the decrease of cosurfactant content as the more cosurfactant in the ME aggregate, the softer the interface and the less energy is required to produce on encounter pair. The activation energies calculated from the temperature dependence according to Arrhenius´ law and compared to the diffusion rate constant increased linearly with decreasing droplet size.

The formation of O/W microemulsions was investigated in transmission, fluorescence and small-angle X-ray scattering mode. Results show that by varying the concentration of solubilised oil, thereby varying the size of the microemulsion aggregates, the logarithm of the coalescence rate depends linearly on the difference in droplet concentration of the two initial MEs during the formation process. This means that the exchange process is the slower the further away in the phase diagram the two starting solutions are located.

Addition of charge by replacing up to 2 wt% of TDMAO with the cationic TTAB leads to a slowing down of both coalescence processes by about one order of magnitude. At the same time, addition of the telechelic polymer to the microemulsion leads to a substantial increase in viscosity of one order of magnitude for Antil and two orders of magnitude for Rewopal, although the number of linking molecules is larger in the case of Antil.

Therefore the existence of a transient, homogeneous network with a polymer-induced transition from randomly to locally ordered droplet arrangements was proposed for all types of thickeners independent of their nature and chain lengths The slowing down was attributed to steric hindrance of the mobility of the droplets due to the polymer network. It was shown that the rate constant for oil exchange is only affected by the ratio of hydrophilic polymer chain length and interparticle distance.

In summary, our experiments show that the stopped-flow technique is very suited for studying coalescence processes in droplet microemulsions and allows discerning in detail effects of the amphiphile composition. These findings are of fundamental interest for a better understanding of the dynamic aspects of microemulsions but they are also of central importance for all solubilisation processes.

In the second part of this thesis the phase diagrams of the ternary system of 200 mM TDMAO in aqueous solution and various esters of intermediate polarity have been presented. The addition of semi-polar additives like esters is an interesting way of formulating amphiphilic systems as their flexible polarity and their character, which is in between that of a typical cosurfactant and that of a solubilisate allows for tuning structures and properties over a large range. With increasing alkyl chain length valerian (VME), capronic (CME), enanthic (EME) and pelargonic methyl ester (PME) were employed. In all cases an L_1-L_α-L_1-transition with increasing concentration of additive is observed, where its location depends on the temperature, being higher in temperature the shorter the ester. Unlike in the case of alcohols as cosurfactants, where the growth of micellar rods is followed by the formation of bilayers, here further addition of the ester at room temperature results in the solubilisation of the additional ester for short esters, while only the longer ones form a vesicle phase. However, upon further addition also these vesicles solubilise the ester into the interior of the aggregates thereby leading to microemulsions, which is clearly different from the case of alcohols. Due to a systematic study with respect to the alkyl chain length of the esters, observations from this chapter should therefore have a profound impact on the general understanding of such mixed amphiphilic systems and allow for a more rational design of them based on properties requested.

The system TDMAO/enanthic methyl ester/water at a constant surfactant concentration of 200 mM was employed to study the formation of vesicles with stopped-flow measurements in transmission, conductivity, small angle X-ray and dynamic light scattering mode. Due to the highly symmetric vesicle phase in the phase diagram with EME it was possible to study the kinetics of the formation process depending on the distance between the starting composition and the final composition and a roughly linear dependency could be found. Accordingly the time constant observed is related to the concentration difference in EME between the two isotropic solutions that are mixed.

The incorporation of the charged TTAB leads to a reduction of this vesicle-to-L_1 transition, the more so the higher the amount of incorporated TTAB. This increased tendency for vesicle formation can be explained by the reduction of the Gaussian bending modulus $\bar{\kappa}$ due to electrostatic interaction that favours the formation of vesicle. The kinetics of vesicle formation depends strongly on the amount of incorporated cationic surfactant and is slowed down by a factor 4 - 5 when 2 wt% surfactant is replaced by TTAB. Apparently the coalescence of amphiphilic domains, which is required in the process of forming multilamellar vesicles starting from micelles and microemulsion droplets, is substantially hindered already by the presence of small amounts of ionic surfactant.

To conclude, the stopped-flow technique is a very useful tool to study the complex process of solubilisation and can be coupled to different, even complementary detection methods in order to obtain detailed information equilibrium dynamics or structural transition in amphiphilic systems.

Future perspectives

During the development of this project and the attempt to study the formation of multilamellar vesicles, new issues appeared and in the following some ideas for possible future research is presented. In chapter 7 the retarding effect of charge incorporated into the surfactant layer on the formation of vesicles was presented. Preliminary results from stopped-flow turbidity measurements show a much higher effect by addition of alkyl ethoxylates. In figure 8.1 the evolutions of the transmission by mixing equal amounts of 200 mM TDAMO and 200 mM TDAMO/450 mM EME, each solution containing 1.00 wt% Brij97 ($C_{18}E_{10}$, circles) and Brij100 ($C_{18}E_{100}$, triangles) respectively are presented. As well as in for the mixing without additive, a two-step process with a pronounced minimum could be observed for both cases. However, the appearance of the minima is delayed by a factor of 10 for Brij100 and by a factor of 100 for Brij97. The higher effect of Brij97 is presumably due to the higher molar concentration compared to the longer additive. However, a very interesting approach would be the quantitative analysis of the retarding effect with respect to the concentration of additive.

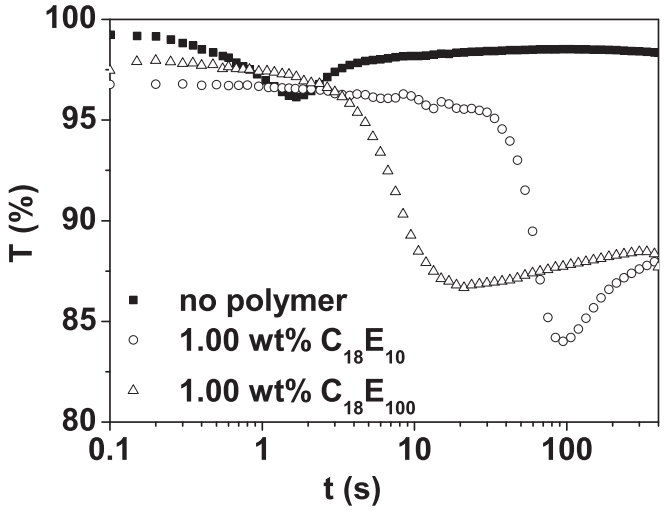

figure 8.1 Stopped-flow transmission measurements of the formation of vesicles according to mixing procedure (**I**) (at 25°C). The influence of polymer on the kinetic of vesicle formation is displayed: no polymer (straight line), 1.00 wt% Brij100 ($C_{18}E_{100}$) and 1.00 wt% Brij97 ($C_{18}E_{10}$)

Another open question is the mechanism of solute exchange in the quaternary system TDMAO/hexanol/decane/water. The zwitterionic surfactant is known to exhibit properties both of ionic and nonionc amphiphiles. As already mentioned in the chapter 1, and in contrary to the nonionic case, observed relaxation rates for microemulsions from ionic surfactants show no dependency on the concentration of `empty` droplets. Therefore first-order kinetics can be observed for ionic surfactants whereas second-order kinetics can be attributed to the nonionic ones. Hence, the question arises wether TDMAO exhibits a first- or second-order mechanism. A direct determination of the exchange mechanism is not possible as dilution with water will induce a shift in the phase diagram into the two-phase region. However, stopped-flow fluorescence measurements in the ternary system TDMAO/cyclohexane/water indicate no correlation between k_{obs} and the concentration of aggregates. An extensive study, e.g. with varying chain length of the zwitterionic surfactant or oil could contribute to the clarification of such a fundamental question.

9 Appendix

9.1 Appendix to Chapter 3

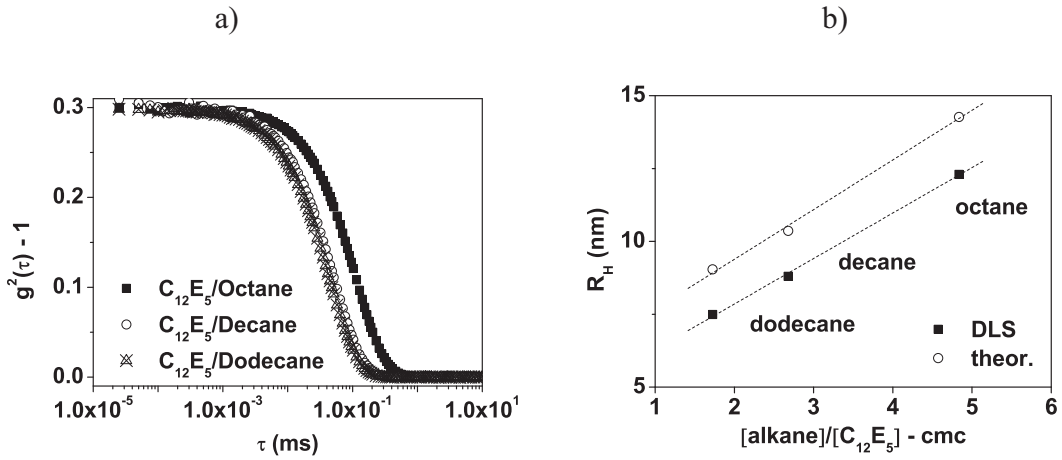

A figure 9.1 a) DLS measurements of ternary MEs with $C_{12}E_5$ and oils of different alkyl chain length (octane, decane, dodecane) at the solubilisation limit (25 °C); b) Hydrodynamic radius derived from DLS measurements (squares) in a) and theoretical values according to equation 3.3 (circles) versus the molar ratio of dispersed component to surfactant within the droplets

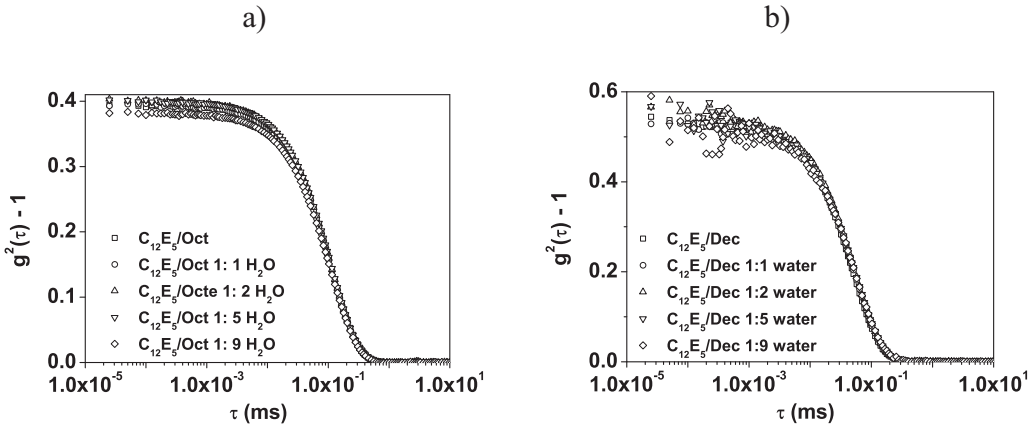

c)

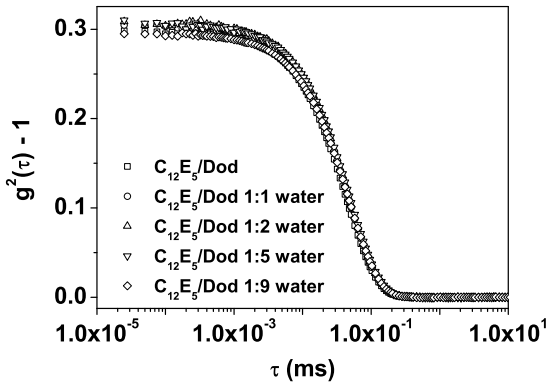

A figure 9.2 DLS measurements of the dilution of ternary MEs with water: a) octane, b) decane and c) dodecane. The droplet size of the single-phase MEs was independent of the concentration of ME aggregates

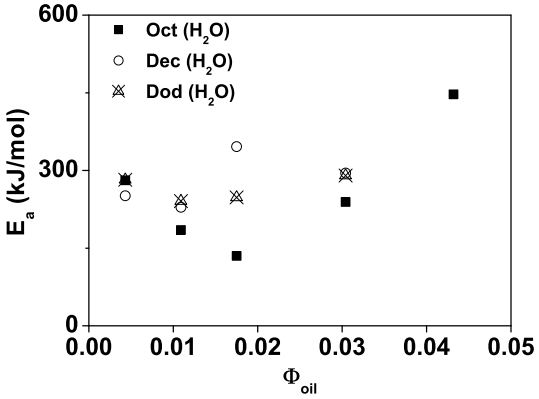

A figure 9.3 Arrhenius´ activation energy from the measurements in figure 3.3; ternary ME with octane (filled squares), decane (circles) and dodecane (triangles) in water

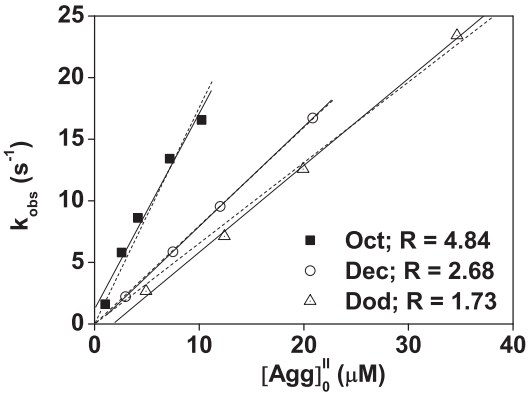

A figure 9.4 Observed relaxation rate versus $[Agg]_0^{II}$ (concentration of unloaded ME aggregates) for three different oils (square: octane, circle: decane, triangle: dodecane) solubilised in the ternary system $C_{12}E_5$/oil/water with the ratio, R of oil to surfactant for each hydrocarbon at the solubilisation limit at 25 °C. Straight lines denote the linear fits to the data; dashed lines the linear fit through the origin

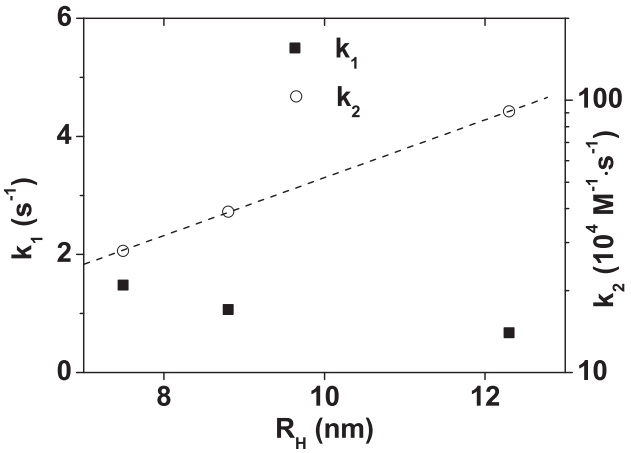

A figure 9.5 First-order and second-order relaxation rates (k_1 and k_2) as function of the hydrodynamic radius; lines mark the linear fits to the data

a) b)

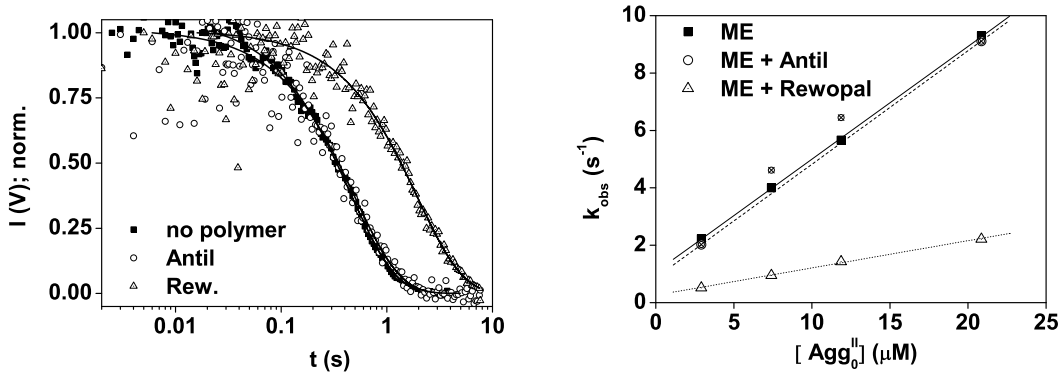

A figure 9.6 a) Stopped-flow fluorescence measurements: 1:1-mixing of two identical MEs with $C_{12}E_5$ and decane in water and the fits (mono-exponential function) at 25 °C: normalized excimer intensity versus measurement time for various concentrations of HM-polymers (square: no polymer, circle: 0.226 wt% Antil, triangle: 0.500 wt% Rewopal). b) Observed relaxation rates for the pure microemulsion $C_{12}E_5$/decane/water (squares), with 0.226 wt% Antil (circles) and 0.5 wt% Rewopal (triangle) versus the concentration of ME aggregates. Lines denote the linear fits of the experimental data; crossed circles denote data points which were not taken into account into the fit because of experimental disturbances

a) b)

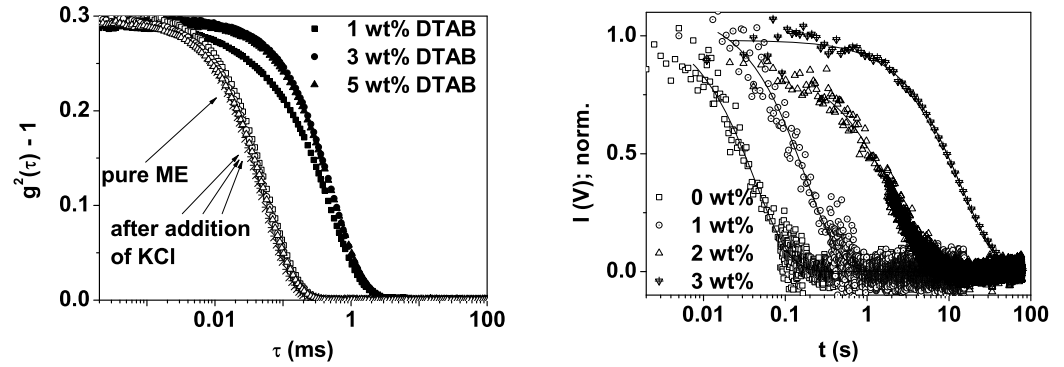

c)

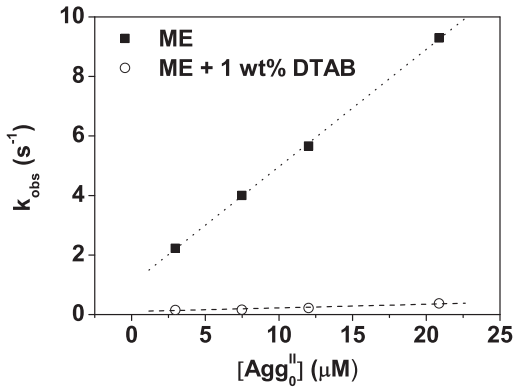

A figure 9.7 a) DLS measurements of ternary MEs with $C_{12}E_5$ and decane with various amounts of DTAB (filled symbols; square: 1 wt%, circle: 3 wt%, triangle: 5 wt%) and after addition of KCl to screen the Coulomb forces (empty symbols) at 25 °C; b) observed relaxation rates for the pure microemulsion $C_{12}E_5$/decane/water (squares), with 1 wt% DTAB (circles) versus the concentration of ME aggregates. Lines denote the linear fits of the experimental data

A table 9.1 First- and second order rate constants calculated from k_{obs} versus [Agg] according to Rharbi et al. and Hilzcer at al. [35, 88]

	(i)			**(ii)**		
k_{obs} versus $[Agg]_0^{II}$	**Oct**	**Dec**	**Dod**	**Oct**	**Dec**	**Dod**
k_1 (10^{-4} $\cdot M^{-1}s^{-1}$)	317.9	162.2	141.1	363.5	131.8	111.4
k_2 (10^{-4} $\cdot M^{-1}s^{-1}$)	79.47	40.54	35.27	90.86	32.95	27.86

9.2 Appendix to Chapter 4

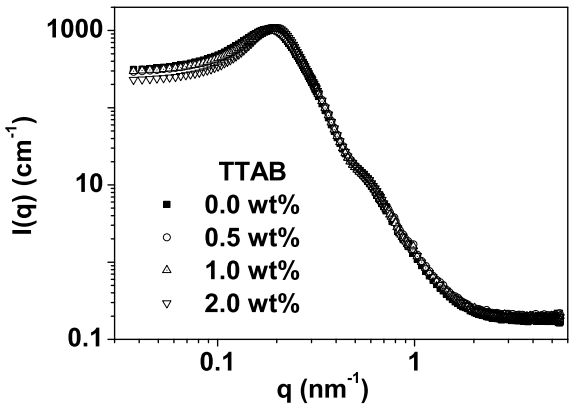

A figure 9.8. Small angle neutron scattering curves for various degrees of ionic substitution in the microemulsion ME2: 0 (squares), 0.5 (circles), 1.0 (triangles) and 2.0 wt% (stars) TTAB

A table 9.2 Relaxation rates, activation energies and additional activation energies due to the charge introduced into the system for the formation of microemulsions by mixing ME1 1:1 ME2 (composition given in table 4.1) at different amount of charge incorporated in the system by replacing x wt% of TDMAO with TTAB

ME2+ME1 [TTAB] (wt%)	**k_{obs}(T) (s^{-1})**	**E_a(T) (kJ/mol)**	**ΔE_{ion}(T) (kJ/mol)**	**k_{obs}(FL) (s^{-1})**	**E_a(FL) (kJ/mol)**	**ΔE_{ion}(FL) (kJ/mol)**
0.0	6.112	224		5.687	164	
0.5	4.562	130	0.9	3.967	214	0.9
1.0	2.779	-	2.2	3.038	148	1.6
1.5	-	255	-	2.778	130	1.8
2.0	1.958	216	3.1	1.823	128	2.8

A table 9.3 SF-fluorescence measurements: observed relaxation rates of the exchange of solubilisate between ME1, ME2 and ME3 with pyrene ester (*Scheme III*). Relaxation rates were obtained from fitting SF-fluorescent curves monitored at λ_{em} = 435 - 600 nm with λ_{ex} = 350 nm fitted with a mono-exponential function

	25 °C			**26 °C**			**27 °C**			
	k_{obs} (s)	**ampl.**	**I_∞ (V)**	**k_{obs} (s)**	**ampl.**	**I_∞ (V)**	**k_{obs} (s)**	**ampl.**	**I_∞ (V)**	**E_a (kJ/mol)**
ME1	3.63	0.638	1.70	4.46	0.629	1.68	5.74	0.640	1.70	171
ME2	8.22	0.274	1.20	9.22	0.268	1.17	11.2	0.261	1.14	114
ME3	3.82	0.095	0.83	4.07	0.093	0.82	4.79	0.093	0.82	84

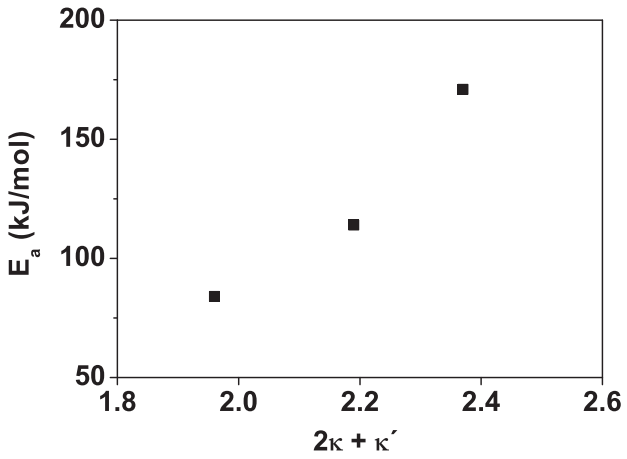

A figure 9.9. Arrhenius´ activation energy of the interpool-exchange of solubilisate, derived from measurements at three different temperatures (25, 26 and 27 °C) as function of the sum $2\kappa + \bar{\kappa}$ of the bending constants of the ME aggregates

9.3 Appendix to Chapter 5

A table 9.4 Calculated observed relaxation rates and effective activation energies for the exchange of oil between microemulsions in the system 100 mM TDMAO/105 mM hexanol/400.5 mM decane with increasing amount of HM-polymers Antil and Rewopal determined from the decrease of the excimer intensity with stopped-flow fluorescence measurements

	Antil				Rewopal		
[Antil] (wt%)	**k_{obs} (s^{-1})**	**ΔE_{eff} (kJ/mol)**	**η (mPa·s)**	**[Rew.] (wt%)**	**k_{obs} (s^{-1})**	**ΔE_{eff} (kJ/mol)**	**η (mPa·s)**
0.000	8.221	27.3	2.2162	0.000	8.221	27.3	2.2162
0.101	7.313	27.6		0.031	7.118	27.6	
0.250	6.411	27.9	2.6244	0.063	7.111	27.6	2.8868
0.500	5.857	28.1	3.3242	0.125	6.045	28.0	3.7908
0.749	5.192	28.4	4.2865	0.250	4.556	28.7	5.8320
0.999	4.291	28.9	7.6982	0.500	2.672	30.1	19.246
1.618	2.932	29.8					

9.4 Appendix to Chapter 6

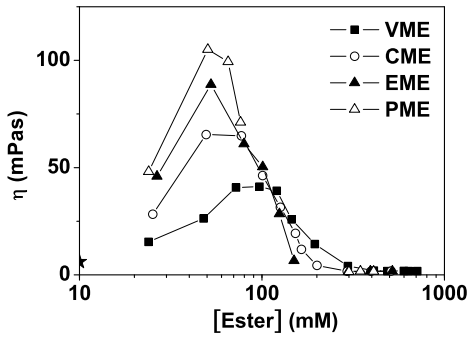

A figure 9.10 Dynamic viscosity η of 200 mM TDMAO for various esters as function of the ester concentration (VME: squares, CME: circles, EME: filled triangles, PME: unfilled triangles; micellar solution: star) at 25°C

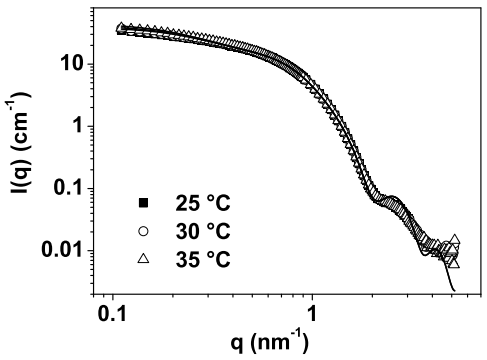

A figure 9.11 SANS intensity as a function of the magnitude of the scattering vector for the system 200 mM TDMAO/ D_2O with 181 mM VME at three different temperatures

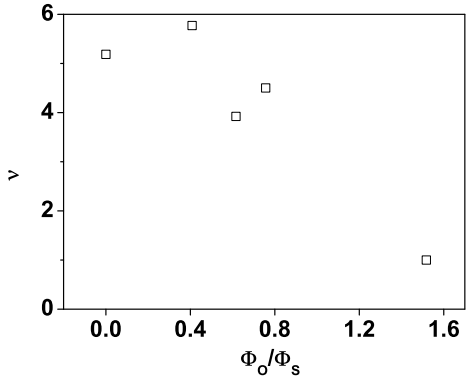

A figure 9.12 Ellipticity ν from the fits versus the ratio of volume fraction of oil to surfactant from the graphs in figure 6.6 for the system 200 mM TDMAO / VME at 25 °C

The porod volume is compared to the volume gained from the fit with the appropriate model deduced from the parameters of the model-free analysis. V_p is proportional to I_0/Inv which should be normalized to S(0), which we used in the fitting model assuming the existence of hard spheres in the system. For simplification we neglected S(0) (equation 6.12, where the hard sphere radius is determined from the dimensions of the ellipsoid and Φ_{HS} is determined from hard sphere radius and the experimental volume fraction.) in the calculation of the Porod volume and normalized V_p to S(0), when comparing it the volume from the fitted parameters. The volume of the aggregates in the system is a highly sensitive parameter and therefore crucial to evaluate the goodness of the fitting model applied (A figure 9.13 a).

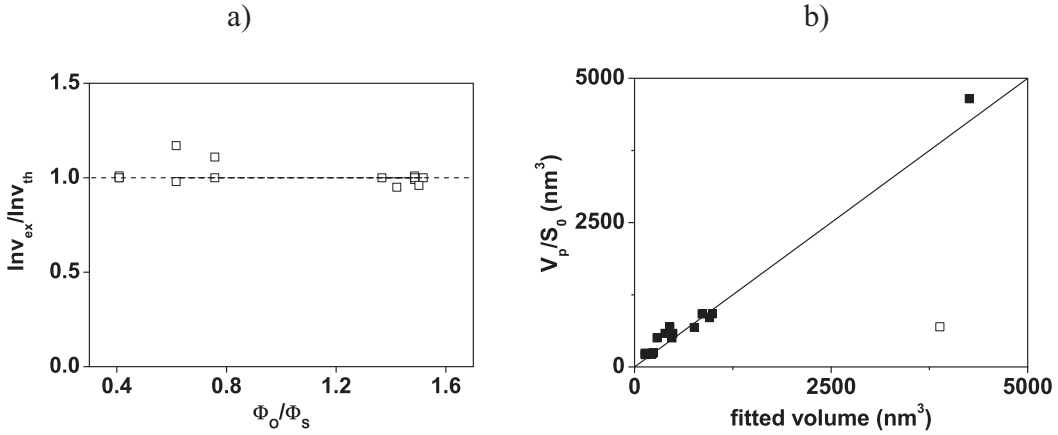

A figure 9.13 a) Ratio of theoretical and experimental invariant as function of the total volume fraction; b) volume from the fits with a model of ellipsoids normalized to S(0) for hard spheres versus calculated volume from the Porod plot (filled squares). The sample with 200 mM TDMAO/273 mM VME at 35 °C (empty square) is in the two-phase region and shows deviations from the linear behavior of the other samples

9.5 Appendix to Chapter 7

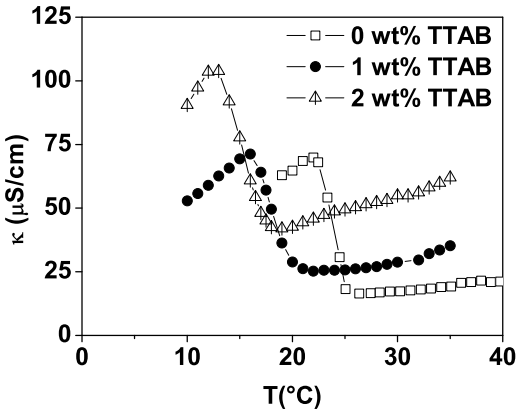

A figure 9.14 Specific conductivity of samples containing 200 mM TDMAO/ 225 mM EME, where 0, 1 and 2 wt% of the surfactant are replaced by the cationic surfactant TTAB

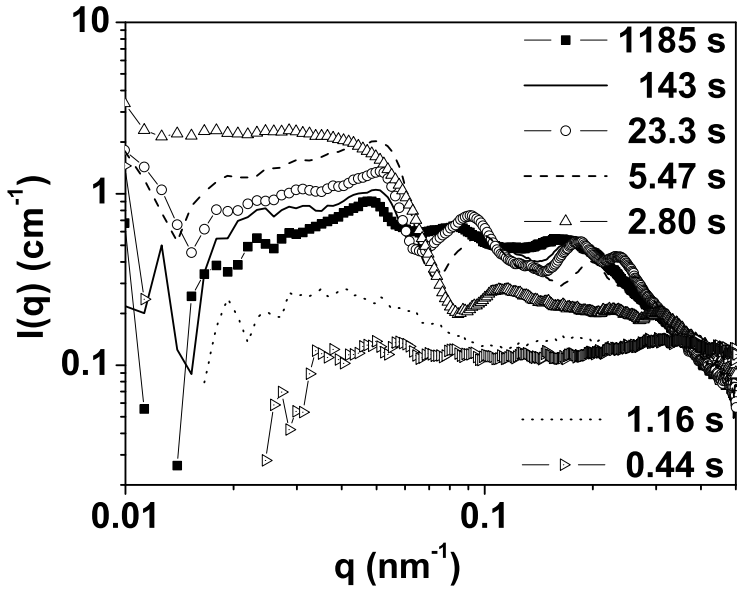

A figure 9.15 SAXS scattering patterns at different times after the mixing of two isotropic L_1-phases (200 mM TDMAO 1:1 200 mM TDMAO/ 450 mM EME) at 25 °C to reach the vesicle phase (200 mM TDMAO/ 225 mM EME) according to mixing procedure (**I**)

A table 9.5 Relaxation times and activation energies from SF-transmission measurements in figure 7.3; mixing of a micellar solution with a microemulsion (200 mM TDMAO 1:1 450 mM EME/ 200 mM TDMAO) to reach vesicle phase; replacement of TDMAO with 0, 1 and 2 wt% TTAB

0 wt% TTAB	**A_1 (%)**	**τ_1 (s)**	**β**	**A_2 (%)**	**τ_2 (s)**	**γ**	**T_∞**
22 °C	46.4	4.02	2.050	-41.4	22.1	1.389	94.7
25 °C	55.4	2.06	2.129	-52.6	8.90	1.265	95.7
28 °C	60.8	1.08	2.122	-61.5	3.93	1.346	97.5
E_a (kJ/ mol)		***162***			***213***		
1 wt% TTAB							
22 °C	40.0	11.3	1.804	-24.3	82.5	1.271	83.0
25 °C	56.2	3.89	1.949	-52.1	12.3	1.198	93.8
28 °C	52.2	2.19	2.426	-49.9	6.53	1.755	92.8
E_a (kJ/ mol)		***202***			***314***		
2 wt% TTAB							
22 °C	32.5	10.7	2.134	-14.1	43.1	1.896	81
25 °C	35.6	4.24	2.024	-31.5	23.8	1.254	95.3
28 °C	43.3	2.45	1.916	-40.8	8.88	1.233	96.9
E_a (kJ/ mol)		***182***			***194***		

References

[1] C. Tanford. *The hydrophobic effect*. Wiley (New York), 2nd edition., 1980.

[2] J.N. Israelachvili, D.J. Mitchell, and B.W. Ninham. Theory of self-assembly of hydrocarbon amphiphiles into micelles and bilayers. *Journal of the Chemical Society-faraday Transactions Ii*, 72:1525–1568, 1976.

[3] P. Ekwall. 2 types of micelle formation in organic solvents. *Journal of Colloid and Interface Science*, 29(1):16–&, 1969.

[4] Y. Chevalier and T. Zemb. The structure of micelles and microemulsions. *Rep. Prog. Phys.*, 53:279–371, 1990.

[5] U. Hornfeck, M. Gradzielski, K. Mortensen, C. Thunig, and G. Platz. Highly swollen lamellar phases in the system calcium dodecyl sulfate, pentanol or hexanol, and water. *Langmuir*, 14(11):2958–2964, May 1998.

[6] H. Hoffmann. Fascinating phenomena in surfactant chemistry. *Advanced Materials*, 6(2):116–129, February 1994.

[7] S. Ristori, J. Appell, and G. Porte. Spontaneous formation of monodisperse vesicles in dilute aqueous solutions of pfpe and betaine. *Langmuir*, 12(3):686–690, February 1996.

[8] J. Oberdisse, O. Regev, and G. Porte. Experimental study of the micelle-to-vesicle transition. *Journal of Physical Chemistry B*, 102(7):1102–1108, February 1998.

[9] M. Gradzielski, M. Valiente, H. Hoffmann, and S. Egelhaaf. Structural changes in the isotropic phase of the ternary surfactant system: Tetradecyldimethylamine oxide/benzyl alcohol/water. *Journal of Colloid and Interface Science*, 205(1):149–160, September 1998.

[10] M. Gradzielski. Vesicles and vesicle gels - structure and dynamics of formation. *J. Phys. Condens. Matter*, 15:R655–R697, 2003.

[11] D. A. Balazs and W.T. Godbey. Liposomes for use in gene delivery. *J. Drug Deliv.*, 2011.

[12] H. Hoffmann, M. Bergmeier, M. Gradzielski, and C. Thunig. Preparation of three morphologically different states of a lamellar phasehoffmann1998. In G. Lagaly, editor, *Horizons 2000 â€“ aspects of colloid and interface science at the turn of the millenium*, volume 109 of *Progress in Colloid and Polymer Science*, pages 13–20. Springer Berlin / Heidelberg, 1998. 10.1007/BFb0118152.

[13] M. Gradzielski. Investigations of the dynamics of morphological transitions in amphiphilic systems. *Current Opinion In Colloid & Interface Science*, 9(3-4):256–263, November 2004.

[14] J.H. Schulman, W. Stoeckenius, and L.M. Prince. Mechanism of formation and structure of micro emulsions by electron microscopy. *Journal of Physical Chemistry*, 63(10):1677–1680, 1959.

[15] H. L. Rosano, J. L. Cavallo, and G. B. Lyons. *Microemulsion Systems*, page 259. Marcell Dekker, 1987.

[16] L. Taisne and B. Cabane. Emulsification and ripening following a temperature quench. *Langmuir*, 14(17):4744–4752, August 1998.

[17] B.K. Paul and S.P. Moulik. Uses and applications of microemulsions. *Current Science*, 80(8):990–2001, 2001.

[18] C. Giordano, C. Erpen, W. T. Yao, and M. Antoniett. Synthesis of mo and w carbide and nitride nanoparticles via a simple "urea glass" route. *Nano Letters*, 8(12):4659–4663, December 2008.

[19] K. Osseo-Asare and F.J. Arriagada. Preparation of sio2 nanoparticles in a non-ionic reverse micellar system. *Colloids and Surfaces*, 50:321–339, 1990.

[20] M. Boutonnet, J. Kizling, and P. Stenius. The preparation of monodisperse colloidal metal particles from micro-emulsions. *Colloids and Surfaces*, 5(3):209–225, 1982.

[21] M. Boutonnet, J. Kizling, R. Touroude, G. Maire, and P. Stenius. Monodispersed colloidal metal particles from nonaqueous solutions - catalytic behavior in hydrogenolysis and isomerization of hydrocarbons of supported platinum particles. *Catalysis Letters*, 9(5-6):347–354, 1991.

[22] P. D. I. Fletcher and D. I. Horsup. Droplet dynamics in water-in-oil microemulsions and macroemulsions stabilised by non-ionic sufactants. *J. Chem. Soc. Faraday Trans.*, 88(6):955–864, 1992.

[23] P. D. I. Fletcher, A. M. Howe, and B. H. Robinson. The kinetics of solubilisate exchange between water droplets of a water-in-oil microemulsion. *J. Chem. Soc., Faraday Trans.*, 83:985–1006, 1987.

[24] P.L. Luisi. Enzymes hosted in reverse micelles in hydrocarbon solution. *Angewandte Chemie-international Edition In English*, 24(6):439–450, 1985.

[25] P.L. Luisi, M. Giomirfi, M.P. Hleni, and B.H. Robinson. Reverse mice|les as hosts for proteins and small molecules. *Biochimica et Biophysica Acta*, 947:209–246, 1988.

[26] P. Lüthi and P.L. Luisi. Enzymatic synthesis of hydrocarbon-soluble peptides with reverse micelles. *J. Am. Chem. SOC.*, 106:7286–7288, 1984.

[27] E. A. G. Aniansson, S. N. Wall, M. Almgren, H. Hoffmann, I. Kielmann, W. Ulbricht, R. Zana, J. Lang, and C. Tondre. Theory of kinetics of micellar equilibria and quantitative interpretation of chemical relaxation studies of micellar solutions of ionic surfactants. *Journal of Physical Chemistry*, 80(9):905–922, 1976.

[28] N. Muller. *Solution Chemistry of Surfactants*, pages 267–295. Plenum: New York, 1979.

[29] J. Gormally, W. J. Gettins, and E. Wyn-Jones. *Molecular Interactions*, volume 2, pages 143–177. Wiley: New York, 1980.

[30] J. Lang and R. Zana. *Surfactant Solutions: New Methods of Investigation*, pages 405–452. Marcel Dekker: New York, 1987.

[31] P. D. T. Huibers, S. G. Oh, and D. O. Shah. *Surfactants in Solution*, volume 64, pages 105–121. Marcel Dekker: New York, 1995.

[32] E. A. G. Aniansson and S. N. Wall. Kinetics of step-wise micelle association. *The Journal of Physical Chemistry*, 78(10):1024–1030, 1974.

[33] M. H. Gehlen and F. C. De Schryver. Time-resolved fluorescence quenching in micellar assemblies. *Chemical Reviews*, 93(1):199–221, January 1993.

[34] Y. Rharbi, N. Bechthold, K. Landfester, A. Salzman, and M.A. Winnnik. Solute exchange in synperonic surfactant micelles. *Langmuir*, 19(1):10–17, January 2003.

[35] Y. Rharbi, M. Li, M. Winnik, and K.G. Hahn. Temperature dependence of fusion and fragmentation kinetics of triton x-100 micelles. *Journal of the American Chemical Society*, 122(26):6242–6251, 2000.

[36] J. Lang, J. J. Auborn, and E.M. Eyring. Kinetics of octylphenyl polyoxyethylene alcohol micelle dissociation by a stopped-flow technique. *Journal of Colloid and Interface Science*, 41(3):484–490, 1972.

[37] T. Yasunaga, K. Takeda, and S. Harada. Kinetic study of sodium dodecyl sulfate micelle dissociation by a stopped-flow method. *Journal of Colloid and Interface Science*, 42(2):457–463, 1973.

[38] T. Inoue, H. Ohshima, H. Kamaya, and I. Ueda. Stopped-flow rapid kinetics of anesthetic-induced phase transition in phospholipid vesicle membranes: nonlocalized fluctuation. *Biochim Biophys Acta*, 818(2):117–122, 1985.

[39] S. Schmölzer, D. Gräbner, M. Gradzielski, and T. Narayanan. Millisecond-range time-resolved small-angle x-ray scattering studies of micellar transformations. *Phys. Rev. Lett.*, 88(25):258301–258304, 2002.

[40] T. M. Weiss, T. Narayanan, C. Wolf, M. Gradzielski, P. Panine, S. Finet, and W. I. Helsby. Dynamics of the self-assembly of unilamellar vesicles. *Phys. Rev. Lett.*, 94:038303–038307, 2005.

[41] S. E. Campbell, Z. Zhang, S. E. Friberg, and R. Patel. Kinetics of formation of vesicles from lecithin/sodium xylenesulfonate micelles from stopped-flow measurements. *Langmuir*, 14(3):590–594, 1998.

[42] M.L. Rogerson, B.H. Robinson, S. Bucak, and P. Walde. Kinetic studies of the interaction of fatty acids with phosphatidylcholine vesicles (liposomes). *Colloids and Surfaces B: Biointerfaces*, 48(1):24–34, 2006.

[43] A. Barth, I. Grillo, and M. Gradzielski. Dynamics of formation of vesicles studied by highly time-resolved stopped-flow experiments. *Tenside Surf. Det.*, 47:300–306, 2010.

[44] J.C. Mathai, S. Tristram-Nagle, J.F. Nagle, and M.L. Zeidel. *Structural Determinants of Water Permeability through the Lipid Membrane*, pages 69–76. The Rockefeller University Press, 2008.

[45] P. G. De Gennes and C. Taupin. Microemulsions and the flexibility of oil/water interfaces. *The Journal of Physical Chemistry*, 86(13):2294–2304, 1982.

[46] D. Langevin. Microemulsions - interfacial aspects. *Advances In Colloid and Interface Science*, 34:583–595, January 1991.

[47] M. Gradzielski, D. Langevin, T. Sottmann, and R. Strey. Droplet microemulsions at the emulsification boundary: The influence of the surfactant structure on the elastic constants of the amphiphillic film. *Journal of Chemical Physics*, 106(19):8232–8238, May 1997.

[48] P. Panizza, P. Roux, V. Vuillaume, C.Y.D. Lu, and M.E. Cates. Viscoelasticity of the onion phase. *Langmuir*, 12(2):248–252, January 1996.

[49] A.D. Bangham, M.M. Standish, and J.C. Watkins. Diffusion of univalent ions across the lamellae of swollen phospholipids. *Journal of Molecular Biology*, 13(1):238–252, 1965.

[50] W. Helfrich. Elastic properties of lipid bilayers - theory and possible experiments. *Z. Naturforsch.*, C 28(11-1):693–703, 1973.

[51] S.A Safran. Curvature elasticity of thin films. *Advances In Physics*, 48(4):395–448, July 1999.

[52] M. Gradzielski. Bending constants of surfactant layers. *Current Opinion in Colloid & Interface Science*, 3(5):478–484, 1998.

[53] F. Sicoli, D. Langevin, and L.T. Lee. Surfactant film bending elasticity in microemulsions - structure and droplet polydispersity. *Journal of Chemical Physics*, 99(6):4759–4765, September 1993.

[54] H. Hoffmann, G. Oetter, and B. Schwandner. The aggregation behaviour of tetradecyldimethylaminoxide. In H. Hoffmann, editor, *New Trends in Colloid Science*, volume 73 of *Progress in Colloid and Polymer Science*, pages 95–106. Springer Berlin / Heidelberg, 1987. 10.1007/3-798-50724-4_68.

[55] H. Katsuura, N. Takisawa, M. Manabe, and H. Maeda. Effect of the protonation equilibrium on the interaction of mixed micelles with their counterions. *Colloid and Polymer Science*, 277(2-3):261–264, February 1999.

[56] R. G. Laughlin. *The Aqueous Phase Behavior of Surfactants*. Academic Press, San Diego, CA, 1994.

[57] M. Gradzielski and H. Hoffmann. Influence of charges on structure and dynamics of an o/w microemulsion - effect of admixing ionic surfactants. *Journal of Physical Chemistry*, 98(10):2613–2623, March 1994.

[58] L.M. Prince. *Microemulsions: Theory and Practice*. Academic: New York, 1977.

[59] D. Langevin. *D. Mol. Cryst. Liq. Cryst.*, 138:259–305, 1986.

[60] M. Gradzielski, H. Hoffmann, J. C. Panitz, and A. Wokaun. Investigations on l(2) phase and cubic phase in the system aot 1-octanol water. *Journal of Colloid and Interface Science*, 169(1):103–118, January 1995.

[61] M. Gradzielski, H. Hoffmann, and D. Langevin. Solubilization of decane into the ternary-system tdmao/1-hexanol/water. *Journal of Physical Chemistry*, 99(33):12612–12623, August 1995.

[62] A.S. Kabalnov, U. Olsson, and H. Wennerström. Polymer effects on the phase-equilibrium of a balanced microemulsion. *Langmuir*, 10(7):2159–2169, July 1994.

[63] F. Witte. *Neuartige Vesikelphasen in Tensidsystemen mit Tetradecyldimethylaminoxid*. PhD thesis, Universität Bayreuth, 1999.

[64] *Manual BioLogic Science Instruments*.

[65] I. Grillo. Applications of stopped-flow in saxs and sans. *Current Opinion In Colloid & Interface Science*, 14(6):402–408, December 2009.

[66] T. Narayanan, O. Diat, and Bösecke P. Saxs and usaxs on the high brilliance beamline at the esrf. *Nuclear Instruments and Methods in Physics Research Section A: Accelerators, Spectrometers, Detectors and Associated Equipment*, 467-468(Part 2):1005–1009, 2001.

[67] B.J. Berne and R. Pecora. *Dynamic Light Scattering With Applications to Chemistry, Biology and Physics*. Dover Publications; Reprint edition, 2000.

[68] P.N. Pusey. *Photon Correlationi Spectroscopy and Velocimetry*. Plenum, New York, 1977.

[69] S.W. Provencher. Contin: A general purpose constrained regularization program for inverting noisy linear algebraic and integral equations. *Computer Physics Communications*, 27(3):229–242, 1982.

[70] S.M. King. Small angle neutron scattering. Technical report, ISIS Facility, Rutherford Appleton Laboratory, 1995.

[71] H. Schnablegger and Y. Singh. *A Practical Guide to SAXS*. Anton Paar GmbH, Austria, 2006.

[72] B. Vonnegut. Rotating bubble method for the determination of surface and interfacial tensions. *Rev. Sci. Instrum 13 (1942) 6*, 13:6–9, 1942.

[73] B. Föllner. PhD thesis, Bochum, 1990.

[74] G. Pößnecker. PhD thesis, Universität Bayreuth, 1992.

[75] R. Kühne, R.-U. Ebert, F. Kleint, G. Schmidt, and G. Schüürmann. Group contribution methods to estimate water solubility of organic chemicals. *Chemosphere*, 30(11):2061–2077, 1995.

[76] J.W. McBain and T.-M. Woo. The solubility of oil-soluble dyes in aqueous solutions of stable protecting colloids as examples of true reversible equilibrium. *Journal of the American Chemical Society*, 60(2):223–227, 1938.

[77] D. Sailaja, K.L. Suhasini, S. Kumar, and K.S. Gandhi. Theory of rate of solubilization into surfactant solutions. *Langmuir*, 19(9):4014–4026, April 2003.

[78] T. Tlusty, S.A. Safran, and R. Strey. Topology, phase instabilities, and wetting of microemulsion networks. *Physical Review Letters*, 84(6):1244–1247, February 2000.

[79] I. Szleifer, D. Kramer, A. Benshaul, D. Roux, and W.M. Gelbart. Curvature elasticity of pure and mixed surfactant films. *Physical Review Letters*, 60(19):1966–1969, May 1988.

[80] A. F. H. Ward and L. Tordai. Time-dependence of boundary tensions of solutions .1. the role of diffusion in time-effects. *Journal of Chemical Physics*, 14(7):453–461, 1946.

[81] A. Kabalnov and J. Weers. Kinetics of mass transfer in micellar systems: Surfactant adsorption, solubilization kinetics, and ripening. *Langmuir*, 12(14):3442–3448, July 1996.

[82] Rharbi and M.A. Winnik. Salt effects on solute exchange and micelle fission in sodium dodecyl sulfate micelles below the micelle-to-rod transition. *Journal of Physical Chemistry B*, 107(7):1491–1501, February 2003.

[83] P. D. I. Fletcher and J. F. Holzwarth. Aggregation kinetics of oil-in-water microemulsion droplets stabilized by c12e5. *Journal of Physical Chemistry*, 95(6):2550–2555, March 1991.

[84] S. Clark, P. D. I. Fletcher, and X. L Ye. Interdroplet exchange-rates of water-in-oil and oil-in-water microemulsion droplets stabilized by c12e5. *Langmuir*, 6(7):1301–1309, July 1990.

[85] M. Gradzielski, D. Langevin, and B. Farago. Experimental investigation of the structure of nonionic microemulsions and their relation to the bending elasticity of the amphiphilic film. *Physical Review E*, 53(4):3900–3919, April 1996.

[86] Y. Rharbi, A. Yekta, and M.A. Winnik. A method for measuring oxygen diffusion and oxygen permeation in polymer films based on fluorescence quenching. *Analytical Chemistry*, 71(22):5045–053, 1999.

[87] Y. Rharbi, V. Kitaev, M.A. Winnik, and K.G. Hahn. Characterizing aqueous micellar triton x-100 solutions of a fluorescent model triglyceride. *Langmuir*, 15(7):2259–2266, 1999.

[88] A. V. Hilczer, M. Barzykin and M. Tachiya. Theory of the stopped-flow method for studying micelle exchange kinetics. *Langmuir*, 17(14):4196–4201, July 2001.

[89] T.K. Wang, I. Iliopoulos, and R. Audebert. Viscometric behaviour of hydrophobically modified poly(sodium acrylate). *Polym. Bull.*, 20:577–582, 1988.

[90] M. Filali, R. Aznar, M. Svenson, G. Porte, and J. Appell. Swollen micelles plus hydrophobically modified hydrosoluble polymers in aqueous solutions:â€‰ decoration versus bridging. a small angle neutron scattering study. *The Journal of Physical Chemistry B*, 103(34):7293–7301, 1999.

[91] K. Thuresson, F.E. Antunes, M.G. Miguel, and B. Lindman. The association between a non-ionic microemulsion and hydrophobically modified peg. a rheological investigation. *Progress in Colloid and Polymer Science*, 123:40–43, 2004.

[92] D.B. Siano, J. Bock, and P. Myer. Interaction of watersolubles polymers with microemulsions and surfactants. *ACS symposium series*, 384:328–337, 1989.

[93] H. Bagger-Jörgensen, L. Coppola, K. Thuresson, U. Olsson, and K. Mortensen. Phase behavior, microstructure, and dynamics in a nonionic microemulsion on addition of hydrophobically end-capped poly(ethylene oxide). *Langmuir*, 13(16):4204–4218, 1997.

[94] D. Vollmer, J. Vollmer, B. Stühn, W. Wehrli, and H.F. Eicke. Polymer-induced ordering in water-oil-surfactant mixtures. *Physical Review E*, 52(5):5146–5155, November 1995.

[95] R. R. Hilfiker, H.F. Eicke, C. Steeb, and U. Hofmeier. Block-copolymer-induced structure formation in microemulsions. *Journal of Physical Chemistry*, 95(3):1478–1480, February 1991.

[96] M. Gradzielski, A. Rauscher, and H. Hoffmann. Hydrophobically cross-linked micellar solutions - microstructure and properties of the solutions. *Journal De Physique IV*, 3(C1):65–79, May 1993.

[97] J. T. Brooks, C. M. Marques, and M. E. Cates. The effect of adsorbed polymer on the elastic moduli of surfactant bilayers. *J. Phys. II (Paris)*, 1(6):673, 1991.

[98] C. Quellet, H.F. Eicke, G. Xu, and Y. Hauser. Transient networks in aba block copolymer-microemulsion systems. *Macromolecules*, 23(13):3347–3352, June 1990.

[99] M. Odenwald, H.F. Eicke, and W. Meier. Transient networks by aba triblock copolymers and microemulsions - a rheological study. *Macromolecules*, 28(14):5069–5074, July 1995.

[100] R.P.W.J. Struis and H.F. Eicke. Polymers in complex fluids - dynamic and equilibrium properties of nanodroplet-aba block copolymer structures. *Journal of Physical Chemistry*, 95(15):5989–5996, July 1991.

[101] F. E. Antunes, K. Thuresson, B. Lindman, and M. G Miguel. A rheological investigation of the association between a non-ionic microemulsion and hydrophobically modified peg. influence of polymer architecture. *Colloids and Surfaces A: Physicochemical and Engineering Aspects*, 215(1-3):87–100, 2003.

[102] F. Molino, J. Appell, M. Filali, E. Michel, G. Porte, S. Mora, and E. Sunyer. A transient network of telechelic polymers and microspheres: structure and rheology. *Journal of Physics-condensed Matter*, 12(8A):A491–A498, February 2000.

[103] M. Filali, M. J. Ouazzani, E. Michel, R. Aznar, G. Porte, and J. Appell. Robust phase behavior of model transient networks. *The Journal of Physical Chemistry B*, 105(43):10528–10535, 2001.

[104] A. Evilevitch, V. Lobaskin, U. Olsson, P. Linse, and P. Schurtenberger. Structure and transport properties of a charged spherical microemulsion system. *Langmuir*, 17(4):1043–1053, February 2001.

[105] U. Olsson and P. Schurtenberger. Structure, interactions, and diffusion in a ternary nonionic microemulsion near emulsification failure. *Langmuir*, 9(12):3389–3394, December 1993.

[106] A. Barth, P. Malo-de Molina, and M. Gradzielski. The kinetics of solubilisate exchange in a zwitterionic microemulsion on addition of hydrophibically end-capped poly(ethylene oxide). *in preparation*.

[107] H. Hoffmann, U. Munkert, C. Thunig, and M. Valiente. The lyotropic mesophases in dilute surfactant mixtures of tetradecyldimethylaminoxide, tetradecyltrimethylammonium bromide, and hexanol - the influence of ionic charge on the mesophases. *Journal of Colloid and Interface Science*, 163(1):217–228, March 1994.

[108] C. Caillet, M. Hebrant, and C. Tondre. Rate of water uptake by water-in-oil microemulsions in relation with the properties of the amphiphilic film. *Langmuir*, 14(16):4378–4385, August 1998.

[109] J.M.G. Sarraguça, A.A.C.C. Pais, and P. Linse. Influence of droplet properties on the formation of microemulsion-aba-triblock copolymer networks. *Soft Matter*, 5:140–147, 2009.

[110] H. Lee, R. M. Venable, A. D. MacKerell, and R. W. Pastor. Molecular dynamics studies of polyethylene oxide and polyethylene glycol: Hydrodynamic radius and shape anisotropy. *Biophysical Journal*, 95(4):1590–1599, August 2008.

[111] A. Barth, S. Prevost, J. Popig, M. Dzionara, G. Hedicke, and M. Gradzielski. Solubilisation of different medium chain esters in zwitterionic surfactant solutions – effects on phase behavior and structure. *J. Colloid Interface Sci.*, page accepted, 2011.

[112] B. G. Schlarb-Ridley, H. L. Mi, W. D. Teale, V. S. Meyer, C. J. Howe, and D. S. Bendall. Implications of the effects of viscosity, macromolecular crowding, and temperature for the transient interaction between cytochrome f and plastocyanin from the cyanobacterium phormidium laminosum. *Biochemistry*, 44(16):6232–6238, April 2005.

[113] N. Kozer and G. Schreiber. Effect of crowding on protein - protein association rates: Fundamental differences between low and high mass crowding agents. *Journal of Molecular Biology*, 336(3):763–774, February 2004.

[114] K. A. Xavier and R. C. Willson. Association and dissociation kinetics of anti-hen egg lysozyme monoclonal antibodies hyhel-5 and hyhel-10. *Biophysical Journal*, 74(4):2036–2045, April 1998.

[115] H. A. Kramers. Brownian motion in a field of force and the diffusion model of chemical re actions. *Physica*, 7:284–304, 1940.

[116] C. J. Feng, R. V. Kedia, J. T. Hazzard, J. K. Hurley, G. Tollin, and J. H. Enemark. Effect of solution viscosity on intramolecular electron transfer in sulfite oxidase. *Biochemistry*, 41(18):5816–5821, May 2002.

[117] M. M. IvkovicJensen and N. M. Kostic. Effects of viscosity and temperature on the kinetics of the electron-transfer reaction between the triplet state of zinc cytochrome c and cupriplastocyanin. *Biochemistry*, 36(26):8135–8144, July 1997.

[118] P.G. De Gennes, P. Pincus, R.M. Velasco, and F. Brochard. Remarks on polyelectrolyte conformation p. 1461. *J. Phys. (Paris)*, 37(12):1461–1474, 1976.

[119] D. Langevin and F. Rondelez. Sedimentation of large colloidal particles through semidilute polymer-solutions. *Polymer*, 19(8):875–882, 1978.

[120] A. Meziani, A. Zradba, D. Touraud, M. Clausse, and W. Kunz. Can aldehydes participate in the nanostructuration of liquids containing charged micelles? *Journal of Molecular Liquids*, 73-4:107–118, November 1997.

[121] A. Meziani, D. Touraud, A. Zradba, M. Clausse, and W. Kunz. Co-surfactant properties of ketones. *Journal of Molecular Liquids*, 84(3):301–311, March 2000.

[122] M. Landgren, M. Aamodt, and B. Joensson. Solubilization of uncharged molecules in ionic surfactant aggregates. 2. phase equilibria. *The Journal of Physical Chemistry*, 96(2):950–961, 1992.

[123] H. Preu, A. Zradba, S. Rast, W. Kunz, E. H. Hardy, and M. D. Zeidler. Small angle neutron scattering of d2o-brij 35 and d2o-alcohol-brij 35 solutions and their modelling using the percus-yevick integral equation. *Physical Chemistry Chemical Physics*, 1(14):3321–3329, July 1999.

[124] E. Caponetti, A. Lizzio, and R. Triolo. Small-angle neutron-scattering study of w/o n-hexadecane, potassium oleate, water, and cnh2n+1oh (n = 5-8) microemulsions - effect of water concentration. *Langmuir*, 6(11):1628–1634, November 1990.

[125] H. Saito and K. Shinoda. The solubilization of hydrocarbons in aqueous solutions of nonionic surfactants. *Journal of Colloid and Interface Science*, 24(1):10–15, 1967.

[126] M. Kahlweit and R. Strey. Phase behavior of ternary systems of the type h2oï£¿oilï£¿nonionic amphiphile (microemulsions). *Angewandte Chemie International Edition in English*, 24(8):654–668, 1985.

[127] D.B. Siano, J. Bock, P. Myer, and W.B. Russel. Thermodynamics and hydrodynamics of a nonionic microemulsion. *Colloids and Surfaces*, 26:171–190, September 1987.

[128] H. Hoffmann and W. Ulbricht. Transition of rodlike to globular micelles by the solubilization of additives. *Journal of Colloid and Interface Science*, 129(2):388–405, May 1989.

[129] G. Oetter and H. Hoffmann. Ringing gels and their fascinating properties. *Colloids and Surfaces*, 38(1-3):225–250, August 1989.

[130] C.A. Miller, M. Gradzielski, H. Hoffmann, U. Krämer, and C. Thunig. Experimental results for the l3 phase in a zwitterionic surfactant system and their implications regarding structures. *Colloid and Polymer Science*, 268(11):1066–1072, November 1990.

[131] F. Schambil and M. J. Schwuger. Cps lg 315 correlation between the phase behavior of ternary systems and removal of oil in the washing process. *Colloid & Polymer Science*, 265:1009–1017, 1987. 10.1007/BF01412405.

[132] M. A. Arandia, A. M. Forgiarini, and J. L. Salager. Resolving an enhanced oil recovery challenge: Optimum formulation of a surfactant-oil-water system made insensitive to dilution. *Journal of Surfactants and Detergents*, 13(2):119–126, April 2010.

[133] L. J. Magid, R. Triolo, and J. S. Johnson. Critical phenomena and aggregate structure in an oil-in-water microemulsion - a small-angle neutron-scattering study. *Journal of Chemical Physics*, 81(11):5161–5166, 1984.

[134] M. Gradzielski, H. Hoffmann, K. Horbaschek, and F. Witte. Thermoreversible vesicles with semipolar additives. In Noboru Oyama Yasuhiro Iwasawa and Hironobu Kunieda, editors, *Proceedings of the International Conference on Colloid and Surface Science, 25th Anniversary of the Division of Colloid and Surface Chemistry, The Chemical Society of Japan*, volume 132 of *Studies in Surface Science and Catalysis*, pages 589–593. Elsevier, 2001.

[135] H. Hoffmann, K. Horbaschek, and F. Witte. Vesicle phases with semipolar additives. *Journal of Colloid and Interface Science*, 235(1):33–45, 2001.

[136] F. Devinsky, A. Letimanovy, I. Lacko, and L. Krasnec. Amine oxides .13. iodine complexes with nonaromatic amine oxides. *Tetrahedron*, 41(23):5707–5709, 1985.

[137] J. D. Fields and P. J. Kropp. Surface-mediated reactions. 9. selective oxidation of primary and secondary amines to hydroxylamines. *Journal of Organic Chemistry*, 65(19):5937–5941, September 2000.

[138] S H Chen. Small angle neutron scattering studies of the structure and interaction in micellar and microemulsion systems. *Annual Review of Physical Chemistry*, 37(1):351–399, 1986.

[139] N. W. Ashcroft and J. Lekner. Structure and resistivity of liquid metals. *Physical Review*, 145(1):83–90, 1966.

[140] H. Hoffmann, C. Thunig, and M. Valiente. The different phases and their macroscopic properties in ternary surfactant systems of alkyldimethylamine oxides, intermediate chain n-alcohols and water. *Colloids and Surfaces*, 67:223–237, November 1992.

[141] M. Bourrel, C. Koukounis, R. Schechter, and W. Wade. Phase and interfacial-tension behavior of non-ionic surfactants. *Journal of Dispersion Science and Technology*, 1(1):13–35, 1980.

[142] R. S. Schechter, W. H. Wade, U. Weerasooriya, V. Weerasooriya, and S. Yiv. Synthesis and performance of isomer-free secondary alkane sulfonate surfactants. *Journal of Dispersion Science and Technology*, 6(2):223–235, 1985.

[143] M. S. Leaver, U. Olsson, H. Wennerström, and R. Strey. Emulsification failure in a ternary microemulsion. *Journal De Physique Ii*, 4(3):515–531, March 1994.

[144] P. Lindner and Th. Zemb. *X-rays and Light: Scattering Methods Applied to Soft Condensed Matter*. North Holland, 2002.

[145] M. Gradzielski. Effect of the cosurfactant structure on the bending elasticity in nonionic oil-in-water microemulsions. *Langmuir*, 14(21):6037–6044, October 1998.

[146] A. Bumajdad, J. Eastoe, and R. K. Heenan. Properties of mixed alcohol-zwitterionic surfactant films in quaternary water-in-oil microemulsions. *Langmuir*, 19(18):7219–7225, September 2003.

[147] G. Oetter and H. Hoffmann. Correlation between interfacial-tensions and micellar structures. *Journal of Dispersion Science and Technology*, 9(5-6):459–492, 1989.

Publications

[1] Anina Barth, Michaela Dzionara, Peggy Heunemann, Jeremie Gummel, Michael Gradzielski
"Kinetic of the Formation of Microemulsions and the Exchange of Oil in a Quaternary Surfactant System - Correlation of Measured Rates with Interfacial Rigidity and Charge"
to be submitted as part of chapter 4

[2] Anina Barth*, Paula Malo de Molina*, Michaela Dzionara, Michael Gradzielski
"The Kinetics of Solubilisate Exchange in a Zwitterionic Microemulsion on Addition of Hydrophibically End-Capped Poly(ethylene oxide)"
to be submitted as part of chapter 5

[3] Anina Barth, Michaela Dzionara, Michael Gradzielski
"The Kinetics of Solubilisate Exchange in a Nonionic Surfactant System - Correlation of Measured Rates with Interfacial Rigidity, Charge and Addition of Polymer"
to be submitted as part of chapter 3

[4] A. Barth, S. Prévost, J. Popig, M. Dzionara, G. Hedicke, M. Gradzielski
"Solubilisation of Different Medium Chain Esters in Zwitterionic Surfactant Solutions – Effects on Phase Behavior and Structure"
Journal of Colloid and Interface Science **2011**, doi:10.1016/j.jcis.2011.06.082
Contains parts of chapter 6

[5] Anina Barth, Isabelle Grillo, Michael Gradzielski
"Dynamics of Formation of Vesicles Studied by Highly Time-resolved Stopped-flow Experiments"
Tenside Surf. Det. **2010**, *47*, 300. *Contains parts of chapter 6 and 7*

** First two authors contributed equally to this work*

Acknowledgements

The present PhD thesis was elaborated under the supervision of Prof. Dr. Michael Gradzielski at the Technical University Berlin in the time of October 2005 to August 2011.

I am heartily thankful to my supervisor, Michael Gradzielski, for giving me the opportunity to work in this laboratory and whose encouragement, guidance and support from the initial to the final level enabled me to develop an understanding of the subject.

I want to thank Prof. Dr. J. Koetz very much for being reviewer of this thesis.

I am grateful to Sylain Prévost, Yun Liu, Jeremie Gummel, Marie-Sousai Appavou and Isabelle Grillo for performing the SANS and SAXS experiments. In particular, it is an honor for me to thank Prof. Mitchell A. Winnik from the University of Toronto for the suggestion of synthesizing the fluorescent probe I used in my experiment.

I owe my deepest gratitude to Gabriele Hedicke, Michaela Dzionara and Jana Lutzki for their kind support with syntheses, surface tension and interfacial tension measurements and their untiring assistance during my thesis. In addition, I would like to thank René Strassnick, Detlef Klabunde, Rolf Kunert, Michael Knuth and Erik Sallwey for servicing the stopped-flow device and for the help with the DLS set-up.

I am indebted to my many of my colleagues to support me and I would like to show my gratitude especially to Claudia Oppel and Jens Popig.

Lastly, I offer my regards to all of those who supported me in any respect during the completion of the project.

Anina Barth